

Role of Neuro-Mesodermal Progenitors in Neural Tube Formation

Dorothee Mugele

Thesis submitted to University College London
for the degree of Doctor of Philosophy

August 2018

Developmental Biology of Birth Defects
Developmental Biology & Cancer Programme
UCL Great Ormond Street Institute of Child Health

DECLARATION

I, Dorothee Mugele confirm that the work presented in this thesis is my own. Where information has been derived from other sources, I confirm that this has been indicated in the thesis.

London, 15th August 2018

ABSTRACT

It has long been thought that neural tube and somites derive from different germ layers, namely the ectoderm and mesoderm. This paradigm was challenged by the discovery of a dual-fated cell population in the mammalian tail bud, the so-called neuro-mesodermal progenitors (NMPs), which give rise to both neuroepithelium and paraxial mesoderm beyond the gastrulation stage. The aim of this PhD thesis was to characterise how NMPs contribute to neural tube formation using mouse embryos as a model system. First, the colonisation of the neural tube by NMPs and related cell populations was studied by labelling with the green fluorescent dye DiO followed by whole-embryo culture. Cells labelled caudal to the node (the NMP location) predominantly colonised the dorsal and dorso-lateral neural tube, but not the ventral domain, which was populated from the node, the node-streak border, and anterior to the node. Next, laser-ablation was used to study the developmental requirement for NMPs. As expected, ablation of the NMP location considerably disturbed the formation of paraxial mesoderm and neuroepithelium, although this effect was only transient, as adjacent cells rapidly re-populated the ablated region. A prevailing assumption is that NMPs co-express the neural marker *Sox2* and the mesodermal marker *T*. However, lineage tracing experiments revealed that the contribution of *Sox2*-expressing cells to the paraxial mesoderm at post-epiblast stages is very infrequent, whereas descendants of *T*-expressing cells extensively colonise both neural tube and somites. This suggested that NMPs are actually *Sox2*-negative. Indeed, when *Sox2* was specifically depleted in the *T*-expressing lineage, the resulting embryos had no mesoderm defect, but substantially reduced *Sox2* mRNA and protein levels in the neural tube with otherwise normal morphology and gene expression domains. This indicates that *Sox2* is not specifically required for neural tube formation and that bi-potent NMPs likely do not express *Sox2*.

IMPACT STATEMENT

The concept of neuro-mesodermal progenitors (NMPs) is incompatible with the traditional germ layer model, which claims that the neural and mesodermal lineages segregate during gastrulation. Therefore, these cells aroused great interest in the scientific community, being considered the exception to the general rule of germ layer formation. My thesis reveals that one of the key assumptions regarding NMPs, i.e. that these cells are characterised by co-expression of *Sox2* and *T*, is a misconception. Furthermore, this work indicates that the NMPs only represent a small piece of a greater phenomenon: The formation of the spinal neural tube is not the only exception to the traditional germ layer model. The data presented here suggest that hindgut and notochord development do not conform to the traditional model either.

These findings emphasise that our perception of early embryonic lineages is flawed and their potency is actually much less restricted than previously assumed. My results will transform the way we think about early embryonic development and stem cell plasticity in general. These new insights are of great significance to various target groups, as follows:

First, they will affect NMP researchers as a large part of the literature is based on the assumption that these cells co-express *Sox2* and *T*. Therefore, it will be necessary to re-assess what we know about these dual-fated progenitors taking into account the revised NMP model I propose here. In addition, it is important to shift the focus away from NMPs and rather concentrate on the bigger picture, that the paradigm of germ layer formation is not universally valid.

The second target group are developmental biologists in general, as germ layer formation is evolutionarily highly conserved. It will be crucial to verify the findings from mouse embryos in other organisms as well to determine if this paradigm is *per se* insufficient, or if only certain species are incompatible with it. Moreover, the results from this thesis will allow us to better understand and model developmental defects related to the axial tissues.

Third, the data will have a great impact on stem cell research in general, offering new possibilities for differentiation protocols, which might become more effective and better reflect the processes *in vivo*. This is not limited to basic research, but might also be exploited for stem cell-based therapies.

Although this PhD thesis is an important first step, more research will be required to fully understand its potential for disease modelling and clinical applications. To communicate these findings to the three target groups identified above, they were summarised in a paper and submitted to a peer-reviewed journal.

This work was funded by a Wellcome Trust 4-year PhD studentship.

ACKNOWLEDGEMENTS

First and foremost, I would like to thank my supervisor Professor Andy Copp for the opportunity to do my PhD in his lab. I am very grateful for your support, not only in the lab but also with my other studies. Thank you for giving me the freedom to make my own decisions and for providing guidance when I needed it. Also, thank you for being so patient with my undiplomatic English.

In addition, I would like to thank my secondary supervisor Professor JP Martinez-Barbera for constantly pushing me out of my comfort zone and for challenging me with unorthodox ideas. I am very glad you did that - turns out you were right! Thank you for all your support.

I would also like to thank Professor Roberto Mayor and Professor Nick Greene for their critical feedback and ideas over the years, which proved to be incredibly helpful.

I am greatly indebted to Dawn Savery and Dale Moulding, who I could always rely on for help and advice. Dawn, thank you for teaching me how to save a ruined experiment, for showing me how to stagger protocols to save time, and for helping me with the mice. No one is more loyal, efficient, or witty than you. I am grateful that I had the opportunity to learn from you. Dale, thank you for helping me so patiently with the laser-ablation and the image analyses. You taught me a lot and, most importantly, it was always great fun with you. I am still laughing at the story you told me about your encounter with the Queen.

I was very lucky to work alongside Sandra de Castro, Ana Rolo, and Paula Alexandre, who I could always turn to for unfailing help. Thank you for all the scientific (and non-scientific) discussions, for technical advice, your honest opinion, and your infectious excitement for science.

I would like to thank all members of the Neural Tube Defects group, past and present, and in particular my fellow PhD students Sonia Sudiwala, Lucy Culshaw, and Chloe Santos for their constant support over the years. My PhD would not have been

the same without Vicky Jones. Thank you for your encouragement and generous support in all aspects of life and thank you for cracking me up every single day. I will very much miss your company.

I would also like to say thank you to Berta Crespo Lopez, Diana Gold Diaz, Scott Haston, and Sarah Ivins, who were always there to help in case of need.

Many thanks to my friends Rachel, Gaile, Kevin, Rani, John, Susan, and Tracey who made my time in London truly special. Special thanks to Kate for cooking for me, travelling with me, and spending countless evenings with me at the Royal Opera House. What a great time we had!

Last but not least, I would like to thank Sanni for everything she has done for me over the last 15 years. You are the best.

TABLE OF CONTENTS

DECLARATION	2
ABSTRACT	3
IMPACT STATEMENT	4
ACKNOWLEDGEMENTS	6
TABLE OF CONTENTS	8
LIST OF FIGURES	13
LIST OF TABLES	15
ABBREVIATIONS	16
CHAPTER 1: INTRODUCTION	18
1.1 Gastrulation and the formation of axial tissues.....	18
1.1.1 The traditional germ layer model.....	18
1.1.2 Different modes of head, upper, and lower body development.....	19
1.1.3 Development of axial and paraxial tissues in the mouse embryo.....	20
1.1.3.1 Primary and secondary neurulation.....	20
1.1.3.2 Somitogenesis.....	22
1.1.3.3 Notochord formation.....	23
1.1.3.4 Hindgut development.....	24
1.2 NMPs – a shared progenitor for somites and spinal neural tube.....	25
1.2.1 NMPs as an exception to the traditional germ layer model.....	25
1.2.2 A brief history of NMPs.....	25
1.2.3 Sox2/T co-expression as a feature of NMPs.....	28
1.2.4 NMPs suggest a new model of body development.....	29
1.2.5 <i>In vitro</i> generation and analysis of NMP-like cells.....	30
1.2.6 NMPs in organisms other than mice.....	32

1.3 NMP research – limitations and open questions.....	34
1.3.1 Technical limitations.....	34
1.3.2 What is the role of NMPs in embryonic development?	34
1.3.3 One single progenitor or a pool of different progenitors?.....	35
1.3.4 Do NMPs form the entire spinal neural tube or only specific parts?	36
1.4 Project aims	37
CHAPTER 2: EXPERIMENTAL PROCEDURES.....	39
2.1 Mouse colonies.....	39
2.1.1 General	39
2.1.2 Wild type and transgenic lines.....	39
2.1.3 Genotyping.....	40
2.1.4 Tamoxifen administration.....	41
2.2 Embryo dissection and procedures	42
2.2.1 Embryo collection and fixation.....	42
2.2.2 Whole-embryo culture.....	42
2.2.3 Rat serum preparation	43
2.2.4 DiO-labelling.....	43
2.3 Expression analysis.....	44
2.3.1 Cryosectioning and immunostaining.....	44
2.3.2 Whole-mount <i>in situ</i> hybridisation.....	46
2.3.2.1 Probe synthesis.....	46
2.3.2.2 Hybridisation of RNA probe	47
2.3.2.3 Post-hybridisation and colorimetric detection	48
2.3.2.4 Vibratome sectioning and imaging.....	48
2.4 Laser-ablation	49
2.5 Image analysis.....	50

2.5.1 General	50
2.5.2 Cell position of DiO-labelled cells	50
2.5.3 Cell fate decision and colonisation of the neural tube by <i>T</i> -expressing cells.....	51
2.6 Statistical analysis	52
2.7 Other software	52
CHAPTER 3: RESULTS	53
3.1. Fate mapping the CLE and node region in E8.5 mouse embryos	53
3.1.1. Introduction and objectives	53
3.1.2. Results: The cellular origins of the neural tube and paraxial mesoderm	54
3.1.2.1 The CLE gives rise to the dorsal neural tube and somites, but only region 1 harbours NMPs	54
3.1.2.2 The ventral-to-dorsal translocation of cells from region 1 of the CLE is specific to the open posterior neuropore region	57
3.1.2.3 The ventral and ventro-lateral neural tube derive from cells located in the node region	60
3.1.3. Discussion: The cellular origins of the neural tube and paraxial mesoderm.....	63
3.1.3.1 Reliability and specificity of DiO-labelling as a method for fate mapping.....	63
3.1.3.2 Inconsistencies in the literature regarding the NMP location	65
3.1.3.3 Conclusion	68
3.2. Laser-ablation of the rostral CLE in E8.5 mouse embryos	69
3.2.1. Introduction and objectives	69
3.2.2. Results: Laser-ablation of the NMP region and its effect on the development of neural tube and paraxial mesoderm	69
3.2.2.1 Ablation of the rostral CLE affects body axis elongation	69
3.2.2.2 Ablating region 1 temporarily disturbs neural tube and somite formation	71
3.2.2.3 Cells located in CLE region 2 compensate for the ablated region 1	73
3.2.3. Discussion: Laser-ablation of the NMPs.....	74

3.2.3.1 Reliability of laser-ablation and its limitations	74
3.2.3.2 Laser-ablation as a method for studying NMPs.....	74
3.2.3.3 Conclusion	75
3.3. <i>Sox2/T</i> double-positive cells in neural tube formation	76
3.3.1. Introduction and objectives	76
3.3.2. Results: Lineage tracing <i>Sox2</i> - and <i>T</i> -expressing cells	77
3.3.2.1 <i>T</i> -expressing cells in the post-gastrulation embryo give rise to neural tube and paraxial mesoderm.....	77
3.3.2.2 <i>Sox2</i> -expressing cells in the post-gastrulation embryo do not give rise to paraxial mesoderm.....	79
3.3.2.3 <i>Sox2</i> -expressing cells in the gastrulating embryo give rise to both neural tube and paraxial mesoderm	84
3.3.3. Discussion: Lineage tracing <i>Sox2</i> - and <i>T</i> -expressing cells.....	87
3.3.3.1 Implications and limitations of genetic lineage tracing	87
3.3.3.2 Contradicting the concept of <i>Sox2/T</i> double-positive NMPs	88
3.3.3.3 Conclusion	89
3.3.4 Results: <i>Sox2</i> and <i>T</i> expression in WT embryos	90
3.3.4.1 <i>Sox2</i> protein is expressed in the CNH.....	90
3.3.4.2 <i>Sox2</i> mRNA is not expressed in the CNH	91
3.3.5 Discussion: <i>Sox2</i> and <i>T</i> expression in WT embryos	93
3.3.5.1 Limitations of WISH and immunostaining	93
3.3.5.2 <i>Sox2/T</i> expression – critique of the literature	94
3.3.5.2 Conclusion	95
3.3.6 Results: Deleting <i>Sox2</i> in the <i>T</i> -expressing lineage.....	96
3.3.6.1 Deleting <i>Sox2</i> in the <i>T</i> -expressing lineage yields embryos with a <i>Sox2</i> - negative neural tube and normal paraxial mesoderm	96
3.3.6.2 $T^{CreERT2}; Sox2^{fl/fl}$ embryos develop a morphologically normal neural tube ...	99
3.3.6.3 Cell fate decision of <i>T</i> -positive cells in $T^{CreERT2/+}; Sox2^{fl/+}$ embryos.....	102
3.3.6.4 Tracing NMPs in $T^{CreERT2/+}; Sox2^{fl/fl}$ embryos.....	104

3.3.7 Discussion: Deleting Sox2 in the <i>T</i> -expressing lineage	106
3.3.7.1 Sox2 is not expressed in NMPs.....	106
3.3.7.2 Sox2 is not required for neural tube formation	106
3.3.7.3 Future work	108
3.3.7.4 Conclusion	110
CHAPTER 4: THESIS DISCUSSION AND CONTROVERSY	111
4.1 Summary of results and new NMP model	111
4.2 Implications for NMP research	113
4.2.1 Common errors in the NMP literature.....	113
4.2.1.1 Location and potency of NMPs.....	113
4.2.1.2 Timing.....	114
4.2.1.3 Sox2/ <i>T</i> co-expression	116
4.2.2 Further support in the literature for the revised NMP model	116
4.2.2.1 <i>In vivo</i> studies	116
4.2.2.2 <i>In vitro</i> studies	120
4.2.2.3 Conclusion	121
4.2.3 Impact of findings.....	122
4.3 Final remarks	123
REFERENCES	125

LIST OF FIGURES

Figure 1. Closure sites during primary neurulation in mouse embryos.	20
Figure 2. Neuroepithelial bending during spinal neurulation.....	21
Figure 3. Location of long-term progenitors for the neural tube and paraxial mesoderm in post-gastrulation mouse embryos.	26
Figure 4. NMP cell fate decision.	31
Figure 5. Non-specific binding of DiO to the headfolds and extraembryonic tissues.	54
Figure 6. NMPs are located in CLE region 1 specifically contribute to the dorsal neural tube. ...	56
Figure 7. Time course tracing DiO-labelled cells from region 1 of the CLE.....	58
Figure 8. Ventral-to-dorsal translocation of cells from CLE region 1 is specific to the posterior neuropore.	59
Figure 9. Ventral and ventro-lateral neural tube arise from cells residing in and around the node.	61
Figure 10. Cellular origins of the neural tube and paraxial mesoderm.	63
Figure 11. Contribution of cells in CLE region 1 and NSB to CNH, notochord, and neural tube.	68
Figure 12. Ablating region 1 of the CLE slows down body axis elongation.	70
Figure 13. Deleting region 1 of the CLE transiently disrupts neural tube and somite formation.	72
Figure 14. Cells expressing <i>T</i> around E8.5 colonise both neural tube and paraxial mesoderm.	78
Figure 15. Cells expressing <i>Sox2</i> around E8.5 colonise the neural tube only (standard dose).	79
Figure 16. Cells expressing <i>Sox2</i> around E8.5 colonise the neural tube only (high tamoxifen dose).	81
Figure 17. Cells expressing <i>Sox2</i> around E8.0 colonise the neural tube and, to a negligible extent, paraxial mesoderm following multiple injections of the high tamoxifen dose.....	82
Figure 18. Cells expressing <i>Sox2</i> around E6.5 colonise both neural tube and paraxial mesoderm.	85
Figure 19. Cells expressing <i>Sox2</i> around E7.5 colonise both neural tube and paraxial mesoderm.	86
Figure 20. <i>Sox2</i> protein is expressed in the CNH.	91
Figure 21. <i>Sox2</i> mRNA is not expressed in the CNH.	92
Figure 22. Deleting <i>Sox2</i> in <i>T</i> -expressing cells results in reduced <i>Sox2</i> mRNA levels in the posterior neuropore, but no visible mesoderm defects.	97

Figure 23. $T^{CreERT2/+}; Sox2^{fl/fl}$ embryos form a Sox2-negative neural tube, but axis elongation and paraxial mesoderm are not affected.	98
Figure 24. Sox2 protein levels are strongly reduced in the neural tube of $T^{CreERT2/+}; Sox2^{fl/fl}$ embryos.....	100
Figure 25. $T^{CreERT2/+}; Sox2^{fl/fl}$ embryos form a normal neural tube in the absence of Sox2.	101
Figure 26. Down-regulation of Sox2 does not affect cell fate decision in T -expressing cells...	103
Figure 27. Cells traced from region 1 of the CLE in $T^{CreERT2/+}; Sox2^{fl/fl}$ embryos show the characteristic NMP pattern, except for DiO accumulation in the tail bud tip.....	105
Figure 28. Current and revised NMP models.....	112

LIST OF TABLES

Table 1. Mouse lines.	39
Table 2. Primer sequences for genotyping.	40
Table 3. Standard PCR reaction for genotyping.	41
Table 4. PCR settings for genotyping.	41
Table 5. Primary antibodies used for immunostaining.	45
Table 6. Secondary antibodies used for immunostaining.	45
Table 7. Plasmid DNA templates used to generate RNA probes for WISH	47
Table 8. Colonisation patterns observed from fate mapping experiments.	62
Table 9. Cell counts of GFP-positive cells in the paraxial mesoderm derived from Sox2 lineage tracing experiments.	83
Table 10. T/Brachyury antibodies tested.	90

ABBREVIATIONS

AP	alkaline phosphatase
AS	antisense
BCIP	5-bromo-4-chloro-3-indolyl phosphate
bp	base pairs
BSA	bovine serum albumin
CLE	caudo-lateral epiblast
CNH	chordo-neural hinge
DAPI	4',6-diamidino-2-phenylindole
DEPC	diethyl pyrocarbonate
DIG	digoxigenin
DLHP	dorsolateral hinge point
DMEM	Dulbecco's Modified Eagle Media
DMSO	dimethyl sulphoxide
DNA	deoxyribonucleic acid
dNTPs	deoxynucleotide triphosphate
E	embryonic day
EYFP	enhanced yellow fluorescent protein
FBS	foetal bovine serum
FGF	fibroblast growth factor
fl	floxed
GFP	green fluorescent protein
MHP	median hinge point
mRNA	messenger RNA
n	sample size
NBT	nitro blue tetrazolium chloride
NMP	neuro-mesodermal progenitor
NSB	node-streak border

NTDs	neural tube defects
PBS	phosphate-buffered saline
PBT	phosphate-buffered saline with 0.1% Tween-20
PCR	polymerase chain reaction
PFA	paraformaldehyde
PNP	posterior neuropore
RA	retinoic acid
RNA	ribonucleic acid
ROI	region of interest
rpm	rotations per minute
RT	room temperature
SDS	sodium dodecyl sulphate
Shh	sonic hedgehog
SSC	saline sodium citrate
SEM	standard error of the mean
ss	somite stage
TBST	Tris-buffered saline with 0.1% Tween-20
WISH	whole-mount <i>in situ</i> hybridisation
WT	wild type

CHAPTER 1: INTRODUCTION

1.1 Gastrulation and the formation of axial tissues

1.1.1 The traditional germ layer model

Gastrulation is an early developmental stage, characterised by dramatic changes in shape, during which the embryo converts from a single layer of pluripotent cells, known as the epiblast, into a tri-laminar structure. These layers are called germ layers and each of them gives rise to specific tissues: the ectoderm layer will eventually form the central nervous system and the epidermis, the mesoderm layer will generate bones and muscles, and the endoderm layer will develop into most of the inner organs including gut, liver, and lungs.

During gastrulation, epiblast cells first invaginate at the midline shaping the so-called primitive streak (Fraser, 1882; Sobotta, 1902; Sobotta, 1911). Subsequently, epiblast cells undergo epithelial-to-mesenchymal transition, ingress through the streak, and give rise to the mesoderm and endoderm layer, while those cells remaining in the epiblast will form the ectoderm (Gardner, 1978; Gardner and Rossant, 1979; Lawson et al., 1991; Lawson and Pedersen, 1992; Poelmann, 1981a; Poelmann, 1981b; Tam et al., 1993). The endoderm layer does not exclusively arise from the epiblast, it also contains cells from the visceral endoderm, which intermingle with each other to form the definitive endoderm (Kwon et al., 2008).

Gastrulation is considered the primary branching point in development as, from this time onwards, the pluripotent epiblast cells of the early embryo become restricted to distinct cell lineages. The segregation into ectoderm, mesoderm, and endoderm is highly conserved among animals with bilateral symmetry and it has been regarded a key paradigm in developmental biology since the early 19th century (Pander, 1817; Remak, 1855).

1.1.2 Different modes of head, upper, and lower body development

In amniotes, head, trunk, and tail form in a sequential manner, which is described as cephalocaudal growth (Kingsbury, 1932). The trunk is defined as the body region from the neck down to the start of the tail, including cervical, thoracic, lumbar, and sacral segments. The tail forms caudal to it at post-sacral levels. Although it is undisputed that head and upper body develop from the germ layers, which were established during gastrulation, lower body development has been the subject of great controversy.

Holmdahl divided body elongation into two separate processes, based on his observations in chick embryos (Holmdahl, 1925): During primary body development, head and upper body arise from the three germ layers. Afterwards, all lower structures, beyond the 30th somite level, are generated by a different mechanism which is called secondary body development. The rostral level of secondary body development corresponds with the transition from primary to secondary neurulation (see Chapter 1.1.3.1 below). According to Holmdahl, tissues of the lower body do not develop from the germ layers but from a homogenous pool of mesenchymal (“blastema”) cells in the tail bud. His model receives support from various studies which show that extirpated, grafted, or isolated tail buds can not only give rise to neural tubes, but also to various mesoderm-derived tail structures (Criley, 1969; Griffith and Sanders, 1991; Schoenwolf, 1978).

On the other hand, Vogt suggested an alternative model, according to which gastrulation continues throughout development until the axis is complete (Vogt, 1926). In favour of Vogt’s view, Pasteels found during studies in amphibian embryos that different locations in the tail bud have variable potential. In particular, he described the chordo-neural hinge, a small region directly caudal to the elongating notochord and hindgut, which gives rise to the neural tube and notochord (Pasteels, 1939; Pasteels, 1942; Pasteels, 1943). These findings contradict Holmdahl’s idea of a homogenous pool of blastema cells.

1.1.3 Development of axial and paraxial tissues in the mouse embryo

1.1.3.1 Primary and secondary neurulation

The central nervous system of vertebrates arises during development from an early embryonic structure known as the neural tube. Neural tube formation is a highly dynamic process which consists of two main mechanisms: Primary neurulation generates those regions of the neural tube, which will later develop into the brain and most of the spinal cord. Here, the flat neural plate, which is ectoderm-derived, folds to form a hollow tube (Waterman, 1976; Waterman, 1979; Wilson and Finta, 1980). However, the spinal cord at lower sacral and coccygeal levels derives from mesenchymal cells in the tail bud, in line with Holmdahl's model of secondary body development. These cells condense and form a rod-like structure which canalises and coalesces with more rostral neural tube aspects, to form a single tube which extends from the brain to the caudal tail end. This mechanism is referred to as secondary neurulation (Schoenwolf, 1984).

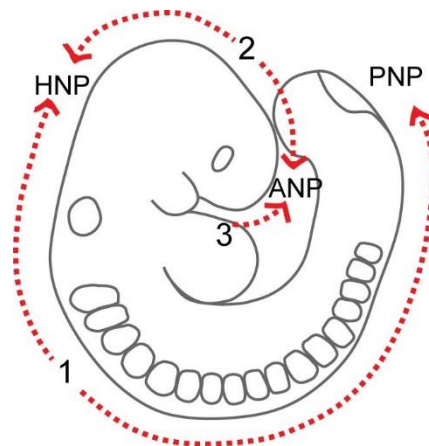


Figure 1. Closure sites during primary neurulation in mouse embryos.

Schematic of an E9.5 mouse embryo. Closure 1 is initiated at the hindbrain-cervical boundary, at the level of the third somite, and progresses bi-directionally. Closure 2 begins at the forebrain-midbrain boundary and extends both rostrally and caudally. Closure 3 progresses caudally only from the rostral end of the forebrain. As closures 1 and 2 meet they close the hindbrain neuropore (HNP), closures 2 and 3 progressively close the anterior neuropore (ANP), and the posterior neuropore (PNP) closes as closure 1 extends caudally. Closure of the PNP around E10.5 marks the end of primary neurulation.

During primary neurulation, neural tube closure initiates at defined axial levels (**Figure 1**) and progresses in a discontinuous manner (Golden and Chernoff, 1993; Sakai, 1989). In mouse embryos, the neural folds initially meet and fuse at the hindbrain-cervical boundary (closure 1) at embryonic day (E) 8.5 and at the forebrain-midbrain boundary at E9.0 (closure 2). Closure extends bi-directionally from these starting points and caudally only from the rostral end of the forebrain (closure 3). These processes continue in a gradual manner and eventually lead to full closure of the open neural tube regions, the so-called neuropores. The anterior neuropore between closures 2 and 3, as well as the hindbrain neuropore between closures 1 and 2, close around E9.0. The posterior neuropore, which is located caudally, closes by E10.5, which completes primary neurulation. Defective closure results in a variety of neural tube defects (NTDs) classified according to the region(s) which fail to close (Copp et al., 2003). For example, failure of posterior neuropore closure results in spina bifida, whereas anencephaly develops as a consequence of persistently open cranial folds.

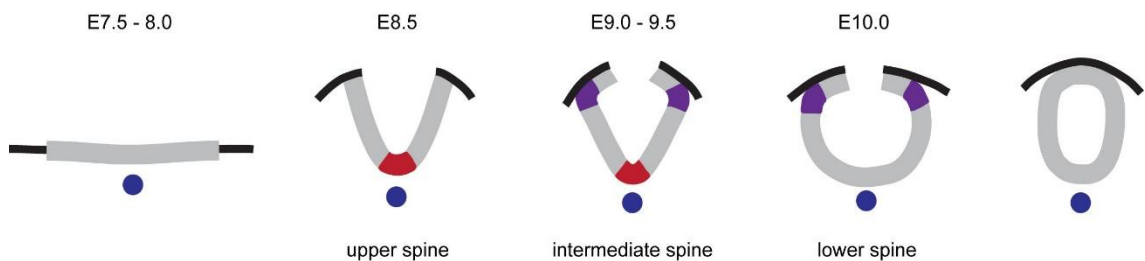


Figure 2. Neuroepithelial bending during spinal neurulation.

The neural plate (grey) is flat at the beginning of primary neurulation. The notochord (blue) induces the formation of the median hinge point (red), which allows the neural plate to bend along the midline. At intermediate and lower spine levels, paired dorsolateral hinge points (purple) direct the tips of the neural folds to the midline. The neural tube at lower spine levels bends without median hinge points. The neural folds fuse and remodel, which results in a closed neural tube which is covered by surface ectoderm (black).

Primary neurulation is further subdivided into neural plate shaping, neural fold elevation, and neural fold fusion. The neural plate is induced during gastrulation as epiblast cells located rostral to the primitive streak thicken and adopt a neural fate in

response to BMP antagonists emanating from the node (Harland, 2000). The neural plate is shaped around E7.5 – 8.0 by a convergent-extension movement: Cells in the neural plate and the underlying axial mesoderm move towards the midline and intercalate, lengthening the neural plate along its rostro-caudal axis and narrowing it along the medio-lateral axis (Copp et al., 2003; Keller, 2002; Keller et al., 2000; Ybot-Gonzalez et al., 2007). During this process, the neural plate begins to bend along the rostro-caudal midline as the underlying axial mesoderm induces the formation of a groove, the so-called median hinge point (MHP; **Figure 2**, left). In addition, the lateral aspects of the neural plate gradually elevate resulting in the characteristic V-shape of the neural plate at E8.5 (**Figure 2**, second from the left). By E9.0, paired dorsolateral hinge points (DLHPs) emerge at the spinal level, which direct the tips of the elevated neural folds to the midline (**Figure 2**, centre). At lower spine levels, which form around E10.0, the MHP is lost (**Figure 2**, second from the right) and bending occurs solely at the DLHPs (Shum and Copp, 1996). Eventually, the neural folds fuse at the dorsal midline, which is guided by cell protrusions at the leading edges of the fold tips (Geelen and Langman, 1979; Pai et al., 2012; Pyrgaki et al., 2010; Rolo et al., 2016). During this step, the neuroepithelium and the surface ectoderm, which initially formed one continuous layer, fuse and remodel generating a closed neural tube which is separated from the overlying surface ectoderm (**Figure 2**, right).

Note that the cranial region closes by a slightly different mechanism: Here, the neural plate initially bends at the MHP, which is followed by thickening of the neuroepithelium, resulting in biconvex folds which are facing away from the midline (Jacobson and Tam, 1982; Morriss-Kay, 1981). As the DLHPs form, the cranial folds adopt a concave shape with the tips of the two folds directed at each other. The cranial neural folds fuse at the midline forming a keyhole-shaped lumen.

1.1.3.2 Somitogenesis

Somites are undifferentiated blocks of mesoderm which can be found in all vertebrate embryos. They are laid down in pairs – one on each side of the neural tube – in a

rostral-to-caudal direction as the embryo elongates. Paraxial mesoderm is formed in mice between E8.0 and E13.0. The rostral-most somites arise from prospective mesodermal cells which migrate anteriorly from the rostral primitive streak, whereas later somites originate from the tail bud mesoderm (Tam and Beddington, 1987). A new pair is pinched off from the rostral end of the pre-somitic mesoderm every two hours at regularly-spaced intervals (Dequeant and Pourquie, 2008). This rhythmic process is guided by a molecular oscillator, the so-called “segmentation clock” (Gomez et al., 2008). It is based on periodic, synchronised transcription of cyclic genes in the pre-somitic mesoderm, which control the specification of paraxial mesoderm. Many of those genes are members of the Notch, Fgf, and Wnt signalling pathways (Krol et al., 2011). The Clock and Wavefront model for somitogenesis proposes that all cells in the pre-somitic mesoderm oscillate in phase, however, only some of these cells are permissive for somite formation (Cooke and Zeeman, 1976). The wavefront is the differentiation front which slowly moves posteriorly as the embryo elongates. Only those pre-somitic cells will form somites, which are in the permissive stage when hit by the wavefront. The somites will later develop into skeletal muscles, vertebrae, ribs, tendons, and dermis.

1.1.3.3 Notochord formation

The notochord, which is also referred to as axial mesoderm, is a transient, bar-shaped structure which is characteristic of chordates. It is present in the mouse embryo from E7.5 until E12.5 and is generally considered to be mesoderm-derived (Chesley, 1935; Gluecksohn-Schoenheimer, 1938; Gruneberg, 1958). The notochord lies centrally, beneath the neural tube, and extends all the way from the prechordal plate to the node. The rostral-most notochord arises from dispersed progenitor cells which converge at the midline (Yamanaka et al., 2007), whereas the notochord in more caudal regions is composed of cells which arise from the node (Beddington, 1994; Yamanaka et al., 2007). The node is the primary organiser in mice, which is located at the rostral end of the primitive streak. However, only the ventral layer of the node gives rise to the

notochord (Wilson and Beddington, 1996), as the dorsal layer generates the floor plate of the neural tube (Sulik et al., 1994). The notochord extends in a rostral-to-caudal direction as the embryo grows, together with the neural tube and hindgut. This elongation is a combined effect of convergent extension, cell division, and addition of cells from the node to the caudal end of the notochord (Sausedo and Schoenwolf, 1994; Yamanaka et al., 2007). Interestingly, Yamanaka and colleagues noticed during live imaging experiments that the distance between the node and the base of the allantois remains constant between 1 – 12 ss (Yamanaka et al., 2007), indicating that the murine node does not regress, unlike Hensen's node, the analogous structure in avians (Schoenwolf, 1992).

The notochord provides stability as some form of embryonic skeleton. In addition, it serves as a signalling centre by secreting factors which pattern the surrounding tissues. For example, Sonic Hedgehog (Shh), which emanates from the notochord, inhibits formation of DLHPs in the upper spinal region (Ybot-Gonzalez et al., 2002). Furthermore, Shh induces the floor plate and thereby establishes the dorso-ventral axis of the neural tube (Echelard et al., 1993; Placzek et al., 1991). The notochord is also required for somite patterning, in particular the differentiation into dermamyotome and sclerotome, which involves Shh and Noggin (Fan and Tessier-Lavigne, 1994; Johnson et al., 1994; McMahon et al., 1998). The sclerotome is the ventral part of the somites which gives rise to the ribs and the skeletal elements of the vertebral column, whereas the dermamyotome differentiates into the dermis and myotome. Further tissues which are patterned by factors originating from the notochord are reviewed in (Corallo et al., 2015).

1.1.3.4 Hindgut development

The hindgut is derived from the endoderm, which was established during gastrulation (Lawson et al., 1986). Folding transforms the endoderm layer into a hollow tube, the so-called gut tube: Around E8.5, the endoderm starts to invaginate at the rostral and caudal end of the embryo, shaping two pockets, the cranial intestinal portal and caudal

intestinal portal, respectively. These are the future fore- and hindgut. The pockets elongate towards each other and become connected as the intervening midgut endoderm folds, forming a contiguous tube by E9.0 (Lawson et al., 1986; Rosenquist, 1971). This tube lies directly ventral to the notochord. The hindgut, which is the caudal-most part of the gut tube, will later develop into the descending colon, sigmoid colon, rectum, and urogenital sinus.

1.2 NMPs – a shared progenitor for somites and spinal neural tube

1.2.1 NMPs as an exception to the traditional germ layer model

Neuro-mesodermal progenitors (NMPs) are a bi-potent progenitor cell population, which resides in the caudal end of the post-gastrulation embryo. These cells can either adopt a neural fate and integrate into the forming spinal neural tube, or they differentiate into paraxial mesoderm and colonise the somites. The concept of a shared progenitor between the neural and mesodermal lineages, which persists in the developing embryo well beyond the gastrulation stage, is difficult to reconcile with the traditional germ layer model, which states that the neural tube is derived from ectoderm and the somites from mesoderm, which segregated during gastrulation. For this reason, the discovery of NMPs has attracted a great deal of attention.

1.2.2 A brief history of NMPs

The idea that the spinal neural tube is actually mesoderm-derived was first introduced in 1884 by Swiss anatomist Albert von Kölliker (Kölliker, 1884). However, the traditional germ layer model, which was proposed by Pander and Remak based on studies in chick embryos (Pander, 1817; Remak, 1855), prevailed and Kölliker's findings were dismissed. Only in 2007, after Cambray and Wilson published two papers on grafting experiments in mouse embryos (Cambray and Wilson, 2002; Cambray and Wilson, 2007), Kölliker's observations gained in importance. Cambray and Wilson

homotopically grafted small pieces of tissue from embryos, which ubiquitously express green fluorescent protein (GFP), into wild type embryos, to analyse how transplanted cells colonise the elongating body axis. They identified two regions in the E8.5 embryo, which harbour cells that provide long-term contribution to both neural tube and paraxial mesoderm. One of them is the area between the caudal node and the rostral end of the primitive streak remnant, the so-called node-streak border (NSB; **Figure 3A**).

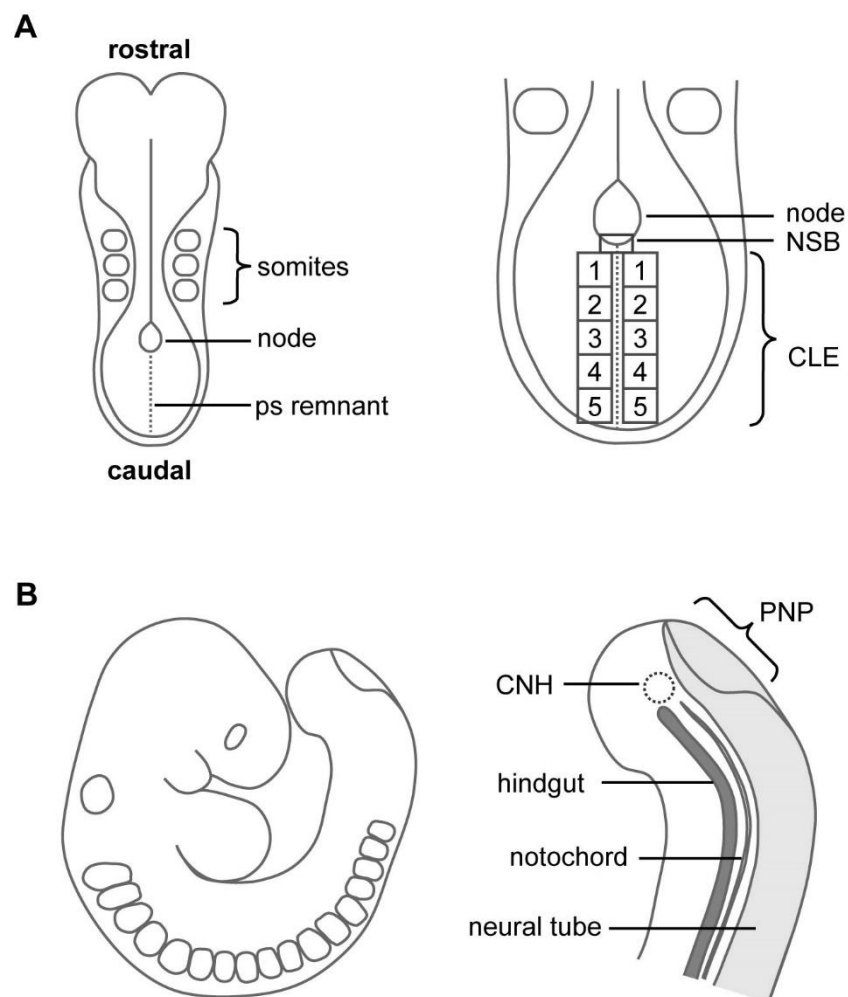


Figure 3. Location of long-term progenitors for the neural tube and paraxial mesoderm in post-gastrulation mouse embryos.

(A) Schematic of an E8.5 mouse embryo. At this stage, long-term progenitors for both neural tube and paraxial mesoderm are located in the NSB and rostral CLE (regions 1 – 3) according to Cambray and Wilson (Cambray and Wilson, 2002; Cambray and Wilson, 2007). **(B)** Schematic of an E9.5 mouse embryo. Following internalisation of the node region around E9.0, these long-term progenitors relocate to the centre of the tail bud, the so-called chordo-neural hinge (CNH). *ps remnant*, primitive streak remnant; *CLE*, caudo-lateral epiblast; *NSB*, node-streak border; *PNP*, posterior neuropore; *CNH*, chordo-neural hinge. Adapted from (Mugele et al., 2018).

In addition, they observed a similar pattern after grafting a piece from the epiblast, which lies on both sides right next to the primitive streak remnant. This epiblast region is referred to as the caudo-lateral epiblast (CLE). However, Cambray and Wilson only observed a lasting colonisation of neural tube and somites after grafting the rostral CLE (spanning regions 1 – 3), but not when analysing regions 4 or 5.

The node and adjacent regions are internalised around E9.0 (Yamanaka et al., 2007) and form the chordo-neural hinge (CNH), which lies underneath the forming neuroepithelium, directly caudal to the extending hindgut and notochord (**Figure 3B**). The long-term progenitors are internalised together with the node and are therefore located in the CNH of E9.0 and older embryos.

Cambray and Wilson further discovered that CNH cells maintain their ability to give rise to paraxial mesoderm and neural tube until E12.5. In addition, they could be serially transplanted through several generations of embryos without affecting their potency (Cambray and Wilson, 2007).

Based on these experiments, NMPs have been defined as cells which are retained in the CNH and whose descendants colonise both spinal neural tube and paraxial mesoderm over long axial distances. Due to these characteristics some authors consider NMPs to be stem cells (Cambray and Wilson, 2007; Cunningham et al., 2015; Kondoh and Takemoto, 2012; Martin and Kimelman, 2012; Olivera-Martinez et al., 2012; Turner et al., 2014; Wilson et al., 2009; Wymeersch et al., 2016), although there is currently no proof for this hypothesis. A stem cell is an undifferentiated cell which has the ability to self-renew and to generate daughter cells which further specialise into different functional cell types. However, the observed colonisation patterns from Cambray and Wilson's transplantation studies do not provide evidence that grafted cells are able to self-renew, as these patterns could equally arise from slowly proliferating progenitor cells.

1.2.3 Sox2/T co-expression as a feature of NMPs

Immunostainings revealed that the NSB and CLE contain cells, which co-express the neural marker Sox2 and the early mesodermal marker T (Henrique et al., 2015; Wymeersch et al., 2016). As this expression pattern coincides with their proposed location and potency, it has since been accepted that the dual-fated progenitors are defined by co-expression of Sox2 and T.

Sox2 is a member of the Sox (Sry-related HMG box) gene family of transcription factors and constitutes the SoxB1 subfamily together with Sox1 and Sox3 (Collignon et al., 1996; Pevny and Lovell-Badge, 1997). Sox2 is originally expressed in the epiblast, from which the three germ layers develop during gastrulation. It is maintained in the ectodermal layer and its derivative, the neural tube, but not in the other two germ layers (Wood and Episkopou, 1999). Sox2-deficient embryos die around implantation as they fail to form epiblast (Avilion et al., 2003), underpinning the critical role of Sox2 in early embryonic development.

T, which is also known as *Brachyury*, is a member of the T-box transcription factor family and required for mesoderm formation (Wilkinson et al., 1990). T is expressed in the nascent mesoderm of the tail bud, but is down-regulated as cells differentiate and move away from the primitive streak. Later, it becomes restricted to the notochord (Kispert and Herrmann, 1994; Wilkinson et al., 1990). Various T mutants have been described, which lead to phenotypes of different severity depending on the gene dosage. These phenotypes range from skeletal abnormalities in heterozygotes (Dobrovolskaia-Zavadskaia, 1927; Gluecksohn-Schoenheimer, 1938; Gruneberg, 1958), to shortened (Chesley, 1935) or absent tails (Gluecksohn-Schoenheimer, 1938; Searle, 1966), and pre-mature body axis truncation in hypomorphs (Cogliatti, 1986; Gruneberg, 1958). Homozygous embryos display severe morphological defects, including early cessation of body axis elongation and the absence of mesoderm-derived structures posterior to the forelimb bud, in particular the notochord and somites (Chesley, 1935; Fujimoto and Yanagisawa, 1983; Gruneberg, 1958). They die early

during development, depending on the allele either at implantation (Gluecksohn-Schoenheimer, 1938) or around E10.5 (Chesley, 1935; Yanagisawa et al., 1981).

1.2.4 NMPs suggest a new model of body development

In relation to the different modes of body development, the NMPs can be considered a modification of Holmdahl's model. Instead of two separate processes, the data on NMPs suggest that the neural tube is formed by three different mechanisms: First, development of the head region which follows the traditional germ layer model; second, the generation of the rostral aspect of the spinal neural tube, which is formed of NMP descendants during primary neurulation; and third, development of the caudal neural tube via secondary neurulation, which also depends on NMPs (Cambray and Wilson, 2007; Olivera-Martinez et al., 2012; Wymeersch et al., 2016). However, it is important to note that Cambray and Wilson's grafting experiments contradict Holmdahl's assumption of a homogenous population of blastema cells in the tail bud and rather suggest that the potency of cells varies in different tail bud regions, in line with Pasteels observations.

The borders between the three sections are well defined. In mouse embryos, primary neurulation ceases with closure of the posterior neuropore around 30 – 32 ss. As to the rostral limit of NMP contribution, lineage tracing experiments have shown that descendants of *T*-expressing cells, which should contain the *Sox2/T* double-positive NMPs, start colonising the forming neural tube beyond the sixth somite level, i.e. from the cervical level onwards (Anderson et al., 2013; Perantoni et al., 2005). This was further confirmed by retrospective clonal analysis in mouse embryos (Tzouanacou et al., 2009). Tzouanacou and colleagues used a method which is based on spontaneous recombination of the inactive *LaacZ* gene into its active *LacZ* form, allowing for long-term tracking of cells and their progeny, in which this rare recombination event took place. They found apparent clones which colonised both neural tube and somites. However, these were only observed caudal to the sixth somite. Altogether, this suggests that the neural tube is formed by three separate mechanisms for the head

(neural tube rostral to the sixth somite level), upper body (between somite level 6 and 30), and lower body (beyond somite level 30).

Interestingly, live imaging experiments by Yamanaka and colleagues indicate that the notochord in mouse embryos is equally formed by three distinct mechanisms: the notochord in the head region is generated independent of the node from dispersed progenitor cells; notochord in the upper body (beyond somite level 2 – 4) is directly derived from the node; and notochord in the lower body section, caudal to the hindlimb (i.e. beyond somite level 28), is formed by node-derived cells, which first need to migrating further caudally before they are incorporated into the growing notochord (Yamanaka et al., 2007). Notably, the authors also found that notochord formation in the upper and lower body, but not in the head region, is dependent on *T*.

1.2.5 *In vitro* generation and analysis of NMP-like cells

Various research groups developed NMP *in vitro* models by mimicking the signalling environment in the caudal mouse embryo (Cunningham et al., 2016; Gouti et al., 2014; Tsakiridis et al., 2014; Turner et al., 2014). Although these protocols differ slightly, they all start off with pluripotent cells, either embryonic or epiblast stem cells. Embryonic stem cells are isolated from the inner cell mass of blastocysts, whereas epiblast stem cells derive from the epiblast layer of post-implantation embryos, which eventually gives rise to the three germ layers. To obtain NMP-like cells, these pluripotent stem cells are treated with Fgf and a Wnt agonist. Depending on the duration and timing when cells are exposed to these factors, they start co-expressing Sox2 and T protein after 3 – 7 days, which is deemed the “NMP stage”. These cells can further be differentiated to express either mesodermal or neural genes (Gouti et al., 2014; Tsakiridis et al., 2014). Moreover, grafting a small number of these stem cell-derived NMP-like cells into chick and mouse embryos showed that descendants of transplanted cells enter both neural tube and paraxial mesoderm (Gouti et al., 2014). In addition, Tsakiridis and Wilson demonstrated that clones derived from single NMP-like cells contain both Sox2- and T-expressing cells (Tsakiridis and Wilson, 2015), confirming

that these *in vitro* protocols generate dual-fated progenitors for both the neural and mesodermal lineages. Similar protocols have also been established for differentiating human pluripotent stem cells into NMP-like cells (Gouti et al., 2014; Lippmann et al., 2015; Verrier et al., 2018).

These *in vitro* systems have been used to model neural tube formation (Lippmann et al., 2015; Verrier et al., 2018) and also to further elucidate the gene regulatory network which guides cell fate decision in NMPs (Cunningham et al., 2016; Gouti et al., 2014; Tsakiridis et al., 2014; Turner et al., 2014). Although it is not clear to what extent these models are consistent with dual-fated progenitors *in vivo*, two recent studies revealed that the *in vitro* data on cell fate decision fits well with transcriptomic analyses of NMPs purified from post-gastrulation mouse embryos (Gouti et al., 2017; Koch et al., 2017).

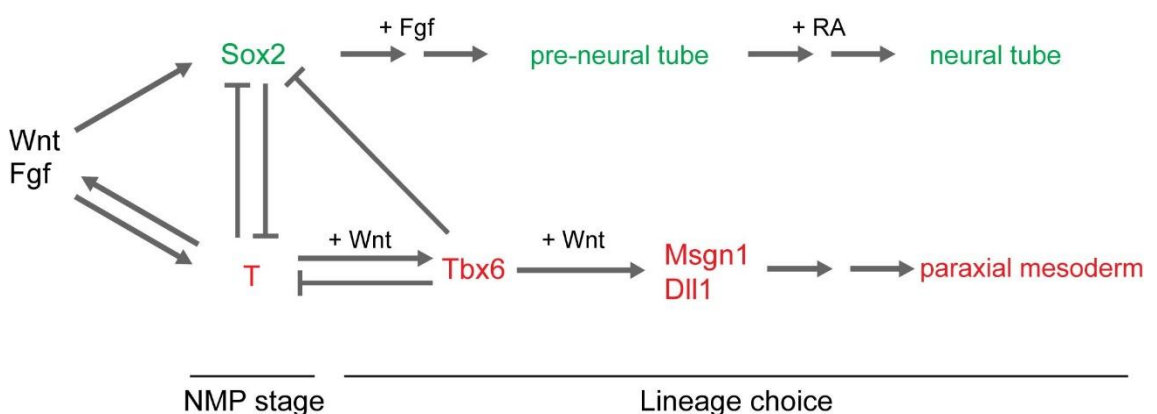


Figure 4. NMP cell fate decision.

Overview of the regulatory network guiding NMP maintenance and differentiation.

A simplified summary of NMP cell fate decision, based on *in vitro* and *in vivo* data, is depicted in **Figure 4**: Wnt3a and Fgf4/8 induce Sox2 and T (Takemoto et al., 2006; Turner et al., 2014; Yamaguchi et al., 1999) and thereby maintain the undifferentiated NMP stage, which is characterised by co-expression of both markers (Gouti et al., 2017; Gouti et al., 2014; Koch et al., 2017; Nowotschin et al., 2012; Olivera-Martinez et

al., 2012; Tsakiridis et al., 2014; Wilson et al., 2009). T further induces canonical Wnt signalling (Martin and Kimelman, 2008), creating a positive feedback loop. Data from stem cell-derived NMP-like cells suggest that prolonged exposure to Wnt favours differentiation into paraxial mesoderm by inducing Tbx6 (Gouti et al., 2014; Tsakiridis et al., 2014). Tbx6 does not only repress Sox2 (Gentsch et al., 2013; Takemoto et al., 2011), synergistic expression of both Wnt and Tbx6 further activates pre-somitic mesoderm genes, including *Mgn1* and the Notch ligand *Dll1* (Chalamalasetty et al., 2014; Hofmann et al., 2004; Wittler et al., 2007). On the other hand, neural differentiation is guided by Fgf and retinoic acid (RA) signalling. Fgf is initially expressed in the pre-neural tube (Wilson et al., 2009). However, it is down-regulated in more rostral regions by RA, which emanates from the somites (Diez del Corral et al., 2003), establishing neural identity. For a more detailed description of the gene regulatory network please refer to (Gouti et al., 2017; Koch et al., 2017).

1.2.6 NMPs in organisms other than mice

NMPs have not only been proposed in mice. Grafting and labelling experiments revealed that many other organisms also have defined regions located at their caudal end, which contain precursors for both paraxial mesoderm and neural tube. In the mouse, NMPs are assumed to reside directly caudal to the node and in the CNH (Cambray and Wilson, 2002; Cambray and Wilson, 2007; Tam and Beddington, 1987; Wilson and Beddington, 1996). Similar regions were described in chick embryos in the rostral primitive streak region (Brown and Storey, 2000; Schoenwolf, 1992) and later in the CNH (McGrew et al., 2008; Olivera-Martinez et al., 2012). In zebrafish embryos, they were found in the caudal-most part of the tail bud (Martin and Kimelman, 2012) and are therefore sometimes referred to as “posterior wall progenitor cells” (Row et al., 2016). NMP-like cells have further been identified in the CNH of *Xenopus* embryos (Davis and Kirschner, 2000; Gont et al., 1993) and in the posterior neural plate of the axolotl (Taniguchi et al., 2017).

Apart from transplantation and labelling studies, immunostainings and *in situ* hybridisation data suggest overlapping expression of the respective Sox2 and T orthologues in these regions. This was shown in chick (Olivera-Martinez et al., 2012), zebrafish (Martin and Kimelman, 2012) and axolotl (Taniguchi et al., 2017). In addition, Olivera-Martinez and colleagues performed double-immunostaining against Sox2 and T in the tail buds of human embryos, showing that these also contain a region where the expression domains of both markers appear to overlap (Olivera-Martinez et al., 2012).

Although the bi-potent progenitors have only been described in a few species, some of the mechanisms underlying posterior development, which are also implicated in NMP regulation, seem to be evolutionarily conserved among most of the animal kingdom: Similar to somite formation in vertebrates, short and intermediate germ-band insects sequentially form segments from a posterior growth zone as the body elongates. Strikingly, this is also regulated by orthologues of the *Wnt* and *Caudal* genes, which are expressed at the posterior end of the embryo (Bolognesi et al., 2008a; Bolognesi et al., 2008b; Copf et al., 2004; Nagy and Carroll, 1994; Ryan and Baxevanis, 2007; Schulz et al., 1998; Shinmyo et al., 2005). In addition to bilaterians, posterior Wnt signalling has also been described in Porifera, Ctenophora, Placozoa, and Cnidaria (Adamska et al., 2007; Nichols et al., 2006; Technau et al., 2005). Although Wnt is known to be involved in patterning the primary body axis in Cnidaria (Hobmayer et al., 2000; Kusserow et al., 2005; Lee et al., 2006), its role in the other three phyla has not been elucidated yet.

Please note, all references given in the Results and Discussion section refer to studies done in the mouse, unless otherwise indicated.

1.3 NMP research – limitations and open questions

1.3.1 Technical limitations

Despite the great interest in NMPs, many questions remain unsolved, which is due to the limited accessibility of these cells. It is not possible to genetically target them as no NMP-specific marker has been identified to date. Instead, researchers have come up with other ideas to study them.

Based on the popular hypothesis that NMPs express both markers, Sox2/T co-expressing cells have been studied extensively *in vivo* (Garriock et al., 2015; Goto et al., 2017; Gouti et al., 2017; Koch et al., 2017; Martin and Kimelman, 2012; Olivera-Martinez et al., 2012; Wymeersch et al., 2016).

Others have grafted the NMP location (Cambray and Wilson, 2002; Cambray and Wilson, 2007; Tam and Beddington, 1987) or labelled cells in this area to assess their contribution to the axial tissues (Cambray and Wilson, 2002; Tam and Beddington, 1987). Although these techniques lack specificity, similar results have been obtained in *Xenopus* (Davis and Kirschner, 2000; Gont et al., 1993), chick (Brown and Storey, 2000; Olivera-Martinez et al., 2012; Schoenwolf, 1992), and zebrafish embryos (Martin and Kimelman, 2012), giving rise to the view that NMPs exist in this embryonic location and are conserved evolutionarily.

1.3.2 What is the role of NMPs in embryonic development?

As NMP descendants colonise both the growing neural tube and paraxial mesoderm, it is assumed they are required for body elongation by supplying the extending axial tissues with cells (Cambray and Wilson, 2007; Cunningham et al., 2016; Garriock et al., 2015; Martin, 2016; Olivera-Martinez et al., 2012; Wilson et al., 2009; Wymeersch et al., 2016). This hypothesis receives support from various loss-of-function studies, which indicate that neural tube and somite formation are closely linked, both spatially and temporarily: For example, the T-box transcription factor *Tbx6* is required for paraxial mesoderm differentiation. It is a down-stream target of *T* (Lolas et al., 2014)

and is expressed in the tail bud and pre-somitic mesoderm after gastrulation. *Tbx6* depletion results in embryos which stop building somites and form ectopic neural tubes instead (Chapman and Papaioannou, 1998). Another, similar example is the *Wnt3a* knock-out, in which embryos also develop an ectopic neural tube at the expense of paraxial mesoderm (Takada et al., 1994; Yoshikawa et al., 1997). *Wnt3a* is expressed in the primitive streak during gastrulation and throughout the tail bud mesoderm in post-gastrulation stages, overlapping with the proposed NMP location (Cambray and Wilson, 2007; Wilson et al., 2009). *Wnt3a* regulates mesoderm specification (Takada et al., 1994), acting directly upstream of *T* (Yamaguchi et al., 1999). In addition, several groups proposed that Wnt/ β -catenin signalling is implicated in NMP cell fate decision (Cunningham et al., 2015; Dunty et al., 2014; Garriock et al., 2015; Goto et al., 2017; Koch et al., 2017; Li et al., 2016; Martin and Kimelman, 2012; Nowotschin et al., 2012; Olivera-Martinez et al., 2012; Tsakiridis et al., 2014).

Interestingly, both *Tbx6* and *Wnt3a* knock-out embryos exhibit premature axis truncation, underpinning the idea that NMPs might be required not only for generating neural and mesodermal cells, but also for body axis elongation. Many more mutations which affect both the neural and mesodermal lineages have been reviewed by Wilson and colleagues (Wilson et al., 2009).

Although the data suggest that neural tube and somite formation are mechanistically linked, they neither provide conclusive evidence that both tissues arise from one shared progenitor cell population, nor do they prove that NMPs drive body axis elongation. More research will be required to define the role of these dual-fated progenitors in the developing embryo.

1.3.3 One single progenitor or a pool of different progenitors?

A couple of different experimental approaches have confirmed that the region caudal to the node contains cells which give rise to spinal neural tube and somites. Yet, none of these studies show specifically that these tissues derive from one shared progenitor. Cambray and Wilson grafted groups of cells in their transplantation experiments

(Cambray and Wilson, 2002; Cambray and Wilson, 2007). Therefore, their experiments do not reveal if true NMPs exist. Similarly, during cell labelling experiments in mouse (Cambray and Wilson, 2002; Tam and Beddington, 1987), *Xenopus* (Davis and Kirschner, 2000; Gont et al., 1993), and chick embryos (Brown and Storey, 2000; Olivera-Martinez et al., 2012) the researchers always marked more than one cell and therefore, the data do not prove the existence of a shared progenitor. Alternatively, the NMP region might contain a heterogeneous pool of progenitor cells with restricted potential for either neural or mesodermal fate.

Tzouanacou and colleagues used retrospective analysis of clonal descendants and they observed apparent clones that spanned both paraxial mesoderm and neural tube (Tzouanacou et al., 2009), suggesting the existence of a shared progenitor. Although unlikely, it cannot be ruled out that the observed pattern might have arisen from recombination in two or more separate cells.

In summary, the accumulated data offer the possibility that paraxial mesoderm and spinal neural tube might arise from a common progenitor, the NMPs. Nevertheless, they do not exclude alternative explanations beyond doubt, in particular the presence of multiple restricted progenitor pools in the caudal embryo, which form either somites or neural tissue.

1.3.4 Do NMPs form the entire spinal neural tube or only specific parts?

Cells which show NMP-like characteristics have been described in various organisms. Yet, it remains unresolved whether the NMPs give rise to the entire spinal neural tube or only to specific domains. Cambray and Wilson reported from their grafting experiments that transplanted cells predominantly colonised the ventral neural tube only (Cambray and Wilson, 2007). However, cells from a few grafts ended up in the dorsal domain, or in both parts. A previous study in our group demonstrated that cells labelled in the elevated neural folds translocate in a ventral-to-dorsal direction as the posterior neuropore closes (McShane et al., 2015). Although the origin of these cells was not identified, they might have arisen from NMPs. On the other hand, lineage

tracing the descendants of *T*-expressing cells revealed that these colonise the entire neural tube along its dorso-ventral axis (Anderson et al., 2013; Perantoni et al., 2005), and since NMPs are believed to co-express *Sox2* and *T*, these findings led many to conclude that the dual-fated progenitors form the entire spinal neural tube, although these results do not fit with the observations from Cambray and Wilson.

This unsolved issue became the starting point for my PhD thesis.

1.4 Project aims

The purpose of this thesis was to better understand the involvement of NMPs in neural tube formation. The two main questions to be answered were:

- i) Which part of the spinal neural tube is derived from NMP descendants?
- ii) What is the function of NMPs in the development of the spinal neural tube?

The results presented in Chapter 3 closely follow these questions and they are subdivided into three main sections, according to the methods used to address them:

Chapter 3.1 deals with the first question by combining vital cell labelling with mouse whole-embryo culture. These experiments aimed to assess how cells located in the CLE and node region contribute to the forming neural tube along its dorso-ventral and rostro-caudal axes.

Chapter 3.2 addresses the second question. To remove NMPs and draw conclusions on their role in embryonic development, I used laser-ablation to extirpate the NMP region, and analysed the effect on neural tube and somite formation.

In Chapter 3.3 I employed genetic techniques to study the descendants of *Sox2*- and *T*-expressing cells in post-gastrulation embryos, which is based on the idea that NMPs are defined by the co-expression of both markers. These experiments

aimed to clarify the nature of the *Sox2/T* double-positive cells and their involvement in neural tube development.

Based on the results obtained from these studies, I propose a new NMP model, which is outlined in Chapter 4.1 of this thesis.

CHAPTER 2: EXPERIMENTAL PROCEDURES

2.1 Mouse colonies

2.1.1 General

All animal studies were performed in accordance with the UK's Animals (Scientific Procedures) Act 1986 and with the Medical Research Council guidance in 'Responsibility in the Use of Animals for Medical Research' (July 1993). The mice were maintained at 22 °C on a 12 h light-dark cycle. They were either mated overnight and checked for a copulation plug the following morning, or they were mated in the morning and checked for a plug in the evening of the same day. The time of plug detection was designated E0.5.

2.1.2 Wild type and transgenic lines

The mouse lines used are summarised in **Table 1**.

Table 1. Mouse lines.

Strain name	Status (background)	Source and reference
CD-1	wild type	Charles River Laboratories (CrI:CD1(ICR))
<i>Sox2</i> ^{CreERT2/+}	mutant (C57BL/6J)	provided by Prof. J.P. Martinez-Barbera (UCL Great Ormond Street Institute of Child Health); previously described in (Andoniadou et al., 2013)
<i>T</i> ^{CreERT2/+}	mutant (C57BL/6J)	The Jackson Laboratory (Tg(T-cre/ERT2)1Lwd); previously described in (Anderson et al., 2013)
<i>Sox2</i> ^{fl/fl}	mutant (C57BL/6J)	The Jackson Laboratory (<i>Sox2</i> ^{tm1.1Lan/J}); previously described in (Shaham et al., 2009)
<i>Rosa26</i> ^{m1mG/m1mG}	mutant (C57BL/6J)	previously described in (Muzumdar et al., 2007)
<i>Rosa26</i> ^{EYFP/EYFP}	mutant (C57BL/6J)	previously described in (Srinivas et al., 2001)

For the experiments shown in **Figures 22 – 27**, the *T*^{CreERT2/+} and the *Sox2*^{fl/fl} lines were initially crossed to obtain *T*^{CreERT2/+}; *Sox2*^{fl/+} males. These were then crossed again with

Sox2^{fl/fl} females to obtain embryos of the genotypes *T^{+/+}; Sox2^{fl/+}*, *T^{+/+}; Sox2^{fl/fl}*, *T^{CreERT2/+}; Sox2^{fl/+}*, and *T^{CreERT2/+}; Sox2^{fl/fl}*. The *Rosa26^{mTmG/mTmG}* line was used for the lineage tracing experiments presented in **Figures 14 – 19** since it is a stronger reporter than *Rosa26^{EYFP/EYFP}*. The *Rosa26^{EYFP/EYFP}* reporter was used for the data shown in **Figures 20 and 26**.

2.1.3 Genotyping

DNA for genotyping was extracted from the yolk sacs of embryos and ear clips of pups and adult mice. Yolk sacs were incubated for 3 h at 55 °C in 25 µl DirectPCR®-Tail Lysis Reagent (Peqlab, 31-102-T), plus 1 µl of 10 mg/ml proteinase K (Roche, 3115852001). Ear clips were lysed overnight at 55 °C in 50 µl of lysis reagent and 1 µl of 10 mg/ml proteinase K. Afterwards, the samples were incubated at 85 °C for 45 min to inactivate the enzyme. The lysate was then added to the PCR reaction mix. Usually, 2 µl contains enough DNA for the reaction, but more can be added if the DNA concentration is low. Primer sequences and band sizes are given below in **Table 2**.

Table 2. Primer sequences for genotyping.

Primer name	Sequence (5' – 3')	Band size
Cre-A	ACCCTGATCCTGGCAATTTTCGGC	500 bp
Cre-B	GATGCAACGAGTGATGAGGTTCGC	
+Ctrl-A	CAAATGTTGCTTGCTGCTGGTG	200 bp
+Ctrl-B	GTCAGTCGAGTGACACAGTTT	
Sox2fl-A	TGGAATCAGGCTGCCGAGAATCC	wild type: 427 bp
Sox2fl-B	TCGTTCTGGCAACAAGTGCTAAAGC	heterozygote: 427 bp & 546 bp
Sox2fl-C	CTGCCATAGCCACTCGAGAAG	mutant: 546 bp

The PCR reaction mix and the PCR settings are detailed below in **Tables 3 and 4**.

Table 3. Standard PCR reaction for genotyping.

Reagent	Stock concentration	Final concentration	Volume per reaction
PCR buffer	10x	1x	5.0 μ l
dNTP mix	2 mM	0.2 mM	5.0 μ l
MgCl ₂	50 mM	1.5 mM	1.5 μ l
Forward primer	40 μ M	0.25 μ M	0.3 μ l
Reverse primer	40 μ M	0.25 μ M	0.3 μ l
Taq polymerase	5 U/ μ l	1 U	0.2 μ l
Template DNA			2.0 μ l
DNase-free water			fill up to final volume
total			50.0 μl

Table 4. PCR settings for genotyping.

Step	Condition		Number of cycles
Initial denaturation	94 °C	2 min	1
Denaturation	94 °C	30 s	
Annealing	63 °C	30 s	29
Extension	72 °C	45 s	
Final extension	72 °C	5 min	1
Final hold	4 °C	∞	1

2.1.4 Tamoxifen administration

CreERT2 recombinase was activated by intra-peritoneal injection of tamoxifen (Sigma-Aldrich, T-5648) as described previously (Danielian et al., 1998). Tamoxifen was first dissolved in 100% ethanol at a concentration of 100 mg/ml. The resulting solution was then further diluted into sterile corn oil (Acros Organics, 10616051-500G) to a final concentration of either 10 mg/ml (used when injecting 2 mg of tamoxifen per 40 g body weight) or 20 mg/ml (used when injecting 4 mg per 40 g body weight), so that a typical mouse of 20 g body weight would be injected with 100 μ l of the tamoxifen solution. The concentrations used for the individual experiments are indicated in the figures and the main text.

2.2 Embryo dissection and procedures

2.2.1 Embryo collection and fixation

Pregnant females were sacrificed by cervical dislocation. The embryos were dissected out of the uterus using a Zeiss SV11 stereomicroscope. The dissection medium contains Dulbecco's Modified Eagle Medium (DMEM) with high glucose and HEPES (Invitrogen, 42430), supplemented with 10% foetal bovine serum (FBS; Sigma-Aldrich, F0679). The dissection medium was warmed to 37 °C beforehand. For each embryo, the somite number and posterior neuropore length were recorded. The latter was measured using an eyepiece graticule. The yolk sacs were washed in cold phosphate-buffered saline (PBS) and stored at -20 °C or used directly for genotyping. Embryos for immunostaining were fixed in 4% paraformaldehyde (PFA) for 2 h at 4 °C and processed for cryosectioning. Embryos to be used for whole-mount *in situ* hybridisation (WISH) were fixed in 4% PFA overnight at 4 °C. They were then washed in PBS, dehydrated in ascending concentrations of methanol (25%, 50%, 75%, 100%), and stored in 100% methanol at -20 °C.

2.2.2 Whole-embryo culture

Embryos were dissected for whole-embryo culture at E8.5 as described previously (Copp et al., 2000; Gray and Ross, 2011). Briefly, the uterus was transferred to warm dissection medium. After trimming blood vessels and fat, the embryos were separated and released from the elastic uterine wall. The conceptus was then gently dissected out of the decidua. Trophoblast and Reichert's membrane were peeled away leaving yolk sac and ectoplacental cone intact. The embryos were then cultured in 0.3 ml rat serum per embryo. Prior to culture, the serum was sterilised by filtration (Medical Millex-HA Syringe Filter Unit, 0.45 µm, Merck Millipore, SLHAM33SS), gassed for 1 min with 5% O₂, 5% CO₂, and 90% N₂, and pre-equilibrated at 37 °C for 30 min. After adding the embryos, the serum was gassed again for 1 min using the same mixture and cultured in a rolling culture incubator at 37 °C for up to 48 h. The embryos were re-

gassed every 6 – 12 h. Once they reached E9.5, the gas mixture was changed to 20% O₂, 5% CO₂, and 75% N₂. After culture, embryo vitality was assessed based on heartbeat, morphology, and yolk sac circulation. Only healthy embryos, which showed a strong heartbeat, vigorous yolk sac circulation and a perfectly round yolk sac, were used for further analyses. Yolk sac and amnion were removed to count somites and measure posterior neuropore length. The yolk sacs were washed in cold PBS and kept for genotyping. Embryos were fixed and processed either for immunostaining or for WISH.

2.2.3 Rat serum preparation

Whole blood was collected from adult Wistar rats (Charles River Laboratories, Crl:WI, strain code 003) at UCL Biological Services Unit. After anaesthetising the animals with isoflurane, their abdomen was opened and the rats were exsanguinated by withdrawing blood from the abdominal aorta with a syringe. To precipitate all cellular components and induce coagulation, the blood was immediately centrifuged for 5 min at 4,000 rpm at room temperature (RT). The clot was allowed to form and then squeezed with flat forceps and the serum was pooled and centrifuged at 4,000 rpm for 5 min at 4 °C to precipitate any remaining blood cells. The serum was heat-inactivated for 30 min at 56 °C, aliquoted, and stored at -20 °C.

2.2.4 DiO-labelling

To track cells and assess their contribution to the closing neural tube, the lipophilic dye DiO (Vybrant® DiO Cell Labelling Solution, Molecular Probes, V22886) was injected into various locations in the posterior neuropore of E8.5 embryos at 1 – 7 ss. The dye solution contains green fluorescent crystals, which intercalate into the cell membrane and thereby mark cells from the region of interest (ROI) as well as their progeny. DiO was injected using glass microinjection needles attached to a mouth pipette. To ensure only few cells were labelled, a small amount of dye solution was taken up and the embryo was pierced with the glass needle at the ROI. Only then was the dye slowly

released, which could be observed through the translucent yolk sac, and the needle was quickly retracted. This resulted in the specific labelling of ~ 5 – 10 cells in the ROI. After culturing these embryos, they were imaged with a Leica DC500 camera attached to a Leica MZ FLIII stereoscope.

2.3 Expression analysis

2.3.1 Cryosectioning and immunostaining

To embed embryos for immunostaining, they were first fixed and then washed twice in PBS. Next, they were cryo-protected at 4 °C by incubating first in 15% sucrose dissolved in PBS, and afterwards in 30% sucrose until they sank to the bottom of the tube. The embryos were then soaked for 2 h at 4 °C in a solution consisting of equal parts of 30% sucrose in PBS and OCT embedding matrix (CellPath, KMA-0100-00A). After removing any residual sucrose-OCT solution, the embryos were placed into an embedding mould filled with OCT and oriented for sectioning. The samples were then snap-frozen in iso-pentane and stored at -80 °C. The blocks were cut with a Leica CM 1900 UV cryostat into 10 µm sections and stored at -20 °C. For immunostaining, sections were first thawed and then washed in PBS for 5 min at RT to remove any residual embedding medium. The sections were then blocked for 2 h at RT using 5% bovine serum albumin (BSA) plus 10% heat-inactivated sheep serum diluted in PBS. Primary antibody was pipetted onto the slides and they were left for 1 h at RT. The slides were subsequently washed in PBS and incubated with the secondary antibody for 1 h at RT. The primary and secondary antibodies were diluted in blocking solution at the concentration detailed in **Tables 5** and **6**. Nuclei were counter-stained for 3 min with 0.5 µg/ml DAPI (Invitrogen, D1306) in PBS and the sections were mounted in Mowiol® 4-88 mounting medium (Sigma-Aldrich, 81381; prepared with glycerol and 0.2 M Tris-HCl pH 6.8). The coverslips were sealed with nail polish and left to dry. The sections were imaged with a Leica DM LB microscope.

Table 5. Primary antibodies used for immunostaining.

Target	Host	Dilution	Supplier (catalogue #)
Cre	mouse (monoclonal)	1:1,000	Merck Millipore (MAB3120)
GFP	chicken (polyclonal)	1:500	Abcam (ab13970)
Nkx6.1	mouse (monoclonal)	1:5	Developmental Study Hybridoma Bank (F55A10)
Pax3	mouse (monoclonal)	1:200	R&D (MAB2457-SP)
Pax6	rabbit (polyclonal)	1:200	BioLegend (901301)
Sox1	rabbit (monoclonal)	1:200	Insight Biotechnology (GTX62974)
Sox2	rabbit (monoclonal)	1:500	Abcam (ab92494)
Sox2	mouse (monoclonal)	1:200	Abcam (ab79351)
Sox3	rabbit (polyclonal)	1:200	Abcam (ab183606)
Sox10	mouse (monoclonal)	1:500	Santa Cruz (sc-365692)
Tbx6	rabbit (polyclonal)	1:500	Abcam (ab38883)

Table 6. Secondary antibodies used for immunostaining.

Target	Host	Conjugate	Dilution	Supplier (catalogue #)
chicken IgY	goat	Alexa Fluor 488	1:500	Life Technologies (A-11039)
mouse IgG	goat	Alexa Fluor 488	1:500	Life Technologies (A-11029)
mouse IgG2a	goat	Alexa Fluor 488	1:500	Life Technologies (A-21131)
rabbit IgG	goat	Alexa Fluor 488	1:500	Life Technologies (A-11070)
mouse IgG	goat	Alexa Fluor 568	1:500	Life Technologies (A-11019)
mouse IgG1	goat	Alexa Fluor 568	1:500	Life Technologies (A-21124)
rabbit IgG	goat	Alexa Fluor 568	1:500	Life Technologies (A-11011)
mouse IgG	goat	Alexa Fluor 647	1:500	Life Technologies (A-21236)
rabbit IgG	goat	Alexa Fluor 647	1:500	Life Technologies (A-21244)

Sections from embryos labelled with DiO were fixed, embedded and sectioned as described above. However, after thawing and washing in PBS to remove the OCT, sections were directly counter-stained with DAPI and mounted.

2.3.2 Whole-mount *in situ* hybridisation

WISH was performed using digoxigenin (DIG)-labelled RNA probes. The solutions used to prepare the probes and those required for the WISH protocol up to the hybridisation step were treated with diethyl pyrocarbonate (DEPC) to inhibit RNAses. They were subsequently autoclaved to inactivate DEPC again.

2.3.2.1 Probe synthesis

To prepare the probes for WISH, DNA plasmids specified in **Table 7** were used as a template. Competent DH5 α cells (Thermo Fisher Scientific, 18265017) were transformed with the plasmid DNA according to standard protocols and plated on LB agar (Invitrogen, 22700-025) plates containing 50 μ g/ml ampicillin (Sigma-Aldrich, 10835269001). Colonies were picked from these plates to grow bacterial cultures. The plasmid DNA was then purified from these cultures using the QIAprep Spin Miniprep Kit (Qiagen, 27106) according to the manufacturer's protocol. The resulting DNA pellet was re-suspended in nuclease-free water (Sigma-Aldrich, W4502). Afterwards, the plasmid was linearised by adding 20 – 50 U of restriction enzyme in 1x restriction enzyme buffer to 3 – 5 μ g plasmid DNA. Nuclease-free water was added to reach a total volume of 50 μ l and the reaction mix was incubated for 2 h at 37 °C. The supplier and catalogue number of the restriction enzymes are given in **Table 7**. Following digestion, the linearised plasmid was purified using the QIAquick PCR Purification Kit (Qiagen, 28106) according to protocol. The purified, linearised plasmid was then transcribed into a DIG-labelled, single-stranded RNA probe using the DIG RNA Labelling Kit (Roche, 11175025910). Briefly, 1 μ g of the linearised DNA was added to 2 μ l of DIG RNA Labelling Mix, 2 μ l transcription buffer, 0.5 μ l RNase inhibitor, and 2 μ l RNA polymerase (specified in **Table 7**). Nuclease-free water was added to obtain a total volume of 20 μ l per reaction, which was then incubated for 2 h at 37 °C. The probes were purified using CHROMA SPIN-100 DEPC-H₂O Columns (Clontech, 636090) and 1 μ l of RNase inhibitor was added to each before storing them at -20 °C.

Table 7. Plasmid DNA templates used to generate RNA probes for WISH

Probe	Antibiotic resistance	Restriction enzyme (supplier, catalogue #)	Polymerase (supplier, catalogue #)	Reference
<i>Dll1</i>	ampicillin	HindIII (Promega, R6041)	T3 (Roche, 11031171001)	(Bettenhausen et al., 1995)
<i>Pax1</i>	ampicillin	XbaI (Promega, R6181)	T3 (Roche, 11031171001)	(Koseki et al., 1993)
<i>Sox2</i>	ampicillin	EcoRI (Promega, R6011)	T3 (Roche, 11031171001)	(Uwanogho et al., 1995)
<i>T</i>	ampicillin	EcoRI (Promega, R6011)	T7 (Roche, 10881775001)	(Herrmann, 1991)

2.3.2.2 Hybridisation of RNA probe

Embryos for WISH were re-hydrated by washing in descending concentrations of methanol (100%, 75%, 50%, 25%; diluted in PBS with 0.1% Tween-20 (PBT)), followed by two washes with PBT. They were bleached for 1 h on ice using 6% H₂O₂, and washed three times with PBT. To permeabilise the embryos, they were first incubated with proteinase K (5 µg/ml diluted in PBT) for 5 min at RT and afterwards treated with 2 mg/ml glycine dissolved in PBT for 5 min at RT to inactivate proteinase activity. After two more washes with PBT, the embryos were re-fixed in 0.2% glutaraldehyde in 4% PFA for 20 min at RT. They were washed again in PBT and transferred to a new tube containing 1 ml of pre-hybridisation buffer, which was warmed up beforehand. The pre-hybridisation buffer is made up of 50% formamide, 5x saline sodium citrate (SSC, pH 4.5), 50 µg/ml yeast RNA (Sigma-Aldrich, R6750), 1% sodium dodecyl sulphate (SDS), and 50 µg/ml heparin (Sigma-Aldrich, H4784) dissolved in DEPC-H₂O. After incubating for 2 h at 70 °C, approximately 1 µg of the DIG-labelled probe was added per 1 ml of pre-hybridisation buffer and the embryos were incubated overnight at 70 °C.

2.3.2.3 Post-hybridisation and colorimetric detection

On the following day, embryos were washed three times in pre-warmed solution 1 at 70 °C for 30 min each, and then twice in solution 2 at 65 °C for 30 min each. Solution 1 contains 50% formamide, 5x SSC, and 1% SDS in DEPC-H₂O. Solution 2 is made up of 50% formamide, 2x SSC, and 1% SDS in DEPC-H₂O. Afterwards, the embryos were washed 3 times for 5 min each at RT in a solution of Tris-buffered saline with Tween-20 (TBST; 50 mM of Tris-HCl pH 7.6 plus 150 mM of NaCl in distilled water, 1% Tween-20). They were blocked for 90 min at RT in 10% heat-inactivated sheep serum in TBST and afterwards incubated with TBST containing 1% sheep serum and the anti-DIG-AP antibody (Roche, 11093274910) diluted 1:2,000. The antibody recognises the DIG-labelled RNA probe and is conjugated with the enzyme alkaline phosphatase (AP), which catalyses the chromogenic reaction to detect the mRNA of interest. After 1 h at RT, the antibody solution was replaced with TBST and the embryos were washed overnight shaking at 4 °C to remove any unbound antibody. The following day, the embryos were washed three times in NTMT solution prepared from 100 mM NaCl, 100 mM Tris pH 9.5, 50 mM MgCl₂, and 1% Tween-20 in distilled water. To detect AP activity, the embryos were incubated at RT with 4.5 µl nitro blue tetrazolium chloride (NBT; Roche, 11383213001) and 3.5 µl 5-bromo-4-chloro-3-indolyl phosphate (BCIP; Roche, 10760994001) per 1 ml of NTMT solution and protected from light until developed sufficiently. AP catalyses the hydrolysis of BCIP and the intermediate product is then oxidised by NBT yielding an insoluble, purple precipitate. To stop the colorimetric reaction, the embryos were washed in PBT and fixed again in 4% PFA for 1 h at RT. Afterwards, they were imaged with a Leica MZ FLIII stereoscope equipped with a Leica DC500 camera and stored in PBT at 4 °C.

2.3.2.4 Vibratome sectioning and imaging

The embryos were embedded in a gelatin/albumin mix consisting of 0.45% gelatin, 27% albumin, and 18% sucrose in PBS. The blocks were cut with a Leica VT1000S vibratome into 40 µm sections. These were then collected on microscope slides and

mounted with a containing equal parts of glycerol and distilled water. The coverslips were sealed with nail polish and left to dry. Vibratome sections were imaged using a Zeiss Axioplan 2 microscope equipped with a Zeiss AxioCam HRc camera.

2.4 Laser-ablation

Region 1 of the CLE, where NMPs are located, was ablated using two-photon microscopy (Zeiss, ZEN 2.1 Imaging Software, black edition). Embryos at the 1 – 7 ss were dissected for culture and the ROI was marked by injecting DiO, to ensure it could easily be identified under the microscope. For ablation, the labelled embryo was transferred to a small petri dish filled with dissection medium, overlying a thin layer of 1% low-melting point agarose (Sigma, A9414). A small cavity was carved into the agarose which allowed for the embryo to be positioned with the node region facing upwards, balancing on the ectoplacental cone. The dish was then placed on the stage of a Zeiss LSM 880 equipped with a Spectra-Physics® Mai Tai® eHP DeepSee™ laser source and an incubation chamber, which was set at 37 °C. The embryo was positioned using an A-Plan 2.5x/0.06 objective (Zeiss). It is important to ensure the entire ROI is flat and perfectly in focus for the ablation to work. Using the DiO-labelled cells as a landmark, region 1 of the CLE was then outlined in the software and the ROI was ablated in a single z-plane using a W Plan-Apochromat 10x/0.50 objective (Zeiss) at 800 nm with 100% laser power and maximum scan speed (1.66 μm pixels, pixel dwell of 0.77 μs). The high scan speed ensured that any heat-induced damage in the adjacent tissues was kept to a minimum. Around 100 iterations were required for complete removal of the ROI (approximately 800 μs per iteration for a typical 60 μm diameter ROI). Successful ablation resulted in the formation of air bubbles and a visible hole in region 1 of the CLE. Thereby, all dye-labelled cells were removed, which was confirmed afterwards by scanning through the z-axis of the embryo while recording both DiO fluorescence and transmitted light. Finally, the embryos were cultured for up

to 24 h to assess how ablation affects neural tube formation and axis elongation. Control embryos were dissected and cultured in parallel, without undergoing ablation.

2.5 Image analysis

2.5.1 General

Images were cropped, adjusted, assembled, and analysed using Fiji image processing software (Schindelin et al., 2012). Only linear adjustments were made and they were applied equally across the whole image.

2.5.2 Cell position of DiO-labelled cells

To analyse how labelled cells contributed to the closing neural tube after injecting DiO into region 1 of the CLE, the embryos were fixed after 24 h culture and processed for cryosectioning. Transverse sections were counter-stained with DAPI and imaged with a Leica DM LB microscope. For each embryo, the relative position of the DiO-positive cells was calculated at three axial levels, namely (i) at the level of the CNH, (ii) further rostral where the neural folds were elevated, and (iii) at the closure point. The Segmented Line Tool in Fiji was used to measure the length of the neuroepithelium from the ventral midline and along its basal side up to the tip of the neural fold for positions (i) and (ii), and to the dorsal midline for position (iii). This template was then used to determine the distance between the ventral midline and the ventral and dorsal border of the labelled cell group. Finally, the position of the DiO-positive cells was expressed as a percentage relative to the dorso-ventral length of the neuroepithelium, to account for any variability in size along the body axis, which was then used for statistical analysis.

2.5.3 Cell fate decision and colonisation of the neural tube by *T*-expressing cells

To address whether different levels of *Sox2* bias cell fate decisions of *T*-expressing cells (i.e. formation of neural tube versus paraxial mesoderm), a $T^{CreERT2/+}; Sox2^{fl/+}$ driver was crossed with the $Rosa26^{EYFP/EYFP}$ reporter line. CreERT2 activity was induced at E8.5 (10 mg of tamoxifen per 40 g body weight) and the embryos were collected 24 h later and processed for immunostaining. Only those embryos with the genotypes $T^{CreERT2/+}; Sox2^{+/+}; Rosa26^{EYFP/+}$ and $T^{CreERT2/+}; Sox2^{fl/+}; Rosa26^{EYFP/+}$ were kept and analysed. Transverse sections were stained for GFP to enhance the signal of the reporter. In addition, these sections were stained for the pre-somitic mesoderm marker *Tbx6* and the neural tube marker *Sox2*. An in-house Fiji macro was used to count *Sox2*/GFP and *Tbx6*/GFP double-positive cells from twelve embryos per genotype and five sections per embryo, which were randomly selected from between the CNH level and the closure point. The macro counts nuclei from the DAPI channel using Difference of Gaussian and Find Maxima to determine the centre of each cell. Cells positive for GFP, *Sox2*, and *Tbx6* were thresholded and counted from masks which were then applied to the counts from the DAPI channel. The macro was written by Dr Dale Moulding and is available for download from <https://www.ucl.ac.uk/ich/core-scientific-facilities-centres/confocal-microscopy/publications>.

The same images were further analysed to compare how GFP-positive cells colonised the neural tube in $T^{CreERT2/+}; Sox2^{+/+}; Rosa26^{EYFP/+}$ and $T^{CreERT2/+}; Sox2^{fl/+}; Rosa26^{EYFP/+}$ embryos. First, the ROI was defined in the GFP channel by drawing along the neuroepithelium with the Segmented Line Tool. The line width was adjusted to the width of the neuroepithelium. The ROI was straightened and a plot profile was calculated from this, which indicates the mean intensity between the apical and basal border along the neuroepithelium. The background was subtracted and the mean values between the left and the right neural fold were calculated (five sections per embryo, twelve embryos per genotype). This was plotted as the mean intensity against the distance from the ventral midline.

2.6 Statistical analysis

Statistical analyses were performed using IBM SPSS Statistics version 23. The p -values are given in the figures and details of the tests performed are specified in the figure legends and the main text. Values below 0.05 were considered statistically significant.

2.7 Other software

All graphs were plotted using GraphPad Prism software version 6. Adobe Illustrator CS4 was used to assemble the figures and draw the schematics.

CHAPTER 3: RESULTS

3.1. Fate mapping the CLE and node region in E8.5 mouse embryos

3.1.1. Introduction and objectives

NMPs are characterised by the following distinctive features: (i) they reside in the tail end of the post-gastrulation embryo and are retained there over a long period of time, and (ii) their progeny populates both the extending neural tube and paraxial mesoderm over long stretches along the rostro-caudal axis (Cambray and Wilson, 2002; Cambray and Wilson, 2007; Tzouanacou et al., 2009). Cambray and Wilson performed grafting experiments which suggest that putative NMPs are located at the border between the node and the primitive streak remnant in E8.5 mouse embryos (Cambray and Wilson, 2007), and, after internalisation of the node around E9.0, in its derivative, the CNH (Cambray and Wilson, 2002). Even though the literature provides extensive evidence that cells located caudal to the node end up in the somites and the neural tube, it remains unclear if these cells randomly integrate into the neural tube or if they populate specific domains along the rostro-caudal and dorso-ventral axes.

In the following chapter, I combined DiO-labelling of cells with mouse whole-embryo culture to further specify where NMPs are located in the E8.5 mouse embryo. For this purpose, I first refined the fate map provided by Cambray and Wilson (Cambray and Wilson, 2002; Cambray and Wilson, 2007). I then labelled cells in the NMP region and traced them into the forming neural tube to address whether they give rise to the whole neural tube or only to specific domains. Finally, I complemented the fate map by assessing how cells from the node and directly rostral to it contribute to the axial tissues.

3.1.2. Results: The cellular origins of the neural tube and paraxial mesoderm

3.1.2.1 The CLE gives rise to the dorsal neural tube and somites, but only region 1 harbours NMPs

To trace cells in the developing embryo, I labelled them by injecting a small amount of DiO into the region of interest. DiO is a lipophilic dye, which consists of green fluorescent crystals in solution. The crystals intercalate into the plasma membrane and thereby mark cells and their progeny, without interfering with normal cellular processes.

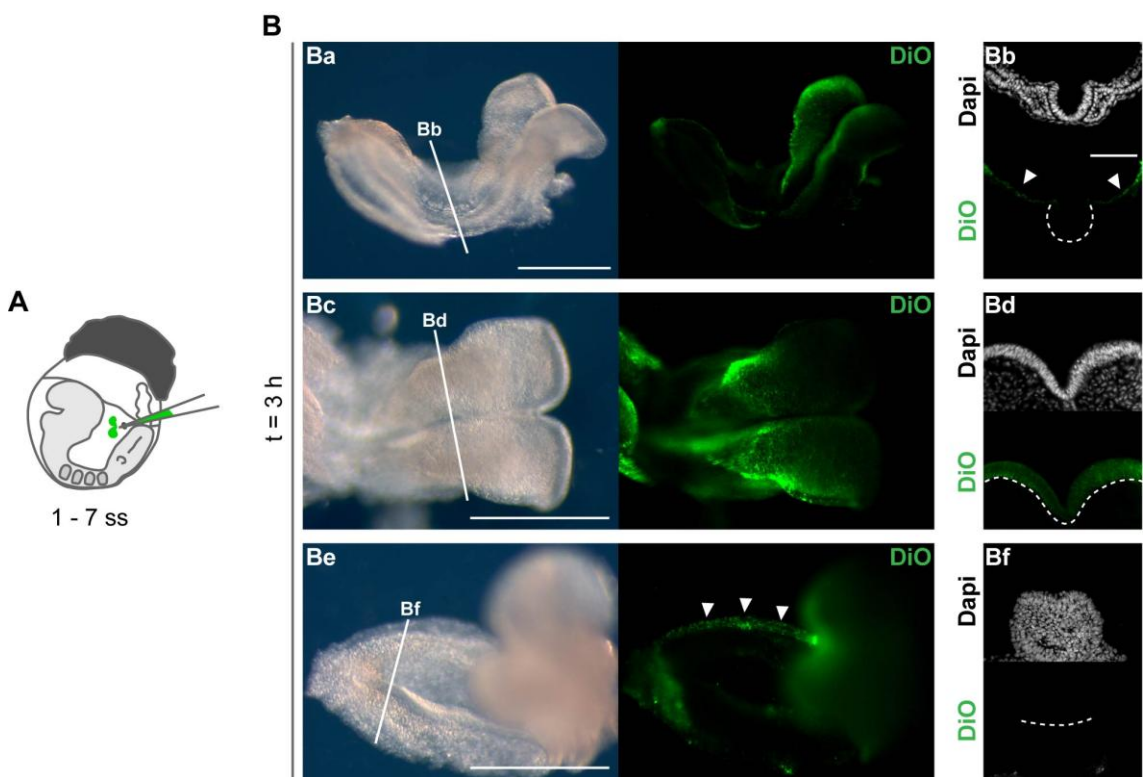


Figure 5. Non-specific binding of DiO to the headfolds and extraembryonic tissues.

(A) To assess non-specific binding of the vital dye DiO, a small amount was injected into the amniotic cavity of E8.5 WT embryos. **(B)** Following 3 h whole-embryo culture, $n = 5/5$ embryos showed non-specific labelling of the headfolds (Bc – Bd), the surface ectoderm (white arrowheads in Bb), and the extraembryonic tissues (white arrowheads in Be). The neuroepithelium caudal to the head region remained DiO-negative in $n = 5/5$ embryos (Ba – Bb, Be – Bf). White dashed lines outline the neuroepithelium. Scale bars, 500 μm in Ba, Bc, Be; 100 μm in Bb. Adapted from (Mugele et al., 2018).

First of all, I evaluated whether dye injection gives any non-specific signal. This was important as most injections release varying amounts of DiO into the amniotic cavity. For this purpose, a small amount of DiO was injected into the amniotic cavity of E8.5

WT embryos (**Figure 5A**). After culturing these embryos for 3 h, dye was trapped in the surface ectoderm as well as in the extraembryonic tissues of $n = 5/5$ embryos (white arrowheads in **Figure 5Bb** and **Be**). The dye also became stuck on the headfolds (**Figure 5Bc – d**; $n = 5/5$ embryos), however, the caudal end of all embryos remained negative (**Figure 5Be – f**; $n = 5/5$ embryos). This shows that if I inject DiO into the posterior neuropore and analyse the caudal part of the embryo, the evolving dye pattern is unlikely to be an artefact due to non-specific binding, but results specifically from labelling cells in this region.

When Cambray and Wilson performed their grafting experiments, they observed NMP-like patterns after transplanting either a piece of tissue spanning regions 1 – 3 of the CLE, or after grafting the NSB. First, I studied the CLE by labelling a small number of cells with DiO in either region 1, 2, 3, 4, or 5 in E8.5 WT embryos. The caudal border of the node served as a landmark to allow for reproducible injection. Since the border is only visible in embryos with 1 – 7 somite pairs, I restricted my labelling experiments to this developmental stage. After 24 h in culture, I analysed the resulting dye pattern in transverse sections (**Figure 6**). The CNH was populated by DiO-positive cells after labelling regions 1 and 2 (white arrowheads in **Figure 6Aa** and **Ba**; pink circles in **Figure 6Ab** and **Bb**). After injecting DiO into regions 3 – 5, labelled cells were present in the tip of the tail bud (**Figure 6Ca, Da, Ea**), which I did not observe after labelling regions 1 or 2. Strikingly, the CNH was DiO-negative in these embryos (pink circle in **Figure 6Cb, Db, Eb**), although labelled cells were accumulated in the tail bud. Independent of the location where dye was injected, DiO-positive cells consistently gave rise to both neural tube and somites, except for region 5 which gave rise to mesoderm only. In line with previous reports, labelled cells contributed less to the neural tube and more towards mesoderm as the dye was injected in more caudal regions (Wymeersch et al., 2016). Surprisingly, cells labelled in regions 1 – 4 gave rise to the dorsal neural tube only (white arrowheads in **Figure 6Ac – d, Bc – d, Cc – d, Dc**), and never to the ventral or ventro-lateral domains.

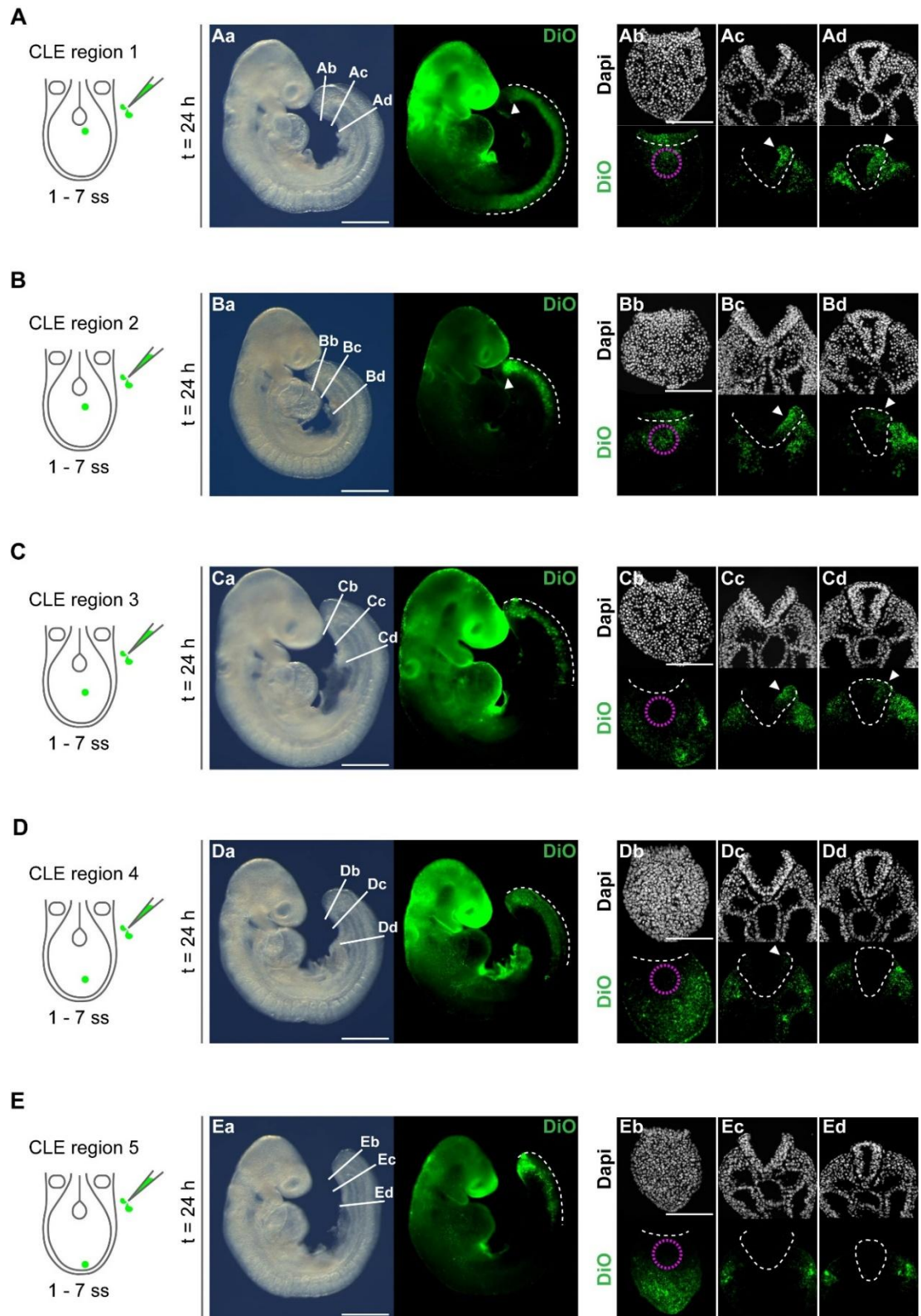


Figure 6. NMPs are located in CLE region 1 specifically contribute to the dorsal neural tube.

(A – E) DiO was injected into regions 1 – 5 of the CLE in E8.5 WT embryos. After 24 h in culture, the contribution of DiO-positive cells to axial tissues was assessed in transverse sections. Please refer to Table 8 for sample sizes and a detailed description of the respective dye patterns. White dashed lines in Aa, Ba, Ca, Da, Ea show the axial levels colonised by DiO-labelled cells. White arrowheads in Aa and Bb point to DiO-positive cells in the CNH. Pink circles in Ab, Bb, Cb, Db, Eb indicate the CNH. White dashed lines in Ab – d, Bb – d, Cb – d, Db – d, Eb – d outline the neuroepithelium. White arrowheads in Ac – d, Bc – d, Cc – d, Dc point to DiO-labelled cells in the dorsal neuroepithelium. Scale bars, 500 μ m in Aa, Ba, Ca, Da, Ea; 100 μ m in Ab, Bb, Cb, Db, Eb. Adapted from (Mugele et al., 2018).

Even when I analysed sections taken from more rostral levels of those embryos which had DiO injected into region 1, I always found labelled cells exclusively in the dorsal domain. Moreover, only cells labelled in region 1 of the CLE showed long-term contribution to the axial tissues (white dashed line in **Figure 6Aa**), but none of the other regions.

Please see **Table 8** for sample sizes and a detailed description of the observed dye patterns. Also note that all of these embryos have green fluorescent heads, which likely stems from the non-specific binding of DiO to the headfolds, as discussed earlier. In summary, only cells located in region 1 of the CLE satisfy the criteria of NMPs, as these cells colonise the CNH and contribute to both neural tube and mesoderm along a considerable length of body axis.

3.1.2.2 The ventral-to-dorsal translocation of cells from region 1 of the CLE is specific to the open posterior neuropore region

To further characterise the nature of cells located in region 1, I performed a time course experiment. First, DiO was injected into region 1 of E8.5 WT embryos followed by culture either for 3 h, 6 h, or 9 h (**Figure 7**; n = 4 embryos per time point). The aim was to determine how long it takes labelled cells to translocate from region 1 to the dorsal neural tube. Since closure 1 of the neural tube occurs around 6 – 7 ss, I only used embryos for this experiment which had 4 – 7 somite pairs. This ensured that the estimated time reflects the true duration and is not delayed by closure 1. Following DiO injection into region 1 of the CLE, labelled cells rapidly dispersed through the neuroepithelium away from the ventral midline and also into the underlying layer (**Figure 7Ba – d**). After 9 h in culture, DiO-labelled cells had entered the dorsal domain of the neural tube, which also coincided with the axial level of the closure point in n = 4/4 embryos (white arrowhead in **Figure 7Bj**).

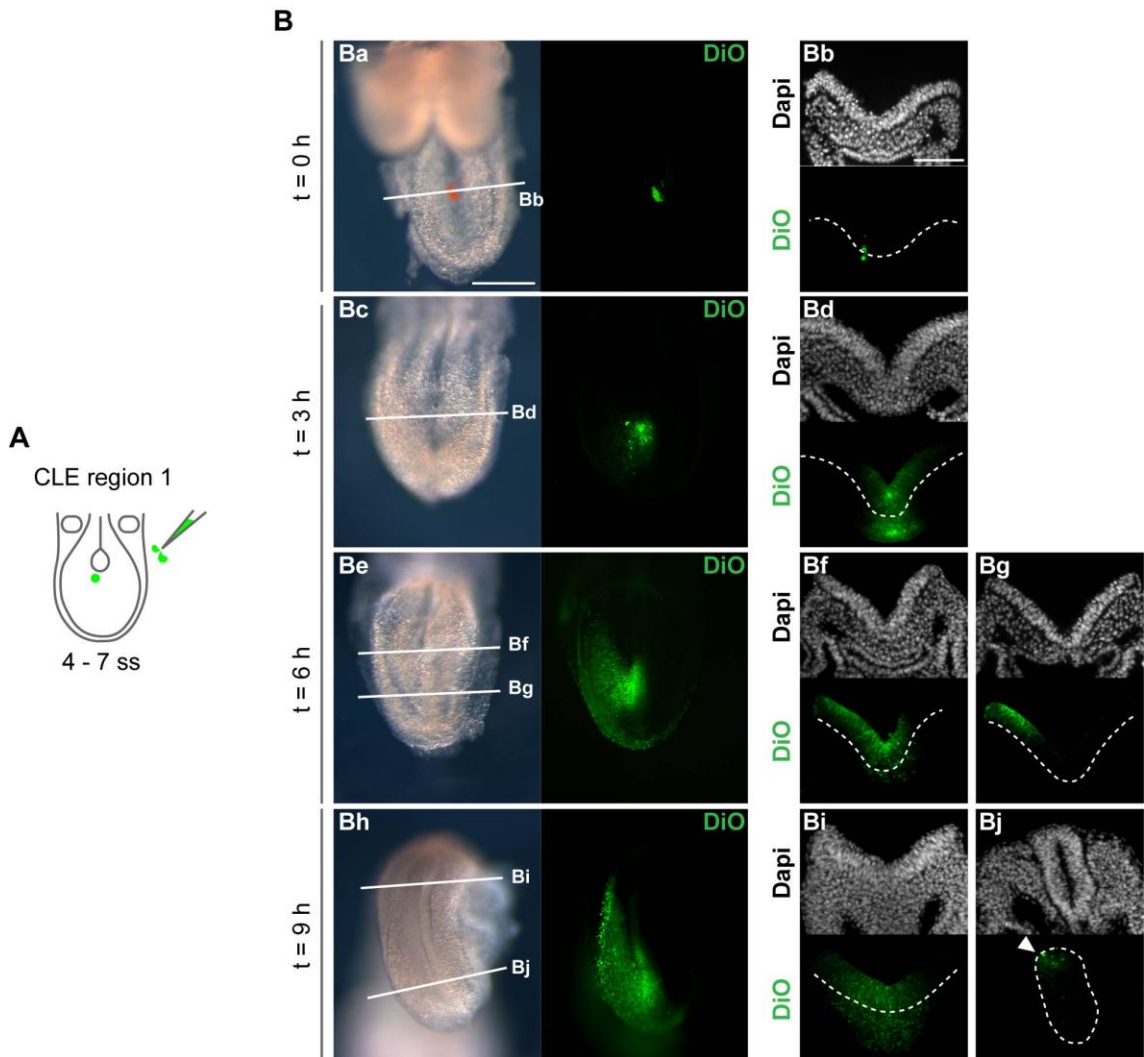


Figure 7. Time course tracing DiO-labelled cells from region 1 of the CLE. (A) DiO was injected into region 1 of the CLE in E8.5 WT embryos (4 – 7 ss). (B) Embryos were cultured either for 0 h, 3 h, 6 h, or 9 h (n = 4 embryos per time point) and the resulting dye pattern was analysed in transverse sections. White dashed lines in Bb, Bd, Bf, Bg, Bi and Bj outline the neuroepithelium. After 9 h in culture, DiO-labelled cells had reached the dorsal neural tube (white arrowhead in Bj; n = 4/4 embryos). Scale bars, 500 μ m in Ba; 100 μ m in Bb. Adapted from (Mugele et al., 2018).

Secondly, I quantified how the labelled cells translocated into the dorsal neural tube. For this purpose, I injected DiO into region 1 of the CLE in E8.5 WT embryos. After 24 h whole-embryo culture, I analysed transverse sections through the posterior neuropore which were taken (i) from the axial level of the CNH, (ii) further rostral where the neural folds were elevated, and (iii) from the closure point (**Figure 8Aa**). I measured the distance between the ventral midline and the dorsal/ventral border of the labelled cell group in these sections and plotted them (**Figure 8Ab**):

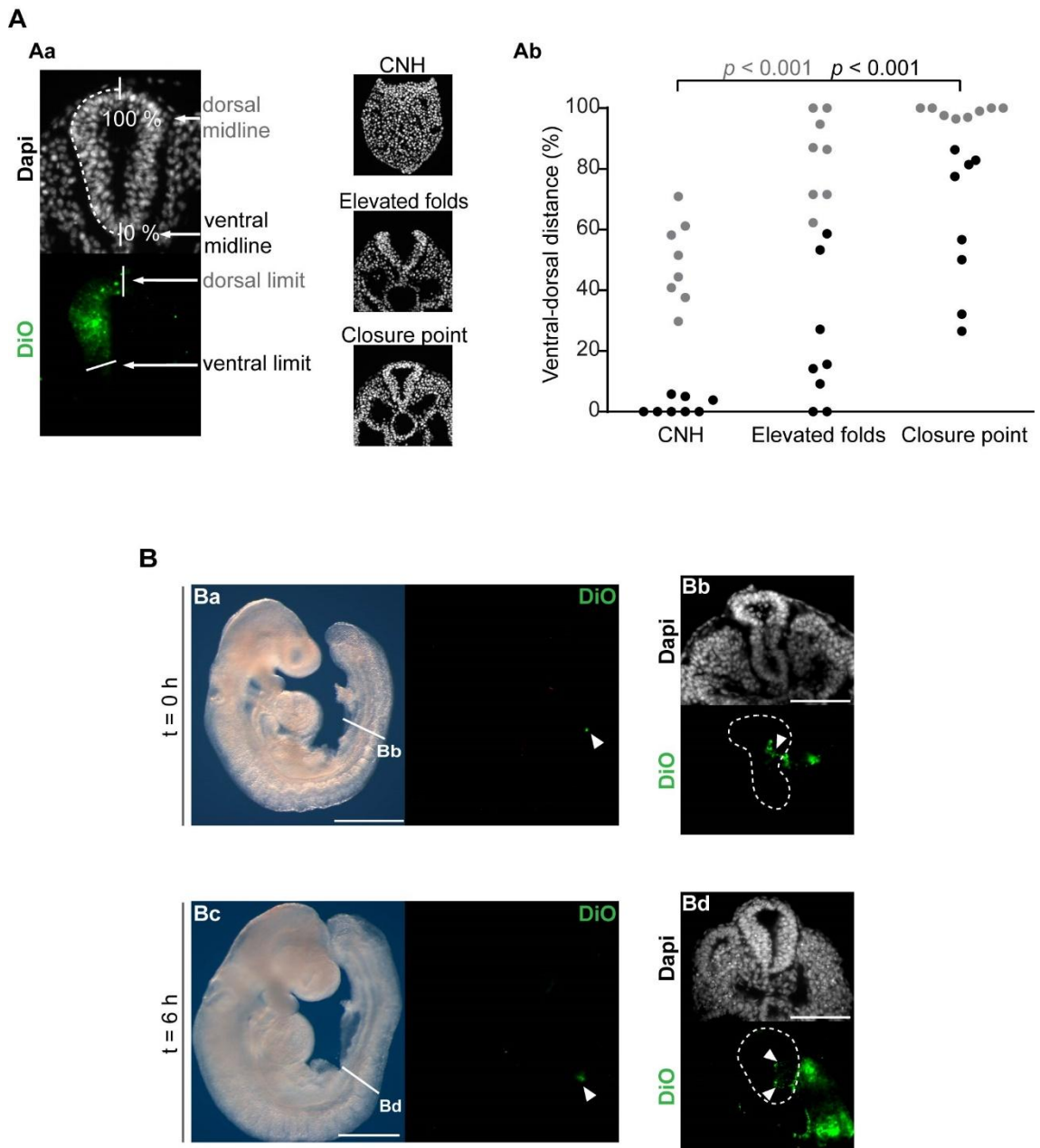


Figure 8. Ventral-to-dorsal translocation of cells from CLE region 1 is specific to the posterior neuropore.

(A) Quantification of cell translocation in E9.5 WT embryos, which had region 1 of the CLE labelled with DiO at E8.5 followed by 24 h whole-embryo culture. Transverse sections from the following regions were analysed: the CNH, the posterior neuropore where the neural folds were elevated, and the closure point of the neural tube. Ventral and dorsal borders of the labelled cell group in the neuroepithelium were measured as shown in Aa. Graph in Ab shows the individual data points for $n = 8$ embryos (grey, dorsal border; black, ventral border); p -values shown for paired, two-tailed Student's t -test. **(B)** The lateral, closed neural tube was labelled by injecting DiO in E9.5 WT embryos (white arrowheads in Ba – Bb). After 6 h in culture, the dye had spread in the lateral domain (white arrowheads in Bc – Bd), yet it did not reach the dorsal neural tube in $n = 5/5$ embryos. White dashed lines in Bb and Bd outline the neural tube. Scale bars, 500 μm in Ba, Bc; 100 μm in Bb, Bd. Adapted from (Mugele et al., 2018).

In $n = 8/8$ embryos, DiO-positive cells translocated in a ventral-to-dorsal direction, away from the ventral midline, and reached the dorsal neural tube at the level of the

closure point. The location of the ventral and dorsal borders in sections from the CNH compared with the closure point were statistically significant (paired Student's *t*-test, two-tailed).

To address whether the observed ventral-to-dorsal translocation is specific to cells originating in the posterior neuropore, I injected DiO into the lateral aspect of the closed neural tube of E9.5 mouse embryos (**Figure 8Ba – b**). Following 6 h in culture, the dye-labelled cells had spread both in the neural tube (white arrowheads in **Figure 8Bc – d**) and the paraxial mesoderm (also directly labelled by this method). However, DiO-positive cells remained in the ventral domain in *n* = 5/5 embryos and did not reach the dorsal neural tube.

3.1.2.3 The ventral and ventro-lateral neural tube derive from cells located in the node region

Cells traced from the CLE into the forming neural tube exclusively colonised the dorsal domain. Hence, the ventral neural tube is likely derived from a different location. Traditionally, floor plate and notochord are believed to arise from the node (Beddington, 1994; Sulik et al., 1994; Wilson and Beddington, 1996). Therefore, I labelled a small number of cells in E8.5 WT embryos by injecting DiO either into the NSB, which contains the rostral aspect of the node (**Figure 9A**), into the centre of the node (**Figure 9B**), or into the region directly rostral to the node (**Figure 9C**). After 24 h in culture, I analysed the contribution of DiO-labelled cells to the axial tissues in transverse sections.

According to Cambray and Wilson, the NSB is the second location in the E8.5 mouse embryo which harbours NMPs, in addition to the rostral CLE (Cambray and Wilson, 2007). The phenotype observed after labelling this region further supports their claim: DiO-positive cells traced from the NSB colonised the CNH (white arrowhead in **Figure 9Aa** and pink circle in **Ab**). Moreover, labelled cells contributed to both neural tube and somites over a long axial distance (white dashed line in **Figure 9Aa**). However, in contrast to region 1, DiO-positive cells ended up in the ventral and ventro-

lateral neural tube only (**Figure 9Ac – d**) and they also colonised in the notochord (white arrowheads in **Figure 9Ac – d**).

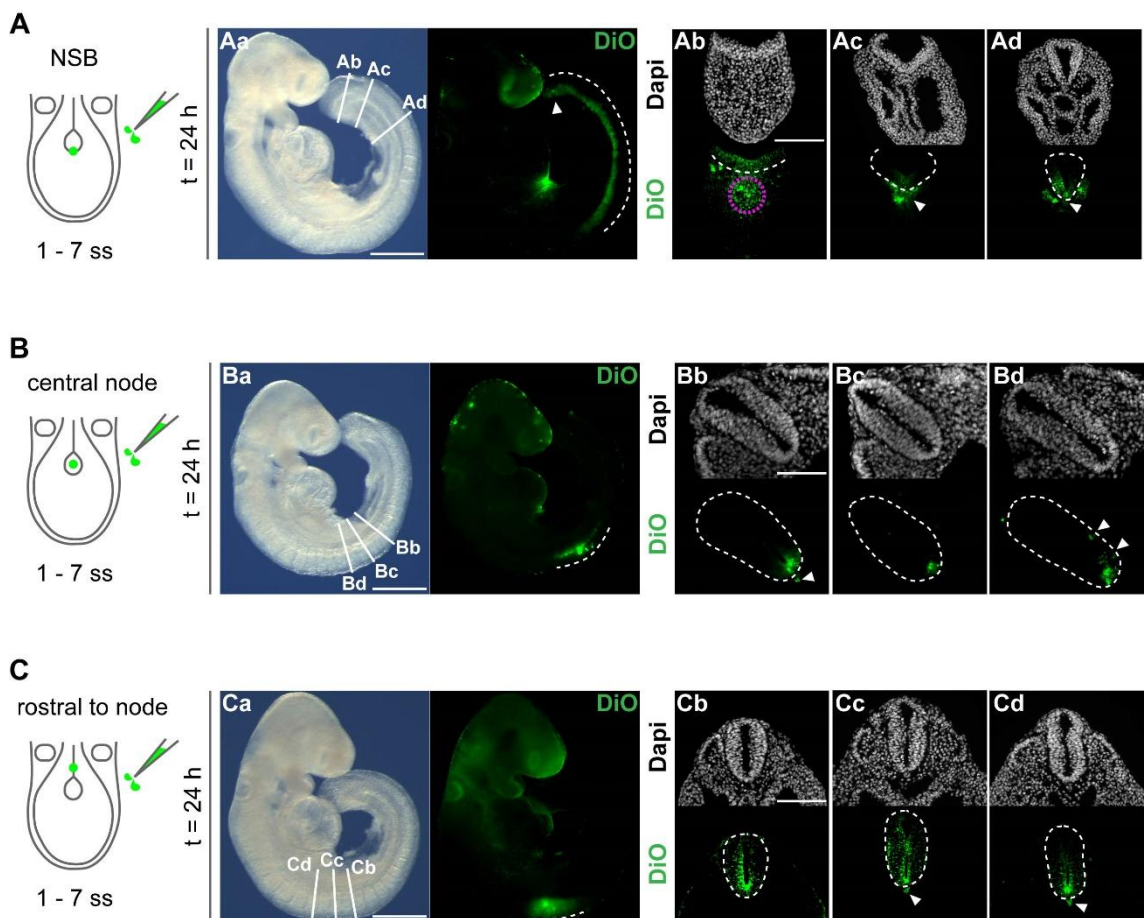


Figure 9. Ventral and ventro-lateral neural tube arise from cells residing in and around the node.

DiO was injected into different locations in the node region in E8.5 WT embryos. Following 24 h whole-embryo culture, the contribution of DiO-positive cells to the extending body axis was analysed in transverse sections. **(A)** Cells labelled in the NSB colonised the CNH (white arrowhead in Aa and pink circle in Ab), the floor plate, the notochord (white arrowheads in Ac – Ad), and the paraxial mesoderm. **(B)** Cells labelled in the centre of the node gave rise to the floor plate, the notochord (white arrowheads in Bb), and the ventro-lateral neural tube (white arrowheads in Bd). **(C)** Labelling rostral to the node revealed cells which contribute to the entire neural tube along its dorso-ventral axis (Cb – Cd), as well as the notochord (white arrowheads in Cc – Cd). Please refer to Table 8 for sample sizes and detailed descriptions of the colonisation patterns. White dashed lines in Aa, Ba, Ca indicate the axial levels colonised by DiO-labelled cells. White arrowhead in Aa points at DiO-positive cells in the CNH. White dashed lines in Ab – d, Bb – d, Cb – d define the neuroepithelium. Scale bars, 500 μ m in Aa, Ba, Ca; 100 μ m in Ab, Bb, Cb. Adapted from (Mugele et al., 2018).

After injecting DiO into the centre of the node, DiO-positive cells contributed to the floor plate (**Figure 9Bb – d**) and the notochord (white arrowhead in **Figure 9Bb**), which is in line with the literature. However, I consistently found labelled cells in the lateral neural

tube as well (white arrowheads in **Figure 9Bd**), which has not been reported so far. Also, DiO-positive cells colonised the notochord and neural tube only over a short stretch along the body axis (white dashed line in **Figure 9Ba**).

Thirdly, I labelled few cells directly rostral to the node. Following 24 h in culture, DiO-labelled cells were present in the neural tube along its entire dorso-ventral axis (**Figure 9Cb – d**). In addition, labelled cells colonised the notochord (white arrowheads in **Figure 9Cc – d**), yet, only over a short axial distance (white dashed lines in **Figure 9Ca**). Please refer to **Table 8** for sample sizes and detailed descriptions of the observed patterns.

Table 8. Colonisation patterns observed from fate mapping experiments.

The data in this table summarise the experiments shown in Figures 6 and 9. Only cells from the NSB and region 1 colonised long stretches along the body axis. Cells from all other locations showed short-term contribution only. *NSB*, node-streak border; *pm*, paraxial mesoderm; *nc*, notochord; *fp*, floor plate; *lnt*, lateral neural tube; *dnt*, dorsal neural tube; *CNH*, chordo-neural hinge; *tbt*, tail bud tip. Adapted from (Mugele et al., 2018).

DiO injection site	n	Contribution to axial tissues					DiO retained in		Comments
		pm	nc	fp	lnt	dnt	CNH	tbt	
Rostral to node	8	0/8	8/8	8/8	8/8	6/8	0/8	0/8	
Central node	8	0/8	8/8	8/8	7/8	0/8	0/8	0/8	
NSB	9	9/9	9/9	9/9	9/9	0/9	9/9	0/9	
CLE region 1	8	8/8	0/8	0/8	8/8	8/8	8/8	0/8	
CLE region 2	8	8/8	0/8	0/8	8/8	8/8	7/8	1/8	region 3 phenotype in 1/8
CLE region 3	7	7/7	0/7	0/7	7/7	7/7	1/7	6/7	region 2 phenotype in 1/7
CLE region 4	7	7/7	0/7	0/7	6/7	6/7	0/7	7/7	region 5 phenotype in 1/7
CLE region 5	8	8/8	0/8	0/8	0/8	0/8	0/8	8/8	

In summary, paraxial mesoderm is derived from cells located between the NSB and region 5 of the CLE. The notochord and floor plate were labelled after injecting DiO into the NSB, the centre of the node, or directly rostral to it. I found DiO-labelled cells in the lateral neural tube after injecting dye into any of the described locations, except for region 5, which gave rise to mesoderm only. The dorsal neural tube is derived from

cells located in regions 1 – 4 of the CLE, as well as directly rostral to the node. The results of these labelling experiments are summarised in **Figure 10**.

The CNH was colonised by labelled cells after injecting DiO either into the NSB, region 1, or region 2. However, tracing cells only from the NSB and region 1 resulted in contribution to tissues along considerable lengths of the body axis. Following dye injection into regions 3 – 5 of the CLE, labelled cells were not retained in the CNH, yet, they were accumulated in the tip of the tail bud.

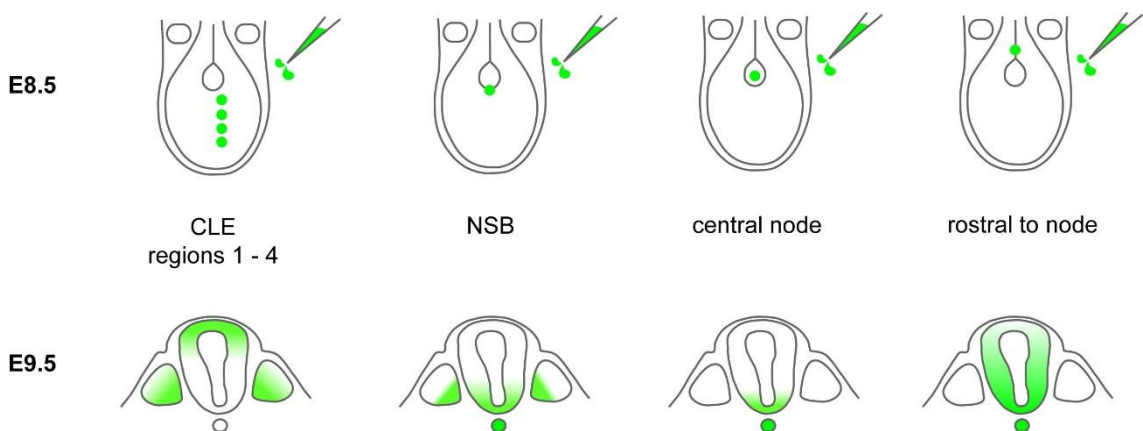


Figure 10. Cellular origins of the neural tube and paraxial mesoderm.

Summary of DiO-labelling experiments corresponding to Figures 6 and 9. Note that only cells labelled in region 1 of the CLE and in the NSB provide long-term contribution to the extending body axis. *CLE*, caudo-lateral epiblast; *NSB*, node-streak border. Adapted from (Mugele et al., 2018).

3.1.3. Discussion: The cellular origins of the neural tube and paraxial mesoderm

3.1.3.1 Reliability and specificity of DiO-labelling as a method for fate mapping

To trace cells from various locations in the post-gastrulation embryo, I labelled them by injecting the vital dye DiO into the region of interest. Regarding the reliability of this method, I only used embryos at 1 – 7 ss, because at this stage the caudal border of the node is visible and the CLE can therefore be easily identified ensuring reproducible injections. However, the definition of the CLE is imprecise as it refers to epiblast adjacent to the primitive streak (Cambray and Wilson, 2007; Wilson et al., 2009), and yet, does not specify how far it reaches laterally. Therefore, I injected DiO as close to

the midline as possible when labelling the CLE, to ensure consistency between the experiments.

The specificity of this method is limited since cells were labelled based on their location in the embryo and not based on their cellular identity. For example, by injecting DiO into region 1 of the CLE I likely labelled some NMPs, because the resulting phenotype after culture fits the proposed characteristics of these cells. Nevertheless, I cannot rule out that I might have labelled some cells other than NMPs, which potentially also contributed to the colonisation pattern. Yet, my results confirm the findings reported by Cambray and Wilson (Cambray and Wilson, 2007), showing that the tail bud of the E8.5 mouse embryo contains two cell populations which are retained in the CNH and show long-term contribution to the axial tissues. Since my data are consistent with the literature, this provides further confidence of the accuracy and reliability of the DiO-labelling technique.

The specificity of this technique is further limited by non-specific labelling of adjacent cells. Initially, I marked only a very small number of cells by injecting DiO into the region of interest. The dye crystals intercalate into cell membranes and thereby allow tracking of these cells and their progeny. Nevertheless, it is possible that neighbouring, unlabelled cells might pick up some DiO crystals and further pass them on to other cells which were not specifically labelled. This would eventually dilute the colonisation pattern. Having said that, I discovered that cells labelled in the CLE specifically colonised the dorsal and dorso-lateral domain of the neural tube, but not the ventral part. Even though this observation would likely be more pronounced under ideal conditions, where only those cells were marked which I labelled initially, it is still informative. In addition, labelling cells in the NSB and region 1 of the CLE resulted in very different colonisation patterns, although both regions are located in close vicinity. This demonstrates that the DiO technique gave sufficient resolution.

3.1.3.2 Inconsistencies in the literature regarding the NMP location

The fate mapping experiments in this chapter have revealed that both neural tube and paraxial mesoderm have multiple cellular origins (**Figure 10**). It is quite remarkable that cells which are located in such close proximity to each other give rise to very different progeny distributions. This applies in particular to the NSB and region 1 of the CLE. Even though these areas are adjacent, cells in the NSB end up in the ventral neural tube only, whereas cells from region 1 colonise the dorsal and dorso-lateral neural tube, but not the ventral domain. When Cambray and Wilson homotopically transplanted the NSB between embryos, they found that cells from the graft consistently colonised the neural tube and paraxial mesoderm, and also the notochord (Cambray and Wilson, 2007). In the same paper they reported that grafted cells from the rostral CLE give rise to the dorsal neural tube and paraxial mesoderm, but sometimes they also colonised the notochord. This suggests that some of their grafts contained cells from both the NSB and region 1.

It is striking that cells located in the NSB and in region 1 of the CLE both satisfy the criteria of NMPs, i.e. retention in the CNH and extensive contribution to neural tube and somites along the body axis. However, they displayed very different colonisation patterns when I traced them. But which of these are the “real” NMPs? The literature is very inconsistent regarding the precise locations of NMPs and many terms, such as NSB and CLE, or NMPs and axial stem cells, are used interchangeably. To shed light on this issue, I revisited the literature and found the following: The concept of a shared progenitor between the neural and mesodermal lineages was first suggested by Swiss anatomist Albert von Kölliker in 1884 (Kölliker, 1884). Nevertheless, this idea was abandoned for many years until Cambray and Wilson published their grafting experiments in 2002 and 2007 (Cambray and Wilson, 2002; Cambray and Wilson, 2007). As discussed above, they discovered that grafts of the NSB gave rise to the paraxial mesoderm, the ventral neural tube, and the notochord. In their papers and also in a later review (Wilson et al., 2009), they referred to these as “axial stem cells” or “axial progenitor cells”. They also reported that the rostral CLE contains cells which

colonise the neural tube and paraxial mesoderm only. Their work aroused great interest and many other research groups became interested in these dual-fated progenitors. The term “neuro-mesodermal progenitors” was first mentioned by Tzouanacou and colleagues in 2009 (Tzouanacou et al., 2009). In their study they used retrospective clonal analysis to address whether neural tube and mesoderm share a common progenitor. However, the authors only counted contribution of traced cells to either neurectoderm or mesoderm, without specifying whether the latter included paraxial mesoderm and notochord, or paraxial mesoderm only. From then onwards, the term neuro-mesodermal progenitors (or NMPs) was commonly used to refer to cells of a particular embryonic region that give rise to paraxial mesoderm and the neural tube (Cunningham et al., 2016; Garriock et al., 2015; Gouti et al., 2014; Henrique et al., 2015; Tsakiridis et al., 2014; Turner et al., 2014; Wymeersch et al., 2016), although some authors refer to them as axial stem cells (Kondoh and Takemoto, 2012; Takemoto et al., 2011; Yoshida et al., 2014), the term Cambray and Wilson used for cells in the NSB which give rise to neural tube, paraxial mesoderm, and notochord. Some others use the terms NMPs and axial progenitor/stem cells interchangeably (Amin et al., 2016; Jurberg et al., 2013; Wymeersch et al., 2016). In line with the majority of the literature, which defines NMPs as those cells which produce neural tube and paraxial mesoderm - but not notochord - I will refer from now on to region 1 of the CLE as the NMP location.

In addition, the area which authors refer to as the NMP location is equally inconsistent in the literature. As discussed before, the NMPs are located in the rostral CLE and give rise to the neural tube and somites. On the other hand, axial stem/progenitor cells are located in the NSB and they form the ventral neural tube, paraxial mesoderm, and notochord. Both regions are internalised together with the node and form the CNH. Cambray and Wilson observed NMP-like colonisation patterns after grafting a piece of tissue comprising regions 1 – 3 of the CLE, however, many authors refer to the entire CLE as the source of NMPs, and not just the rostral part

(Henrique et al., 2015; Koch et al., 2017; Kondoh and Takemoto, 2012; Rodrigo Albers et al., 2016; Takemoto et al., 2011; Yoshida et al., 2014).

Similarly, the location of the CNH, where NMPs and axial stem/progenitor cells are retained after E9.0, is highly variable between different papers. After labelling region 1 of the CLE, I found DiO-positive cells specifically retained in a small region directly caudal to the forming notochord and hindgut, underneath the forming neuroepithelium. When collecting transverse sections of an E9.5 embryo from rostral to caudal, this region is present in the first three sections, after the lumen of the hindgut has become no longer visible. At this axial level, the overlying neuroepithelium is completely flat (for example, see **Figure 6Ab**). After labelling cells in the NSB, I found DiO-positive cells in the exact same location, however, they also extended further rostrally into the area of the forming notochord as depicted in **Figure 11**. In Figure 1 of their 2007 paper, Cambray and Wilson depicted a transverse section through the region which they defined as the CNH, where they found graft-derived cells accumulated in E9.5 embryos following transplantation of the NSB: the hindgut lumen and notochord are visible and the neural folds are elevated (Cambray and Wilson, 2007). However, this is not the same region where I found DiO-labelled cells after injecting region 1 of the CLE. The sections they showed were taken from a region rostral to the CNH where labelled cells are consistently retained after labelling the NSB, but not after labelling region 1 of the CLE. After revisiting the literature, I found several papers (Gouti et al., 2017; Rodrigo Albers et al., 2016; Wilson et al., 2009; Wymeersch et al., 2016) in which the authors, similar to Cambray and Wilson, referred to an area as the CNH, which was actually located rostral to the CNH, as defined in my work, i.e. colonised following DiO injections into NSB or CLE region 1.

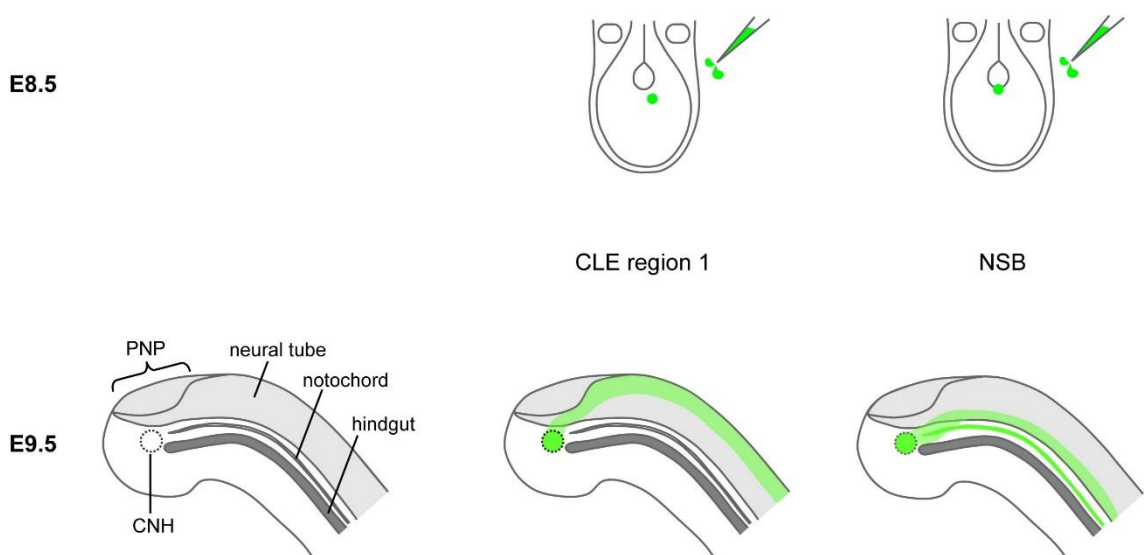


Figure 11. Contribution of cells in CLE region 1 and NSB to CNH, notochord, and neural tube.

After injecting DiO into region 1 of the CLE, the caudal end of the extending notochord in E9.5 embryos remained DiO-negative, whereas CNH and dorsal neural tube were labelled (green, middle). In contrast, cells labelled in the NSB contributed to the CNH, notochord, and ventro-lateral neural tube (green, right). The E9.5 diagrams are “reconstructions” from analysis of serial transverse sections. *PNP*, posterior neuropore; *CNH*, chordo-neural hinge; *CLE*, caudo-lateral epiblast; *NSB*, node-streak border. Adapted from (Mugele et al., 2018).

3.1.3.3 Conclusion

Altogether, the described inconsistencies in the literature make it very difficult to compare the results from different studies. Considering the diverse colonisation patterns described here which arose from cells labelled in neighbouring regions in the posterior neuropore, it is likely that several of the published studies did not actually capture the NMPs. To avoid further confusion, it is important to standardise the nomenclature and clearly describe which locations in the embryo are labelled/transplanted, and then subsequently analysed.

For the remainder of my thesis, I will refer to NMPs as those cells, which are located in region 1 of the CLE at E8.5 and later give rise to the dorsal neural tube and paraxial mesoderm.

3.2. Laser-ablation of the rostral CLE in E8.5 mouse embryos

3.2.1. Introduction and objectives

NMPs are believed to be required for body axis elongation providing the growing neural tube and paraxial mesoderm with cells (Cambray and Wilson, 2007; Cunningham et al., 2016; Garriock et al., 2015; Martin, 2016; Olivera-Martinez et al., 2012; Wilson et al., 2009; Wymeersch et al., 2016). Yet, the lack of NMP-specific markers complicates the analysis of this cell population. Here, I used multiphoton microscopy to specifically ablate region 1 of the CLE, where NMPs are located. The main objectives of this experiment were to investigate the idea that NMPs are required for body axis extension and to dissect their function during embryonic development, focussing in particular on neural tube formation. As shown in the previous chapter, cells from the rostral CLE colonise paraxial mesoderm and specifically the dorsal neural tube. Therefore, I expected deletion of region 1 to disturb both neural tube and somite formation, and potentially interfere with neural tube closure since ablation removes those cells which are eventually forming the dorsal domain.

3.2.2. Results: Laser-ablation of the NMP region and its effect on the development of neural tube and paraxial mesoderm

3.2.2.1 Ablation of the rostral CLE affects body axis elongation

To ablate the region which harbours NMPs, I first dissected E8.5 WT embryos for culture (1 – 7 ss) and labelled the region of interest (ROI) with DiO to ensure it can be easily identified under the microscope (**Figure 12A**). Next, I defined the shape and position of the area to be extirpated. I chose to delete a circular area in region 1 with a diameter of ~ 60 µm. The chosen diameter was selected after doing a test trial where I ablated areas of various sizes in the rostral CLE. However, I found that removing larger areas significantly affected the survival rate of the embryos. This is also the reason why I extirpated region 1 of the CLE only on one side, and not bi-laterally. Consequently, the size of the ROI is a trade-off between targeting as many NMPs as possible and at

the same time ensuring that the embryos survive the procedure. Please refer to the Methods section for details on the microscope settings.

After ablation, the embryos were put into culture for up to 24 h. As a control, I used embryos which were kept under similar conditions and cultured in parallel, but had not been ablated. Although the resulting embryos were alive and did not show any obvious morphological defects (**Figure 12A**), signs of toxicity became apparent in both control and laser-ablated embryos when cultured for more than 24 h. This is most likely due to the lengthy ablation procedure during which the embryos were kept under suboptimal conditions.

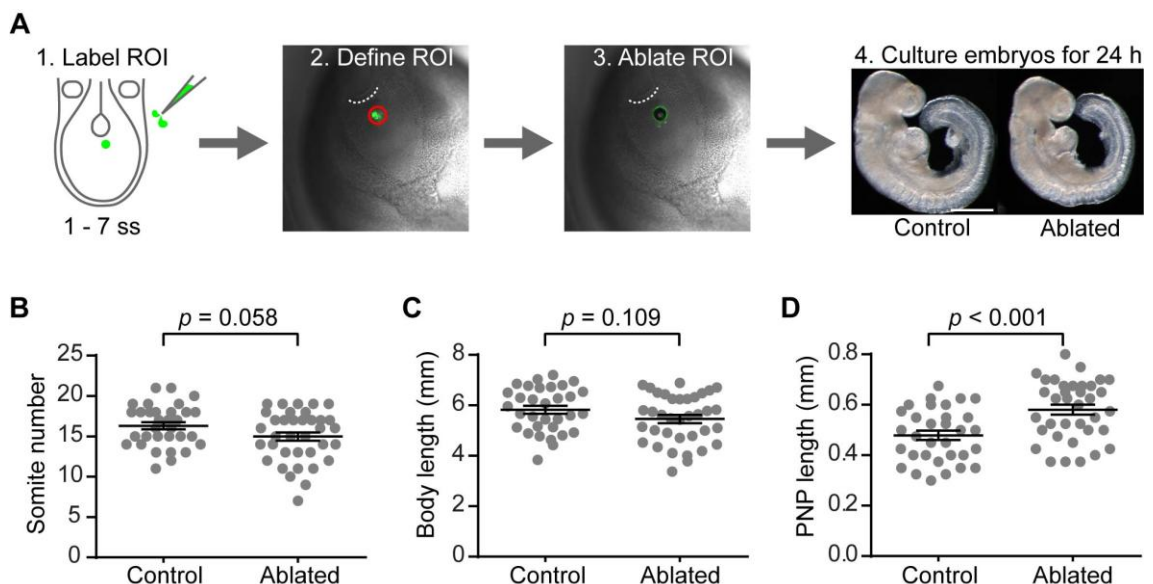


Figure 12. Ablating region 1 of the CLE slows down body axis elongation.

(A) Schematic of the ablation procedure. E8.5 WT embryos were dissected and the ROI was labelled by injecting DiO. The embryos were positioned under the microscope and the region to be deleted was outlined in the software (red circle) and lasered. The white dotted lines indicate the caudal border of the node. Following 24 h whole-embryo culture, ablated embryos had a smaller somite number **(B)**, they tended to be slightly shorter **(C)**, and their posterior neuropore length was significantly larger **(D)** compared to non-ablated control embryos. Data in B, C, and D shown as mean \pm SEM including the individual data points, with $n = 32$ control and $n = 36$ ablated embryos. Unpaired Student's t -test, two-sided. Scale bar, 500 μ m in A. ss, somite stage, ROI, region of interest, PNP, posterior neuropore. Adapted from (Mugele et al., 2018).

After culture, I first analysed the effect of laser-ablation on body axis elongation ($n = 32$ control embryos, $n = 36$ ablated embryos). For this purpose, I measured the length of

the embryos from the forebrain along the dorsal midline to the caudal tip, as well as their somite number and posterior neuropore length. These measures help to define the developmental stage of the embryos, as their somite number naturally increases as they grow and the size of their open posterior neuropore decreases over time. The results from control and laser-ablated embryos were compared using Student's *t*-test (unpaired, two-sided). The data revealed that ablated embryos had a marginally reduced somite number (**Figure 12B**) and they tended to be slightly smaller (**Figure 12C**), even though the observed trend was not significant. None of the ablated embryos showed pre-mature axis truncation ($n = 0/36$). The size of the posterior neuropore was significantly larger in ablated embryos compared to the control group (**Figure 12D**). Yet, although significant, the effect size was small and none of the posterior neuropore lengths is considered abnormal for this developmental stage (van Straaten et al., 1992). Altogether, this suggests that ablating region 1 of the CLE results in embryos which tend to be mildly developmentally delayed. Next, I analysed whether extirpation of this region affects the development of the neural tube and somites, as both tissues are derived – at least in part – from cells located in this region.

3.2.2.2 Ablating region 1 temporarily disturbs neural tube and somite formation

First, I analysed serial sections through laser-ablated and control embryos to assess how deletion of the rostral CLE affects the development of the neural tube (**Figure 13A**). To better identify neural tube and somites, I stained these sections for Pax3, which labels the dorsal neural tube and the dermamyotome. Surprisingly, both tissues appeared normal along the entire body axis (**Figures 13Ab** and **Ad**), except for a short region of neural tube of ~30 – 40 μm in length, where neural tube morphology was severely disrupted with apparently excessive neural tissue (**Figure 13Ac**; $n = 13/17$ ablated embryos, $n = 0/13$ control embryos). The positioning of this abnormal region suggested it had resulted from the earlier CLE region 1 ablation, although such a “short-lived” (limited axial extent) phenotype suggests that the embryos were able to recover from ablation. The dorsal neural tube, which was specifically labelled when

tracing DiO-positive cells from region 1 of the CLE, did actually form in the ablated embryos, as confirmed by Pax3 staining.

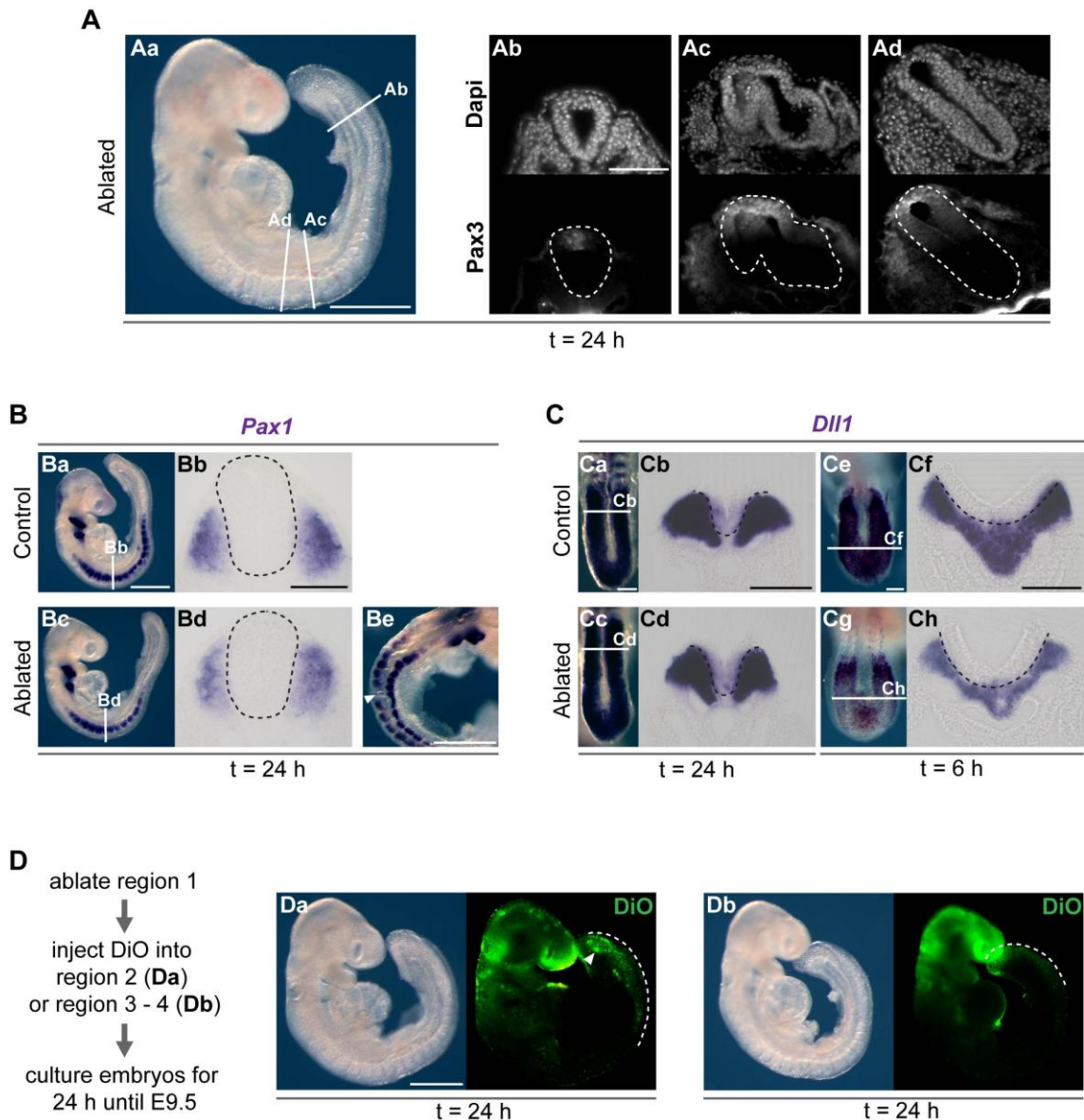


Figure 13. Deleting region 1 of the CLE transiently disrupts neural tube and somite formation.

(A) Ablated embryos featured a highly malformed neural tube ($n = 13/17$ ablated and $n = 0/13$ control embryos). However, only a short region was affected. (B) WISH for the sclerotome marker *Pax1*. No difference was visible in expression between control ($n = 10$) and laser-ablated embryos ($n = 7/8$), except for $n = 1/8$ ablated embryos, which was lacking a somite (white arrowhead in Be). (C) WISH for the pre-somitic mesoderm marker *Dll1* showed comparable expression in control ($n = 7$) and ablated ($n = 11$) embryos (Ca – Cd). Ablated embryos cultured for 6 h only (Ce – Ch) had clearly reduced *Dll1* expression levels ($n = 11/11$) compared to controls ($n = 7$). (D) Cells in region 2 of the CLE, which were labelled with DiO following deletion of region 1, re-populated the CNH after 24 h (white arrowhead in Da, $n = 7/8$ embryos), but not cells labelled in region 3 – 4 (Db; $n = 0/8$ embryos). White dashed lines in A and black dashed lines in B and C outline the neuroepithelium. White dashed lines in D indicate the contribution of DiO-labelled cells along the body axis. Scale bars, 500 μm in Aa, Ba, Be, Da; 100 μm in Ab, Bb, Ca, Cb, Ce, Cf. Adapted from (Mugele et al., 2018).

Second, I performed WISH for the sclerotome marker *Pax1* (**Figure 13B**; n = 10 control and n = 8 ablated embryos) and the pre-somitic mesoderm marker *Dll1* (**Figure 13Ca – d**; n = 7 control and n = 11 ablated embryos) to examine whether extirpation of region 1 interferes with somite formation. However, I did not detect any visible differences in the expression of both markers. Only 1/8 ablated embryos had a single somite missing after 24 h culture, as indicated by a gap in the *Pax1* expression domain (white arrowhead in **Figure 13Be**).

Given that deleting region 1 of the CLE disrupted neural tube formation only transiently, which is consistent with a minor delay in body axis elongation, any effect of ablation on mesoderm formation should be equally short-lived. Therefore, I repeated the laser-ablation experiment, but cultured the embryos for 6 h only (**Figure 13Ce – h**; n = 7 control and n = 11 ablated embryos). When analysing the formation of pre-somitic mesoderm by WISH for *Dll1*, I found the marker considerably down-regulated in the caudal region of 11/11 ablated embryos compared to controls (**Figures 13Cg – h**).

3.2.2.3 Cells located in CLE region 2 compensate for the ablated region 1

The previous experiments indicate that ablation of the rostral CLE affects axis elongation by producing what appears as excessive neural tissue at the expense of mesoderm. However, the transient nature of this phenotype suggests that region 1 may be re-populated shortly after ablation. But where do the re-populating cells come from? When I traced cells from the CLE by labelling various locations in the posterior neuropore with DiO, I found that cells in region 2 of the CLE gave a colonisation pattern very similar to region 1, including DiO-positive cells populating the CNH (**Figure 6B**). Yet, cells originating from region 2 contributed only to a short stretch of axial tissues compared to region 1. To test whether the rostral CLE is re-populated by cells from the more caudal CLE, I deleted region 1 in WT embryos at 1 – 7 ss as before and injected DiO either into region 2 or into regions 3 – 4 of the CLE (on the same side where CLE region 1 was ablated) before culturing the embryos for 24 h. Only when DiO was injected specifically into region 2 of the CLE did the embryos resemble those after

injecting region 1: 7/8 of these embryos showed DiO accumulated in the CNH (white arrowhead in **Figure 13Da**). Moreover, DiO-labelled cells from region 2 colonised axial tissue over a longer axial distance than cells labelled in regions 3 – 4 following ablation (white dashed lines in **Figure 13D**), but also for a longer distance than in non-ablated embryos labelled in region 2 (see **Figure 6B**). In contrast, DiO injection into regions 3 – 4 yielded embryos which exhibit the same appearance as described in **Figure 6C – D**, where DiO-positive cells are retained at the very tail bud end, but not in the CNH (n = 8/8 embryos).

3.2.3. Discussion: Laser-ablation of the NMPs

3.2.3.1 Reliability of laser-ablation and its limitations

NMPs are difficult to study, because there is no known marker, which is specifically expressed in these cells. Therefore, knock-out mouse models and other genetic approaches cannot be applied here, or only to a limited extent. To overcome this challenge, I used laser-ablation to destroy the region which harbours NMPs, hoping that the resulting phenotype would reveal more about NMP function in development. Even though the microscope settings ensure reliable ablation conditions, this method has limitations which need to be taken into account. First, laser-ablation creates heat which will damage not only the ROI, but to some degree also the adjacent tissue. This effect was reduced as much as possible by setting the scanning speed to maximum. Nevertheless, it likely still caused some damage in neighbouring cells. Second, the deleted region was relatively small, only ~ 60 µm in diameter, suggesting that ablation did not target all NMPs, which might explain why the observed phenotype was relatively mild. Similarly, I potentially extirpated cells other than NMPs, which might have contributed to the phenotype as well.

3.2.3.2 Laser-ablation as a method for studying NMPs

The laser-ablation experiments confirm that region 1 of the CLE is linked via cell lineage to neural tube and somite formation. Interestingly, ablation of the NMP location

appeared to induce excessive neural tissue, whereas mesoderm formation was down-regulated as indicated by reduced *Dll1* mRNA expression in the caudal region. Both tissues were severely affected by ablation, yet, only for a short period of time. This means that either laser-ablation did not remove the entire NMP population, or the ablated region was soon re-populated by cells from the surrounding CLE. My data support the latter, although a contribution from the first explanation is likely as well. The fact that the embryos recovered from ablation suggests that NMPs are not only produced once early during development, but that new NMPs can be recruited from region 2 of the CLE, thereby compensating for the loss of region 1.

3.2.3.3 Conclusion

Although my laser-ablation experiments have shed new light on NMP behaviour in axial development, the embryos recovered quickly from the intervention. Therefore, it is not a suitable system for studying the long-term effects of NMP ablation on neural tube formation. In the following chapter, I employ a genetic approach to permanently delete NMPs, which is based on the prevalent assumption that these cells co-express the neural marker *Sox2* and the early mesodermal marker *T* (Cambray and Wilson, 2007; Garriock et al., 2015; Tsakiridis et al., 2014; Wymeersch et al., 2016).

3.3. Sox2/T double-positive cells in neural tube formation

3.3.1. Introduction and objectives

The same area in the mouse tail bud, which Cambray and Wilson identified as the NMP location (Cambray and Wilson, 2002; Cambray and Wilson, 2007), harbours cells which co-express the early mesodermal marker *T* and the neural marker *Sox2* (Henrique et al., 2015; Wymeersch et al., 2016). This expression pattern is quite remarkable, since it is inconsistent with the traditional view that all cells within the embryo commit towards a specific germ layer during gastrulation. Yet, it matches the controversial potency proposed for the bi-potent progenitors and was therefore soon accepted as the distinctive feature of NMPs. Since then, many researchers have defined putative NMPs solely based on the co-expression of *Sox2* and *T* (Amin et al., 2016; Cunningham et al., 2016; Garriock et al., 2015; Gouti et al., 2017; Gouti et al., 2014; Javali et al., 2017; Koch et al., 2017; Rodrigo Albors et al., 2016; Tsakiridis et al., 2014; Turner et al., 2014; Wymeersch et al., 2016).

In the following chapter, I made use of this assumption to further explore NMP function in neural tube formation. First, I performed lineage tracing experiments in post-gastrulation embryos for both *Sox2*- and *T*-expressing cells to assess their contribution to the extending body axis. In addition, I revisited their expression pattern in WT embryos. Thirdly, I crossed a $T^{CreERT2/4}$ driver with a line homozygous for floxed *Sox2* ($Sox2^{fl/fl}$) to specifically delete *Sox2* in the *T*-expressing lineage. This system allowed precise timing of *Sox2* knock-out in relation to the emergence of NMPs in mouse embryos at E8.5. If NMPs truly co-express *Sox2* and *T*, this experiment might yield embryos with a phenotype similar to the one I observed after laser-ablating the rostral CLE. However, the effects are likely to be more extreme and affect longer stretches along the body axis since tamoxifen-induced CreERT2 recombination permanently deletes *Sox2*. Besides, it was suggested that NMPs account only for a fraction of the *Sox2*/*T* double-positive population in the tail bud (Wymeersch et al., 2016), with the

residual cells being progenitors committed to either neural or mesodermal fate. Therefore, this approach might potentially create phenotypes unrelated to the NMPs.

The main objectives of these experiments were to address how Sox2- and *T*-expressing cells behave under normal conditions and to characterise how Sox2 knock-down in *T*-expressing cells affects the development of NMP-derived tissues, focussing in particular on the neural tube.

3.3.2. Results: Lineage tracing Sox2- and *T*-expressing cells

3.3.2.1 T-expressing cells in the post-gastrulation embryo give rise to neural tube and paraxial mesoderm

If the hypothesis is true that NMPs co-express Sox2 and *T*, then tracing either lineage should result in significant contribution to both neural tube and somites. To begin with, I crossed a $T^{CreERT2/+}$ driver with the $Rosa26^{mTmG/mTmG}$ reporter line, which ubiquitously expresses the red-fluorescent protein tdTomato (mT) in all cell membranes. Following tamoxifen administration, cells which are positive for CreERT2, as well as their future progeny, will express membrane-localised GFP (mG) instead. This allows tracking of *T*-positive cells and their descendants as they colonise the extending axial tissues. CreERT2 activity was induced by injecting the pregnant females with 2 mg of tamoxifen per 40 g body weight at E8.5 (**Figure 14A**). At this developmental stage, gastrulation has ceased and NMPs have started giving rise to paraxial mesoderm and neural tube. The injection time point therefore ensures that the NMPs are targeted as part of the *T*-expressing lineage and will hence be labelled by GFP. I collected the embryos 24 h later at E9.5 (**Figure 14B**) and immuno-stained transverse sections for GFP expression, to enhance the signal of the reporter. A similar experiment had been published already by Anderson and colleagues (Anderson et al., 2013) and I was able to confirm their results: GFP-positive cells extensively colonised both the paraxial mesoderm and the neural tube, which was labelled by staining for Sox2 (**Figure 14C**; n = 8/8 embryos). In addition, I consistently found labelled cells in the CNH (pink circle in **Figure 14Ca**), as well as the notochord (orange arrowhead in **Figure 14Cb – c**).

Surprisingly, GFP-positive cells also colonised the hindgut roof (white arrowheads in **Figure 14Cb – c**; n = 8/8 embryos).

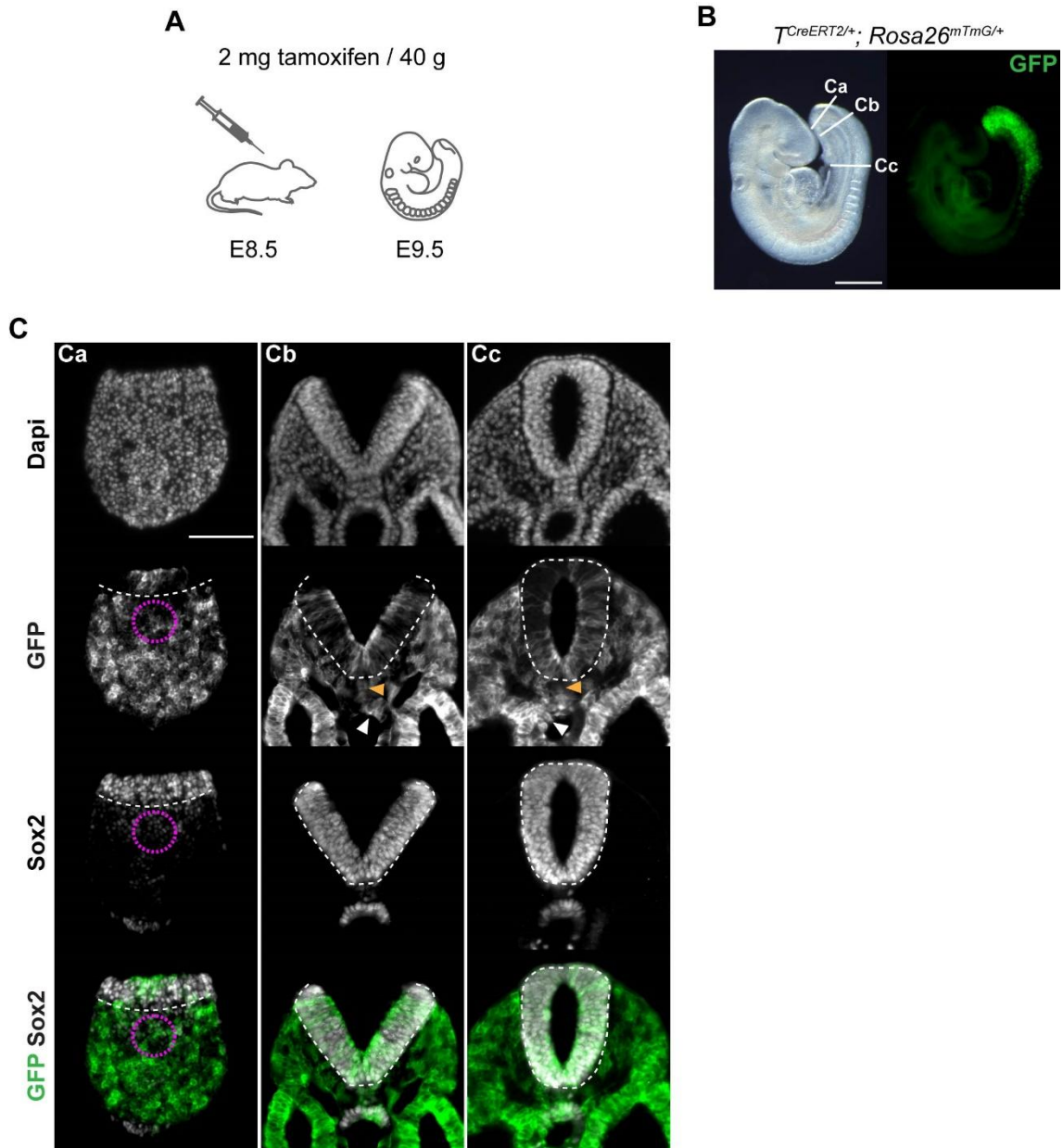


Figure 14. Cells expressing *T* around E8.5 colonise both neural tube and paraxial mesoderm.

(A) Tamoxifen was injected into the pregnant females at E8.5 at a concentration of 2 mg per 40 g body weight. **(B)** The embryos were collected at E9.5. **(C)** Transverse sections show that traced cells substantially contributed to the forming neural tube and paraxial mesoderm, as well as the CNH in n = 8/8 embryos. In addition, GFP-positive cells colonised the notochord (orange arrowheads in Cb – c) and the hindgut (white arrowheads in Cb – c). White dashed lines in C indicate the basal border of the neuroepithelium. Pink circles in Ca outline the CNH. Scale bars, 500 μ m in B; 100 μ m in Ca. Adapted from (Mugele et al., 2018).

3.3.2.2 Sox2-expressing cells in the post-gastrulation embryo do not give rise to paraxial mesoderm

Subsequently, I did the reverse experiment, by crossing a $Sox2^{CreERT2/+}$ driver with the $Rosa26^{mTmG/mTmG}$ reporter.

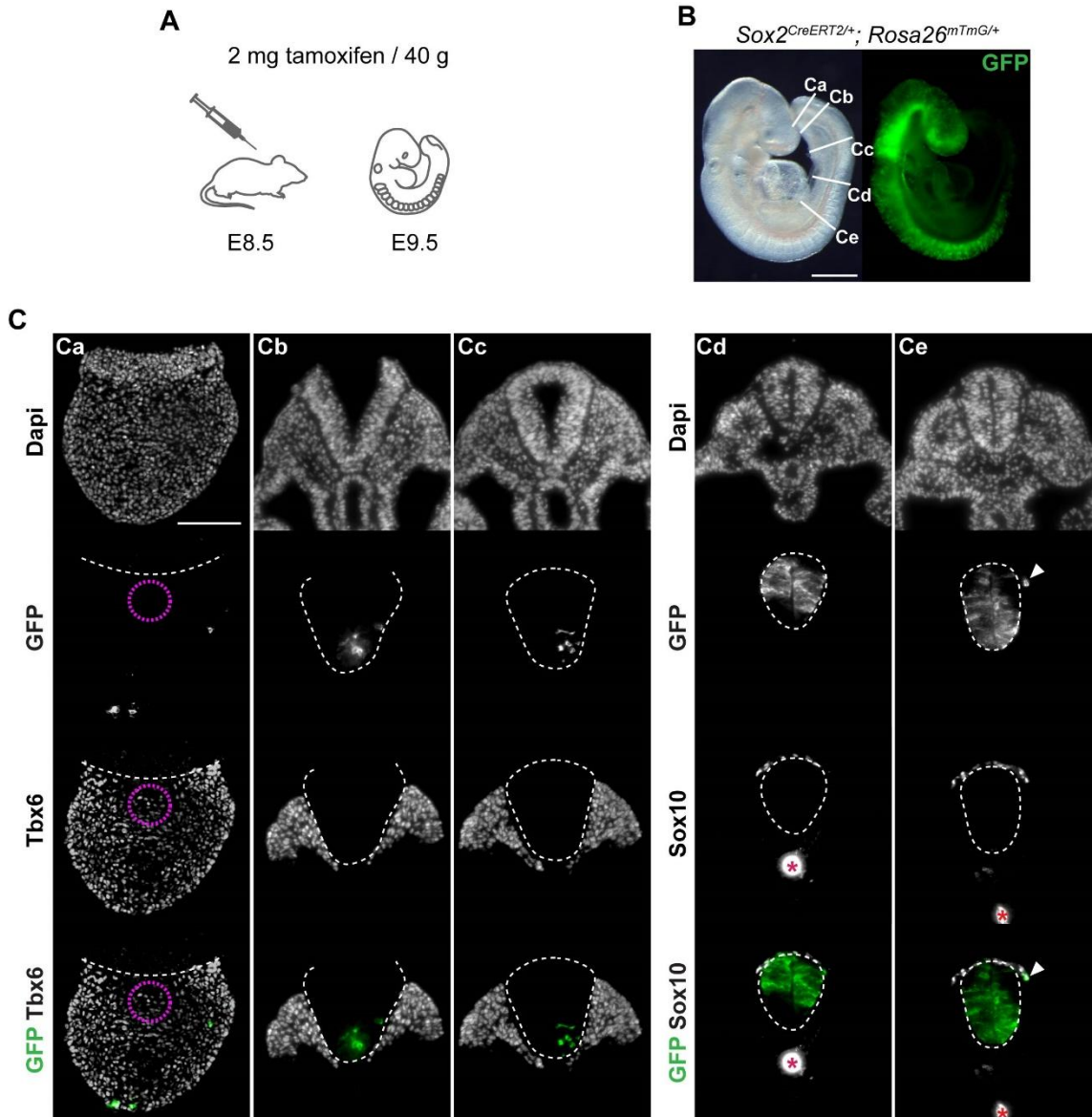


Figure 15. Cells expressing Sox2 around E8.5 colonise the neural tube only (standard dose).

(A) Tamoxifen was injected into pregnant females at E8.5 at a concentration of 2 mg per 40 g body weight. (B) The embryos were collected at E9.5 (n = 6). (C) Transverse sections show that traced cells colonised the neural tube, but neither the paraxial mesoderm, nor the CNH. Those few GFP-positive cells found outside the neuroepithelium were Sox10-expressing neural crest cells (white arrowheads in Ce). The white dashed lines in C indicate the basal border of the neuroepithelium. Pink circles in Ca highlight the CNH. Red asterisks in Cd – e mark non-specific trapping of secondary antibody in the hindgut lumen. Scale bars, 500 μ m in B; 100 μ m in Ca. Adapted from (Mugele et al., 2018).

In spite of an extensive literature search, I was not able to find any indication that this experiment had been done previously with reference to NMPs. Similar to the previous lineage tracing experiment, pregnant dams were injected with 2 mg of tamoxifen per 40 g body weight at E8.5 and the embryos were collected 24 h later (**Figure 15**; n = 6 embryos). They were sectioned and immuno-stained for the pre-somitic mesoderm marker Tbx6 and for GFP, to enhance the signal of the reporter line. I screened every transverse section from all six embryos, from the caudal tip to hindbrain level and found GFP-expressing cells in the neural tube only without any contribution to paraxial mesoderm (**Figure 15Ca – d**). Individual GFP-positive cells were present outside the neural tube. Yet, overlapping Sox10 expression identified these as neural crest cells (white arrowheads in **Figure 15Ce**). The CNH did not contain any GFP-labelled cells at all in these embryos.

Although 2 mg of tamoxifen per 40 g body weight is a standard dose for inducing CreERT2 activity (Feil et al., 2009), I doubled the dosage to ensure sufficient recombination. The *Sox2^{CreERT2/+}* driver was crossed with the *Rosa26^{mTmG/mTmG}* reporter line, and pregnant female were injected with 4 mg of tamoxifen per 40 g body at E8.5 (**Figure 16**; n = 8 embryos). I did not observe any undue toxicity when using this high dose. Nevertheless, I obtained the same phenotype as before even though I screened every transverse section from all eight embryos: GFP-positive cells colonised the neural tube only and those few cells found outside the neural tube were all Sox10-positive neural crest cells (white arrowheads in **Figure 16Cd – e**). Again, the CNH was GFP-negative.

To increase recombination even further, I repeated the experiment using the high dose of 4 mg of tamoxifen per 40 g body weight and injected the pregnant females three times at 12 h intervals at E8.0, E8.5, and E9.0. The embryos were collected 12 h after the last injection at E9.5 (**Figure 17**; n = 12 embryos). Only 1/8 litters collected showed signs of toxicity and these embryos were excluded from analysis. Similar to the previous experiments, GFP-positive cells mainly contributed to the neural tube. GFP-expressing cells located in the paraxial mesoderm stained positive for the neural crest

marker Sox10. Yet, a very small number of 1 – 23 GFP-positive cells per embryo were actually Sox10-negative (blue arrowheads in **Figure 17b – d**). Please refer to **Table 9** for the cell counts. Interestingly, GFP-expressing cells were also found in the notochord of $n = 12/12$ embryos (orange arrowheads in **Figure 17c – d**).

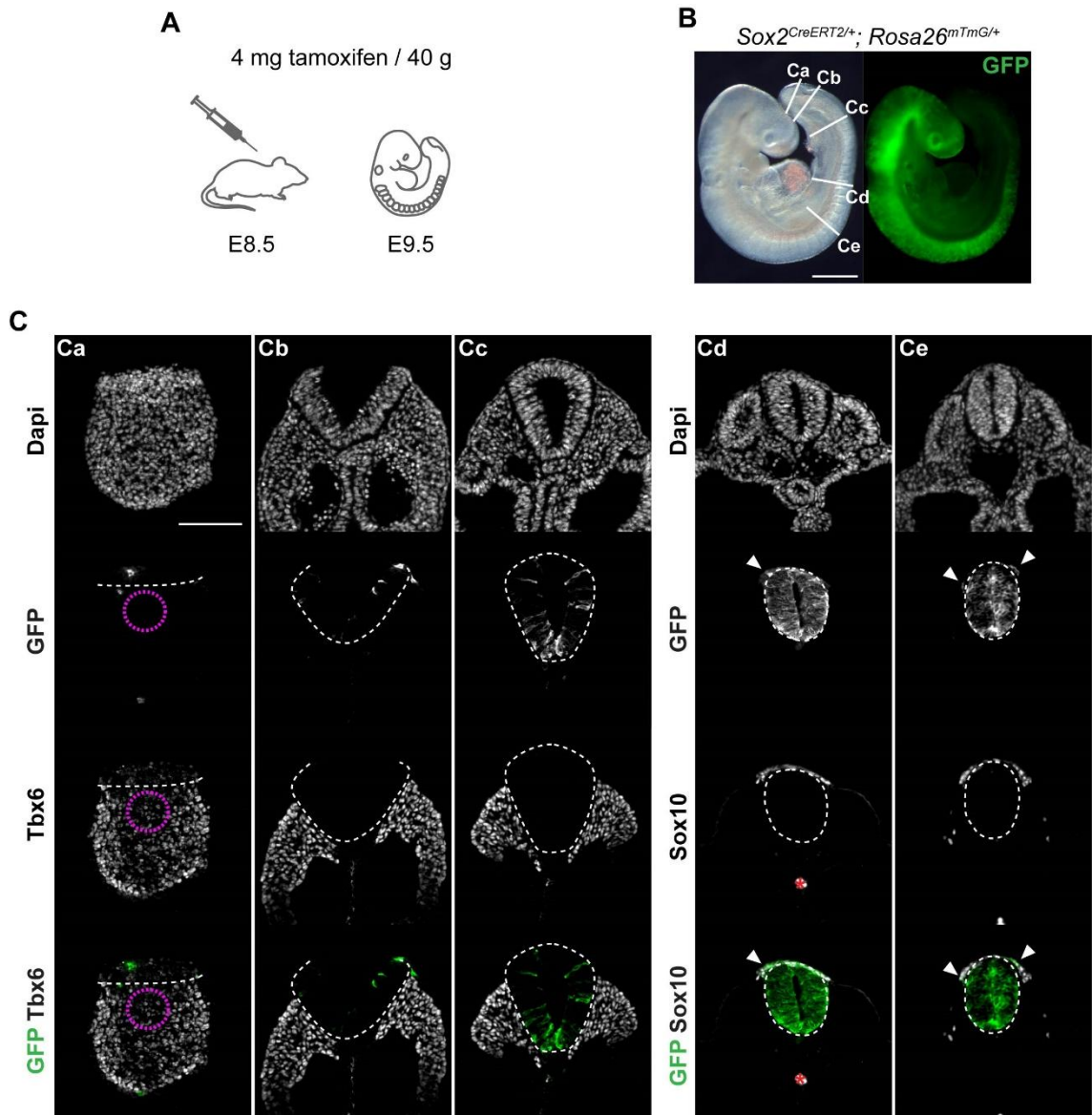


Figure 16. Cells expressing Sox2 around E8.5 colonise the neural tube only (high tamoxifen dose). (A) Tamoxifen was injected into the pregnant dams at E8.5 at a concentration of 4 mg per 40 g body weight. (B) The embryos were collected at E9.5 ($n = 8$). (C) Transverse sections reveal that traced cells contributed the neural tube, but neither to the paraxial mesoderm, nor to the CNH. All GFP-positive cells identified in the paraxial mesoderm were neural crest cells as they co-expressed Sox10 (white arrowheads in Cd – e). The white dashed lines in C outline the neuroepithelium along its basal border. Pink circles in Ca indicate the CNH. Red asterisks in Cd label non-specific trapping of secondary antibody in the hindgut lumen. Scale bars, 500 μ m in B; 100 μ m in Ca. Adapted from (Mugele et al., 2018).

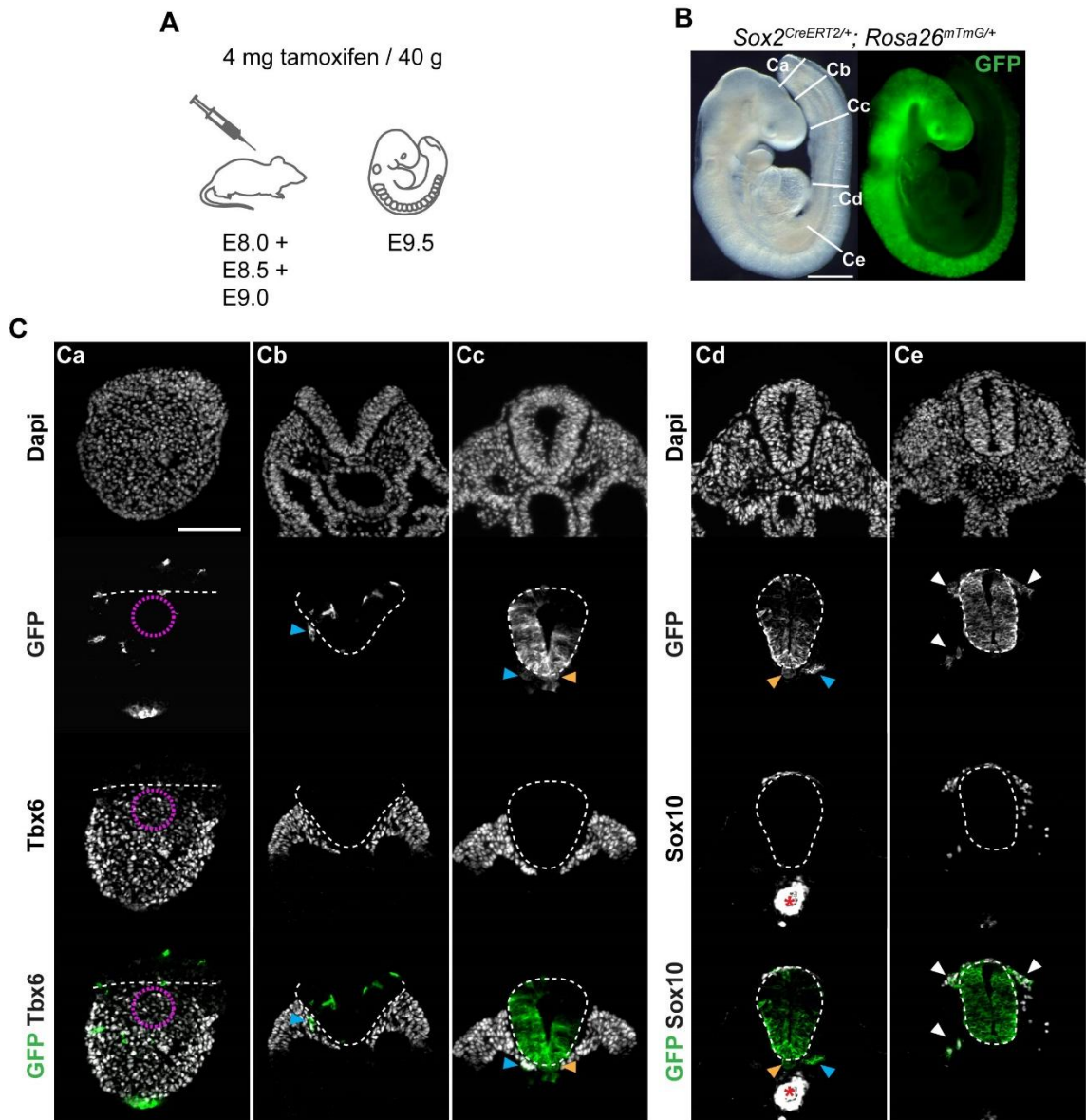


Figure 17. Cells expressing Sox2 around E8.0 colonise the neural tube and, to a negligible extent, paraxial mesoderm following multiple injections of the high tamoxifen dose.

(A) Tamoxifen was injected into the pregnant females at E8.0, E8.5, and E9.0 at a concentration of 4 mg per 40 g body weight. **(B)** The embryos were collected at E9.5. **(C)** Transverse sections show that traced cells contributed significantly to the neural tube. Of GFP-positive cells that were found outside the neural tube, most co-expressed the neural crest marker Sox10 (white arrowheads in Ce). Yet, a very small number of GFP-positive cells in the paraxial mesoderm were indeed Sox10-negative (blue arrowheads in Cb – Cd, n = 12/12 embryos). Orange arrowheads in Cc – d point to GFP-positive cells in the notochord. White dashed lines in C delineate the basal border of the neuroepithelium. Pink circles in Ca indicate the CNH. Red asterisks in Cd mark non-specific trapping of secondary antibody in the hindgut lumen. Scale bars, 500 μ m in B; 100 μ m in Ca. Adapted from (Mugele et al., 2018).

Table 9. Cell counts of GFP-positive cells in the paraxial mesoderm derived from Sox2 lineage tracing experiments.

This table refers to the data shown in Figures 15 – 17. For each embryo, every transverse section from the tail bud to the hindbrain level was stained and screened. “# GFP-positive/Tbx6-positive cells in the open region” refers to those GFP-positive cells which were found in the pre-somitic mesoderm of transverse sections between the CNH and closure point. “# GFP-positive/Sox10-negative cells in the paraxial mesoderm” refers to the number of GFP-positive cells per embryo found outside the neural tube in the closed region, which were also Sox10-negative. Adapted from (Mugele et al., 2018).

Day of tamoxifen injection	Day of embryo collection	Tamoxifen concentration	n	Embryo ID	Somite stage at collection	# GFP-positive cells in CNH per embryo	# GFP-positive/Tbx6-positive cells in the open region per embryo	# GFP-positive/Sox10-negative cells in paraxial mesoderm per embryo	Location of GFP-positive/Sox10-negative cells in paraxial mesoderm			
												
E8.5	E9.5	2 mg / 40 g	6	A1	21	0	0	0				
				A2	16	0	0	0				
				A3	17	0	0	0				
				A4	18	0	0	6			1	5
				A5	15	0	5	0				
				A6	17	0	0	4			4	
E8.5	E9.5	4 mg / 40 g	8	B1	18	0	0	0				
				B2	18	0	0	0				
				B3	17	0	0	0				
				B4	18	0	0	0				
				B5	17	0	0	0				
				B6	15	0	0	0				
				B7	18	3	0	4	2		1	1
				B8	21	1	1	0				
E8.0, E8.5, E9.0,	E9.5	4 mg / 40 g	12	C1	15	0	3	1	1			
				C2	19	2	1	5	3		1	1
				C3	19	0	1	5	1	3		1
				C4	21	2	0	16	8	4	3	1
				C5	18	4	4	3	2	1		
				C6	21	3	3	6	3	1	1	1
				C7	23	0	0	23	10	6	6	1
				C8	20	3	0	17	6	3	5	3
				C9	23	0	1	3	1	1	1	
				C10	19	0	2	6	1		4	1
				C11	18	3	4	8	3	3	1	1
				C12	19	0	0	14	4	5	1	4

3.3.2.3 Sox2-expressing cells in the gastrulating embryo give rise to both neural tube and paraxial mesoderm

The germ layers arise during gastrulation from the epiblast layer, which also expresses Sox2 (Avilion et al., 2003; Wood and Episkopou, 1999). Consequently, if Sox2-positive cells are traced from this developmental stage until E9.5 they are expected to show considerable contribution to both neural tube and paraxial mesoderm. After tracing Sox2-expressing cells from E8.0, I found that labelled cells gave rise to the forming neural tube, but only scarcely to the paraxial mesoderm (**Figure 17**). To further specify the time point when Sox2 expression becomes restricted to cells with a neural fate, I repeated the lineage tracing experiment by crossing the Sox2^{CreERT2/+} driver line with the Rosa26^{mTmG/mTmG} reporter. To induce CreERT2 activity, pregnant dams were injected with 4 mg of tamoxifen per 40 g body weight either at E6.5, which is an early gastrulation stage (**Figure 18**; n = 12 embryos), or at E7.5, which is a late gastrulation stage (**Figure 19**; n = 10 embryos). The litters were collected at E9.5. As expected, all of these embryos showed substantial contribution of GFP-positive cells to both paraxial mesoderm and neural tube (**Figures 18C** and **19C**). However, it was notable that embryos treated with tamoxifen at E6.5 contained more GFP-positive mesodermal cells than those treated at E7.5. In addition, all embryos had some GFP-positive cells located in their CNH (pink circles in **Figures 18Ca** and **19Ca**).

In summary, Sox2-expressing cells which were traced following tamoxifen administration at E8.0 or later, were fated exclusively for the neural lineage, except for a very low number of GFP-positive/Sox10-negative cells, which ended up in the paraxial mesoderm. However, when the drug was given at E7.5 or earlier, labelled Sox2-expressing cells and their progeny extensively gave rise to both neural tube and paraxial mesoderm.

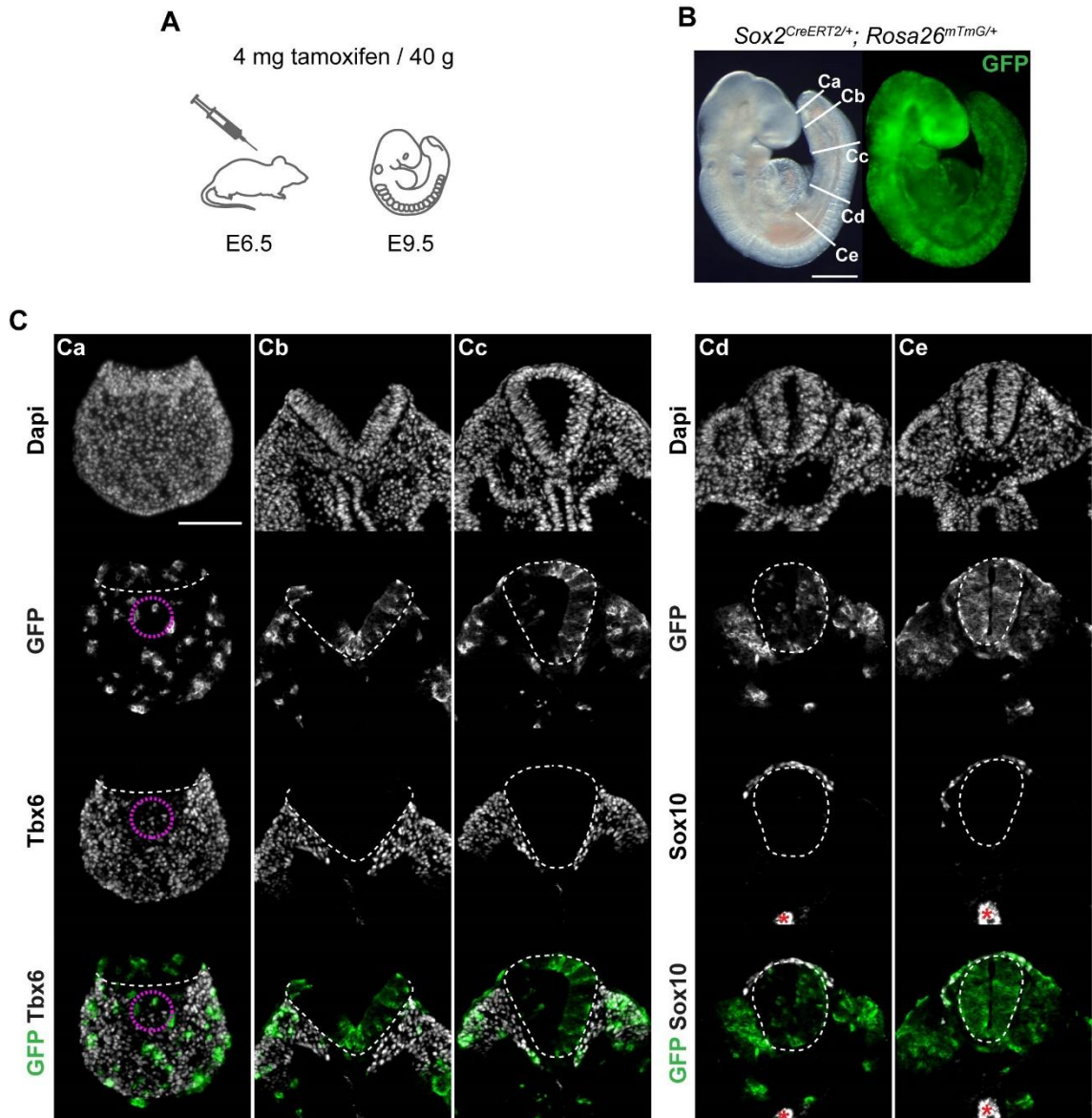


Figure 18. Cells expressing Sox2 around E6.5 colonise both neural tube and paraxial mesoderm.

(A) Tamoxifen was injected into the pregnant females at E6.5 at a concentration of 4 mg per 40 g body weight. (B) The embryos were collected at E9.5. (C) Transverse sections demonstrate that traced cells substantially contributed to the neural tube and paraxial mesoderm, as well as the CNH in $n = 12/12$ embryos. The white dashed lines in C mark the basal border of the neuroepithelium. Pink circles in Ca highlight the CNH. Red asterisks in Cd – e indicate non-specific trapping of secondary antibody in the hindgut lumen. Scale bars, 500 μm in B; 100 μm in Ca. Adapted from (Mugele et al., 2018).

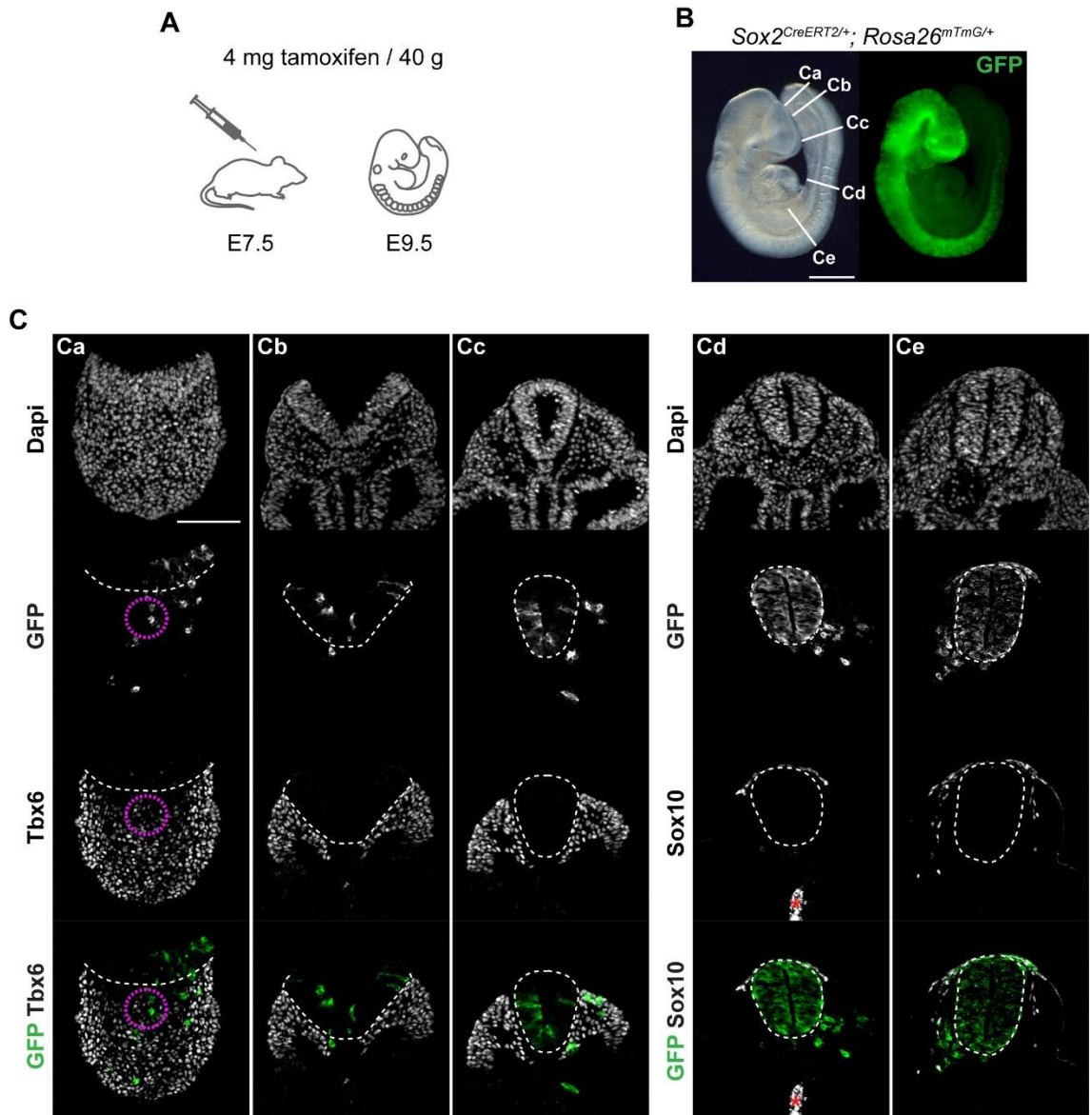


Figure 19. Cells expressing *Sox2* around E7.5 colonise both neural tube and paraxial mesoderm. (A) Tamoxifen was injected into pregnant dams at E7.5 at a concentration of 4 mg per 40 g body weight. (B) The embryos were collected at E9.5. (C) Transverse sections show that traced cells contributed to neural tube, paraxial mesoderm, and the CNH in $n = 10/10$ embryos. White dashed lines in C outline the neuroepithelium. Pink circles in Ca define the CNH. Red asterisks in Cd mark non-specific trapping of secondary antibody in the hindgut lumen. Scale bars, 500 μm in B; 100 μm in Ca. Adapted from (Mugele et al., 2018).

3.3.3. Discussion: Lineage tracing Sox2- and T-expressing cells

3.3.3.1 Implications and limitations of genetic lineage tracing

For the lineage tracing experiments I used mice which express the inducible CreERT2 recombinase under the control of either the *Sox2* or *T* promoter. CreERT2 is activated by the tamoxifen metabolite trans-4-OH-tamoxifen. Therefore, recombination can be timed by tamoxifen administration. Pharmacokinetic studies in mice showed that reporter genes were induced within 6 – 12 h following injection of a single dose of tamoxifen into the peritoneum of CreERT2 mice and they remained active for ~ 24 – 36 h (Dymecki and Kim, 2007). Hence, recombination occurs over a time period of ~ 24 h and starts with a delay of ~ 6 – 12 h after tamoxifen administration. In line with this study, GFP expression was first visible ~ 8 h after tamoxifen injection (data not shown). Regarding my *Sox2* lineage tracing experiments, this means that *Sox2* expression becomes limited to cells with a neural fate around E8.0, since tamoxifen administration at E7.5 resulted in GFP-labelled cells in both neural tube and paraxial mesoderm, but not when tamoxifen was given at E8.0 or later. This time point also coincides with the end of gastrulation. To ensure consistency and comparability between all lineage tracing experiments presented in this chapter, I only included those embryos in the analysis, which had 15 – 23 somite pairs when collected at E9.5.

In addition to the timing, it is also important to consider that CreERT2 activity is induced in a concentration-dependent manner. The higher the tamoxifen dose, the more recombination events occur, until the system is saturated which gives the maximum recombination rate. However, higher doses also increase the risk of drug-related side-effects. Therefore, it is generally not possible to achieve 100% recombination. I started with a concentration of 2 mg of tamoxifen per 40 g body weight, which is the standard dose used by most research groups, including my own. It is a trade-off between good recombination and low drug-related toxicity. I only observed toxicity after injecting three doses of the high tamoxifen, i.e. 4 mg per 40 g body weight, which equally affected all embryos in the litter, independent of their genotype. Those few embryos which were affected were excluded from analysis. That

said, I cannot rule out any residual tamoxifen-induced side-effects, although these are more common following long-term exposure to the drug. Since I only traced cells and did not delete any crucial genes, CreERT2-mediated side-effects were not expected.

3.3.3.2 Contradicting the concept of Sox2/T double-positive NMPs

If the neural tube and somites shared a common *Sox2/T* double-positive progenitor, then tracing either lineage should have shown substantial contribution to both tissues. Surprisingly, I found that *Sox2*-positive cells almost exclusively adopted a neural fate after gastrulation, whereas descendants of *T*-positive cells extensively colonised both neural tube and somites. NMPs are believed to form the spinal neural tube and paraxial mesoderm from the axial level of the sixth somite onwards (Perantoni et al., 2005; Tzouanacou et al., 2009), which corresponds to E8.5. Therefore, they should have been labelled following tamoxifen administration at E8.5.

This finding is further supported by the fact that the tail bud tips of *Sox2^{CreERT2/+}; Rosa26^{mTmG/+}* embryos were completely GFP-negative – except for a few sparse cells – when CreERT2 activity was induced after E8.0. Considering the lag in reporter expression following tamoxifen administration, this phenotype suggests that those cells which follow the neural lineage immediately leave the tail bud and integrate into the forming neural tube. Therefore, labelled cells are scarce in the caudal part of the tail bud but they continuously increase in number at more rostral levels, where > 90% of the cells in the neural tube are GFP-positive (see for example **Figure 19Cd-e**). Since this pattern is consistent among the *Sox2* lineage tracing experiments and is independent of the point of injection, it likely reflects the lack of *Sox2* expression in the caudal end of the E9.5 embryo and the lag in reporter gene expression, rather than insufficient recombination. Although it is likely that higher doses of tamoxifen might have resulted in a higher number of GFP-positive/*Sox10*-negative cells in the paraxial mesoderm, the fact that their number is extraordinarily small, even in more rostral sections which show high recombination, suggests that this contribution is not biologically significant. Another explanation for the low number of GFP-positive/*Sox10*-

negative cells in the somites is that NMPs might express *Sox2* only transiently and might therefore not be sufficiently targeted in this experiment. However, this is again inconsistent with the idea of a *Sox2/T* double-positive progenitor population which persists in the CNH, as suggested by the work performed by Wilson and colleagues (Cambray and Wilson, 2002; Cambray and Wilson, 2007; Wilson et al., 2009; Wymeersch et al., 2016).

Even though I might have lost a few sections in the cryostat, the total number of GFP-positive/*Sox10*-negative cells I found in the paraxial mesoderm indicates that this contribution is negligibly small. This means that somites are not derived from *Sox2/T* double-positive cells, but from *T*-positive cells only. Interestingly, I noticed that GFP-positive/*Sox10*-negative cells in the paraxial mesoderm were not equally spread along the body axis, but were usually accumulated in one to two adjacent sections. For example, all five GFP-positive cells I found in the centre of the somite of embryo A4 (see **Table 9**), were all within the same transverse section, suggesting that these might be clones (i.e. mitotic descendants of a single cell). This further emphasises that the contribution of *Sox2*-positive cells to the paraxial mesoderm is a highly exceptional case.

3.3.3.3 Conclusion

The concept of a *Sox2/T* double-positive progenitor cell population which gives rise to the spinal neural tube and paraxial mesoderm after E8.5 is inconsistent with the results I obtained from my lineage tracing experiments. The hypothesis that NMPs co-express *Sox2* and *T* was based on the discovery of double-positive cells in the NMP region as shown by both WISH and immunostaining in mouse embryos (Henrique et al., 2015; Wymeersch et al., 2016). These findings were also confirmed in other species including zebrafish (Martin and Kimelman, 2012), chick (Olivera-Martinez et al., 2012), and axolotl (Taniguchi et al., 2017). To get to the bottom of this problem, I repeated both immunostaining and WISH for the markers, which will be discussed next.

3.3.4 Results: Sox2 and T expression in WT embryos

3.3.4.1 Sox2 protein is expressed in the CNH

First, I repeated the immunostaining for Sox2 and T (**Figure 20**) by staining transverse sections of E9.5 embryos, since the NMPs are spatially confined to the CNH at this stage. Unfortunately, I was not able to find an antibody against T which gave me a reliable and sufficiently specific staining. **Table 10** lists the antibodies tested. Therefore, I opted for an indirect readout of T protein expression by crossing the $T^{CreERT2/+}$ line with the $Rosa26^{EYFP/EYFP}$ reporter.

Table 10. T/Brachyury antibodies tested.

Host	Supplier (catalogue #)	# of batches tested
goat (polyclonal)	R&D (AF2085)	3
goat (polyclonal)	Santa Cruz (sc-17743)	1
mouse (monoclonal)	Santa Cruz (sc-166962)	1
mouse (monoclonal)	Santa Cruz (sc-374321)	1
mouse (monoclonal)	Developmental Study Hybridoma Bank (PCRP-T-1A5)	1
rabbit (polyclonal)	Thermo Fisher Scientific (PA5-23405)	1
rabbit (polyclonal)	Abcam (ab20680)	1

CreERT2 activity was induced at E8.5 by injecting 2 mg of tamoxifen per 40 g body weight into the pregnant females. The embryos were collected 24 h later at E9.5 and transverse sections were immuno-stained for Cre, Sox2, and also GFP, to enhance the signal of the reporter. Active, nuclear Cre served as an indirect indication of T protein expression. In line with previous studies, transverse sections through the tail bud revealed that both Sox2 and active (nuclear) Cre are expressed in the CNH in $n = 7/7$ embryos (pink circles in **Figure 20Ca**). Note that Sox2 expression is much weaker in the tail bud and CNH compared to the neuroepithelium.

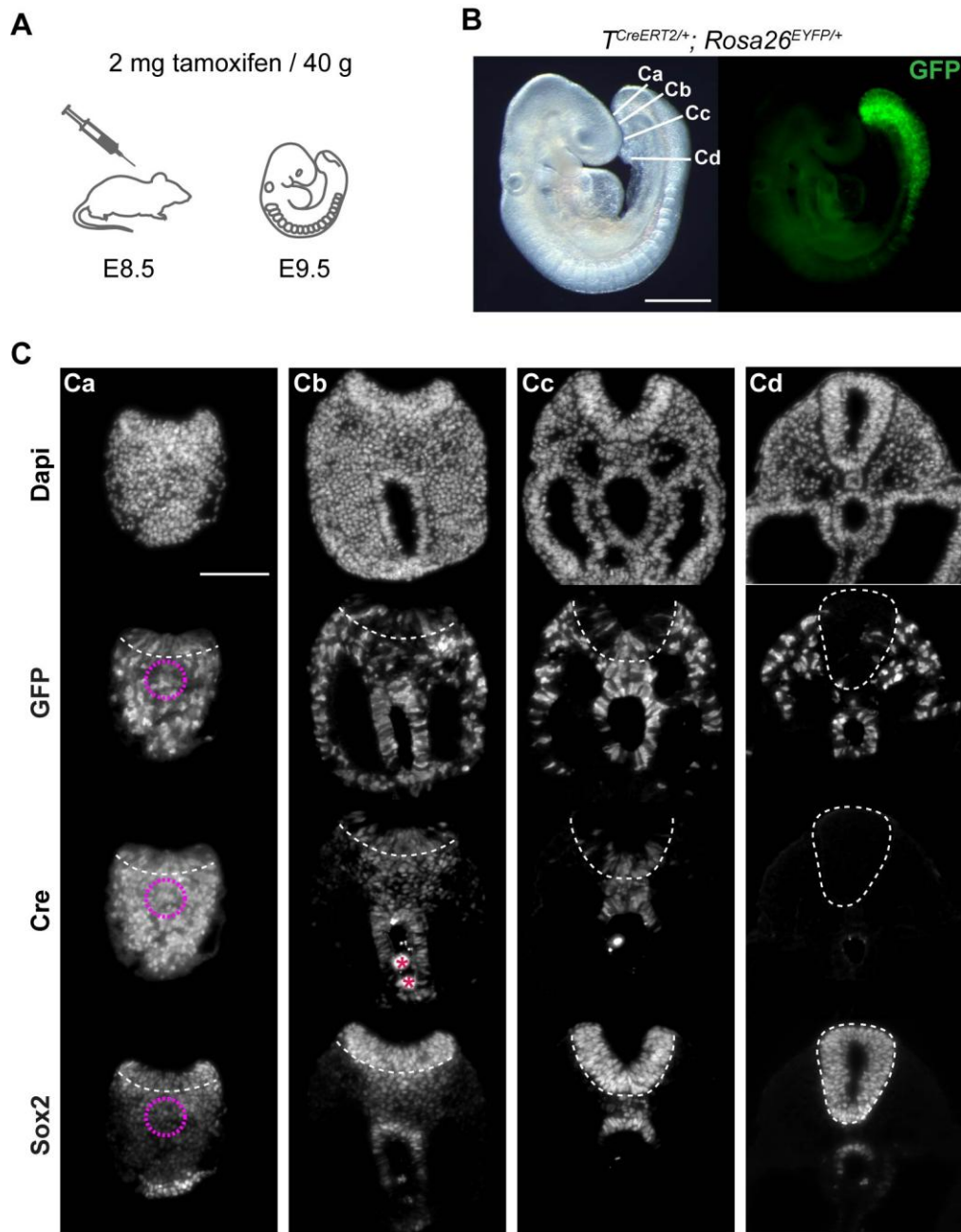


Figure 20. Sox2 protein is expressed in the CNH.

(A) A $T^{CreERT2/+}$ driver was crossed with $Rosa26^{EYFP/EYFP}$ reporter. Tamoxifen was injected at E8.5 at a concentration of 2 mg per 40 g body weight. (B) The embryos were collected at E9.5. (C) Both Sox2 and active (nuclear) Cre are clearly expressed in the CNH of $n = 7/7$ embryos (pink circles in Ca). White dashed lines in C mark the basal border of the neuroepithelium. Red asterisks in Cb indicate non-specific trapping of secondary antibody in the hindgut lumen. Scale bars, 500 μm in B; 100 μm in Ca. Adapted from (Mugele et al., 2018).

3.3.4.2 Sox2 mRNA is not expressed in the CNH

Secondly, I performed WISH for Sox2 and *T* in E8.5 (5 – 6 ss) and E9.5 (16 – 21 ss) WT embryos (Figure 21). At E8.5, *T* mRNA is strongly expressed at the caudal end of the embryo, and is not only present in the pre-somitic mesoderm, but also in the

forming neuroepithelium in $n = 4/4$ embryos (**Figure 21Aa – Ae**). In contrast, *Sox2* mRNA expression is restricted to the neuroepithelium in $n = 5/5$ embryos (**Figure 21Af – Aj**). The sections shown in **Figure 21Ad** and **Ai** were taken through the rostral CLE.

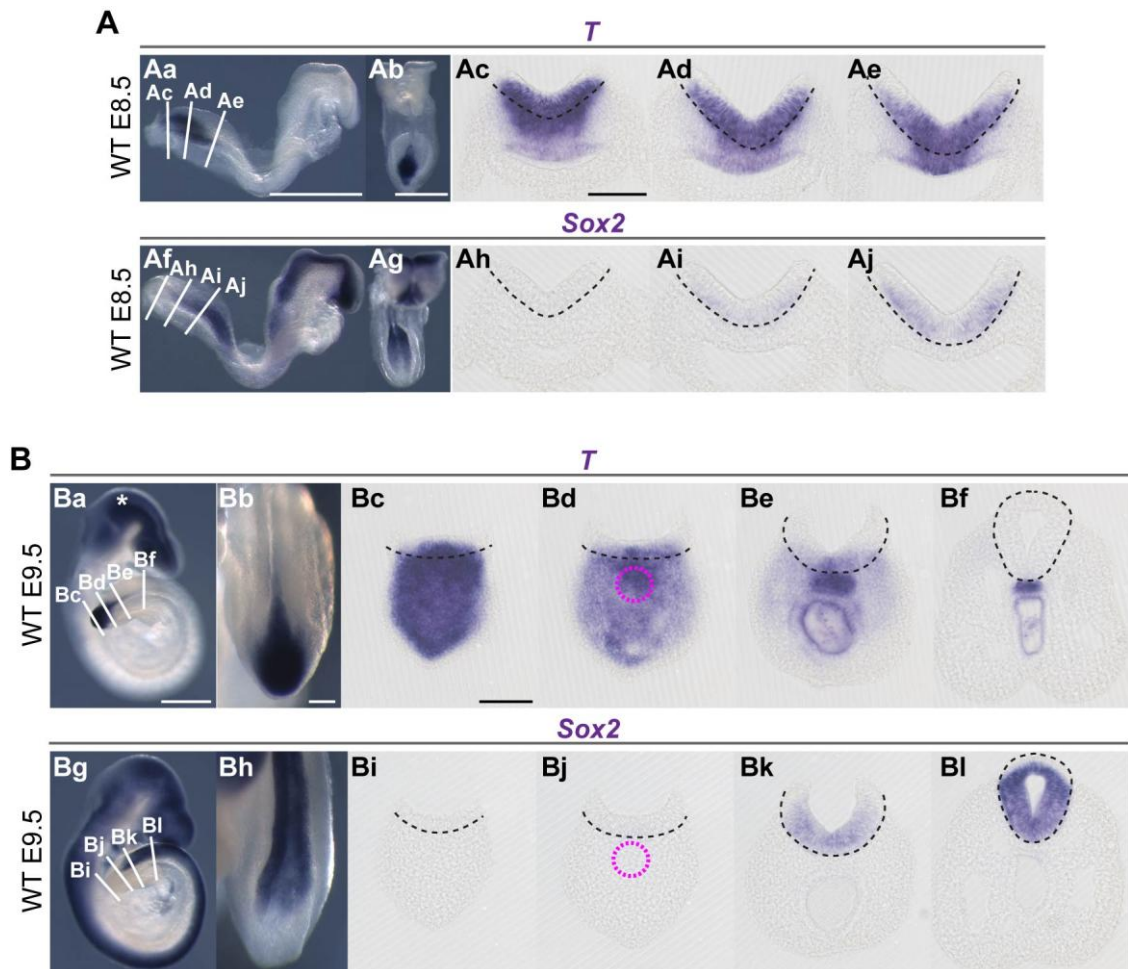


Figure 21. *Sox2* mRNA is not expressed in the CNH.

(A) WISH for *T* ($n = 4$) and *Sox2* ($n = 5$) in E8.5 WT embryos, viewed from lateral (Aa, Af) and from dorsal (Ab, Ag). **(B)** WISH for *T* ($n = 5$) and *Sox2* ($n = 5$) in E9.5 WT embryos, shown from lateral (Ba, Bg) and their posterior neuropore viewed from dorsal (Bb, Bh). Black dashed lines in Ac – Ae, Ah – Aj, Bc – Bf, and Bi – Bl outline the neuroepithelium. Pink circles in Bd and Bj indicate the CNH. White asterisk in Ba marks non-specific trapping of the probe in the head region. Scale bars, 500 μm in Aa – Ab, Ba; 100 μm in Ac, Bb – Bc. Adapted from (Mugele et al., 2018).

Similarly, *T* mRNA is strongly expressed in the posterior neuropore of E9.5 embryos in both mesoderm and neuroepithelium. Only rostral to the closure point does expression become limited to the notochord (**Figure 21Ba – Bf**). In addition, *T* mRNA is present in the CNH in $n = 5/5$ embryos (pink circle **Figure 21Bb**). Note that *T* mRNA expression

correlates well with the immunostaining for Cre presented in **Figure 20**. *Sox2* mRNA, on the other hand, is expressed in the neuroepithelium only (**Figure 21Bg – BI**) and most importantly, is absent from the CNH in n = 5/5 embryos (**Figure 21Bj**).

3.3.5 Discussion: *Sox2* and *T* expression in WT embryos

3.3.5.1 Limitations of WISH and immunostaining

Both WISH and immunostaining are standard methods and I followed the same protocols that have been used in our group for many years (Henderson et al., 1999), without any modifications.

Beforehand, I tested and optimised the antibody against *Sox2*, which gave me - as expected - strong and specific staining in the neural tube without any background. I consistently found *Sox2* expression in the CNH, which is in line with the literature. In addition, I tested a second antibody against *Sox2*, which was raised in a different species and I obtained the same results (data not shown).

Regarding the WISH for *Sox2* mRNA, I did this experiment twice and the second time I left the embryos for an extended period in the developing solution. Although this resulted in stronger staining, there was still no visible expression of *Sox2* mRNA in the CNH. The probes were not designed in our lab, but they have been used many times in the past by us and other groups. Please refer to **Table 7** in the Methods section for details on the probe and source. In addition, I compared the expression pattern I obtained with published *Sox2* WISH data and found them to appear fairly similar, for example (Takemoto et al., 2011; Wood and Episkopou, 1999; Wymeersch et al., 2016; Yoshida et al., 2014).

An alternative approach would have been to use RNAscope (Wang et al., 2012) to detect *Sox2* mRNA. This method works similar to WISH, but with a much higher sensitivity and specificity. Therefore, it would help to determine if *Sox2* mRNA is truly absent from the CNH, or if its concentration is simply too low to be detected via WISH. However, due to time constraints I was not able to perform this experiment yet.

3.3.5.2 Sox2/T expression – critique of the literature

So what is the explanation for the discrepancy between Sox2 mRNA and protein expression? After reviewing the literature on embryonic Sox2/T mRNA expression, I noticed that almost all papers on NMPs, including those in non-mammalian species, showed whole embryos only and either no sections at all or sections through regions other than the NMP location. Nevertheless, the authors concluded that both markers have overlapping expression patterns (Martin and Kimelman, 2012; Olivera-Martinez et al., 2012; Takemoto et al., 2011; Taniguchi et al., 2017; Yoshida et al., 2014). I only found two papers which actually included sections showing the same pattern I observed: In Figure 3A of the paper published by Wymeersch and colleagues, the authors performed double *in situ* hybridisation in E8.5 and E9.5 mouse embryos against both Sox2 and *T* (Wymeersch et al., 2016). Although the authors drew a different conclusion, the sections show that Sox2 mRNA expression is restricted to the neuroepithelium at both stages. Similarly, Delfino-Machin and colleagues performed WISH for Sox2 and *T* in the chick embryo at various developmental stages as shown in Figure 1 of their paper (Delfino-Machin et al., 2005). Transverse sections reveal that Sox2 mRNA is expressed in the neuroepithelium only. Moreover, they also show that *T* mRNA is expressed both in the tail bud mesoderm and the neuroepithelium from Hamburger and Hamilton Stage 8 onwards, similar to what I observed in WT mouse embryos at E8.5. This discovery has some important implications: Since *T* mRNA is expressed in the ventral domain of the forming neuroepithelium, it is no surprise that lineage tracing *T*-expressing cells from E8.5 onwards led to substantial contribution of labelled cells to the neural tube. In other words, the phenotype which has so far been attributed to the NMPs could actually be caused – to some extent or entirely – by *T*-expressing cells in the neuroepithelium.

But how does this fit with Sox2 protein expression in the CNH? Studies in the early mouse embryo and in cancer stem cells have shown that Sox2 protein is very stable. Depending on the system in which it is studied, Sox2 protein can persist for ~ 40 – 48 h, or even longer (Avilion et al., 2003; Ji et al., 2018; Lee et al., 2015; Luo et

al., 2011). Therefore, Sox2 protein expression in the CNH presumably stems from the epiblast, a Sox2-positive structure from which the germ layers arise during gastrulation (Wood and Episkopou, 1999). In this context it is also important to remember that there is no functional data suggesting that NMPs express Sox2. The immunostaining only suggests that some cells in the posterior neuropore express very low levels of Sox2, but there is no proof that these cells actually are NMPs. Moreover, it is not clear if the protein detected is functional or not. However, Sox2 protein stability is well-studied and therefore, it is reasonable to assume, that some (or all) of the Sox2 protein in the CNH in E9.5 embryos date from the epiblast.

3.3.5.2 Conclusion

The fact that Sox2 mRNA cannot be detected in the CNH, the NMP location, is consistent with the results from my lineage tracing experiments, which showed that Sox2-expressing cells in the post-gastrulation embryo give rise to the neuroepithelium, but only to a negligible extent to paraxial mesoderm. Consequently, if Sox2 is deleted in all *T*-expressing cells, then this should affect the neural tube only, but not somite formation. This experiment will be discussed next.

3.3.6 Results: Deleting Sox2 in the T-expressing lineage

3.3.6.1 Deleting Sox2 in the T-expressing lineage yields embryos with a Sox2-negative neural tube and normal paraxial mesoderm

To delete Sox2 specifically in T-expressing cells, I first crossed the $T^{CreERT2/+}$ driver with the Sox2^{fl/fl} line to obtain $T^{CreERT2/+}; Sox2^{fl/+}$ males, which were then crossed again with Sox2^{fl/fl} females to produce litters which contain the following genotypes: (i) $T^{+/+}; Sox2^{fl/+}$, (ii) $T^{+/+}; Sox2^{fl/fl}$, (iii) $T^{CreERT2/+}; Sox2^{fl/+}$, and (iv) $T^{CreERT2/+}; Sox2^{fl/fl}$ (**Figure 22A**).

To assess the effect of Sox2 depletion on the neural tube, I performed WISH for Sox2 in n = 4 embryos per genotype at E9.5 (**Figure 22B**). Sox2 mRNA expression was slightly reduced in the posterior neuropore of $T^{CreERT2/+}; Sox2^{fl/+}$ embryos (n = 4/4), and was absent from this region in $T^{CreERT2/+}; Sox2^{fl/fl}$ embryos (n = 4/4). WISH for the pre-somitic mesoderm marker *Dll1* and the sclerotome marker *Pax1* did not reveal any discernible differences in mesoderm formation between the different genotypes (**Figure 22C**; n = 4 embryos per genotype).

Since these experimental conditions affected only a short part of the caudal region, I crossed the same lines again but induced CreERT2 activity by tamoxifen injection at E7.5 and collected the embryos 48 h later at E9.5 (**Figure 23A**). This was expected to result in a more pronounced phenotype. As the NMPs are believed to be required for body axis elongation, I counted their somite number (**Figure 23B**), measured their body length from the forebrain along their dorsal side to the tail bud tip (**Figure 23C**), and determined the size of their posterior neuropore (**Figure 23D**). If there was any difference between the various genotypes, it would be most obvious comparing $T^{CreERT2/+}; Sox2^{fl/fl}$ embryos with those negative for CreERT2. Therefore, I pooled the data from $T^{+/+}; Sox2^{fl/+}$ (n = 19) and $T^{+/+}; Sox2^{fl/fl}$ embryos (n = 22), and compared it with the values obtained from $T^{CreERT2/+}; Sox2^{fl/fl}$ embryos (n = 20) using an unpaired Student's *t*-test (two-sided). Yet, none of the three parameters was significantly different between the two groups, suggesting normal growth in embryos lacking Sox2 in the T domain (see **Figure 23B – D** for the *p*-values). Note that none of the embryos had a neural tube defect or any other morphological abnormality.

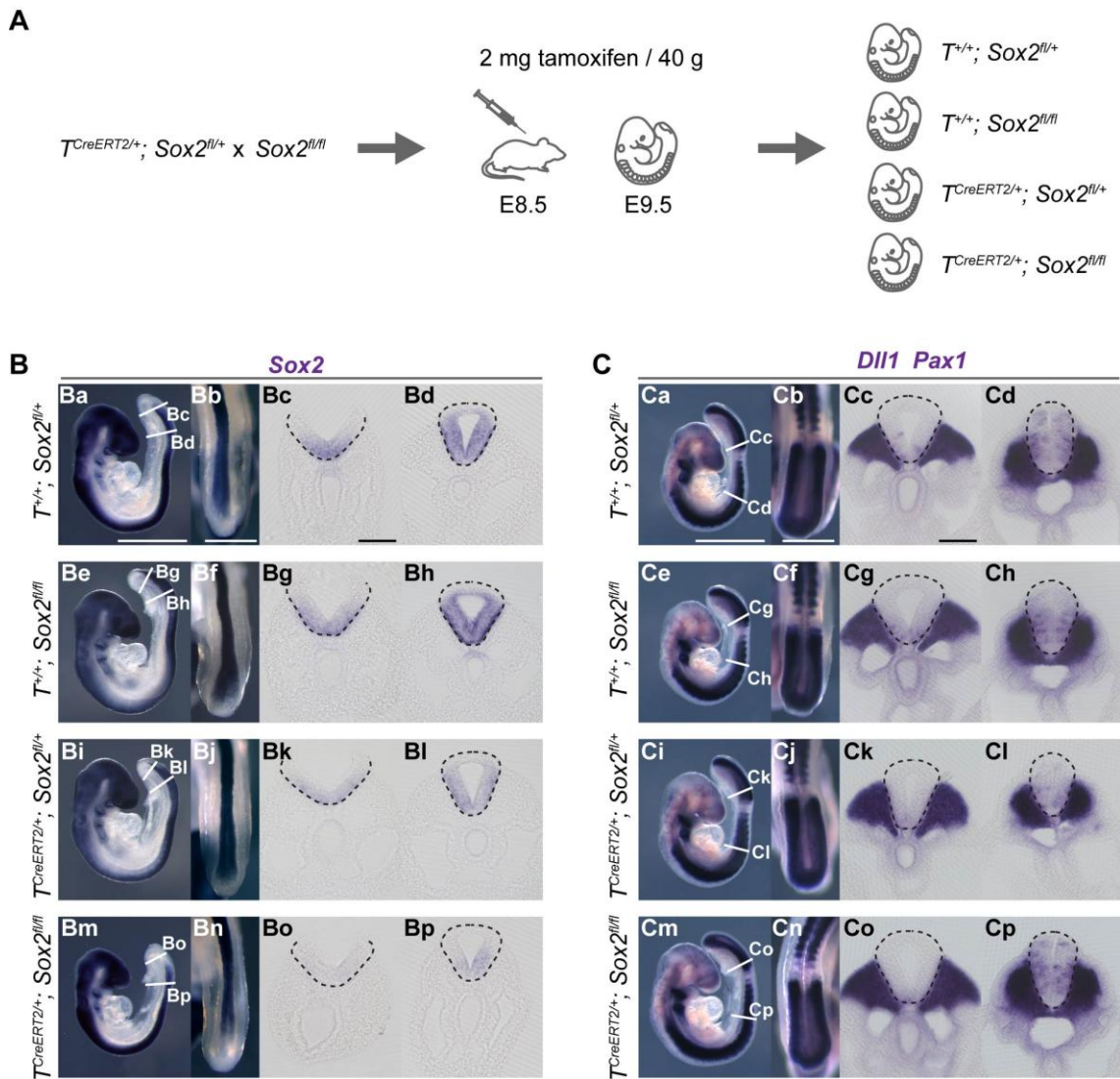


Figure 22. Deleting *Sox2* in *T*-expressing cells results in reduced *Sox2* mRNA levels in the posterior neuropore, but no visible mesoderm defects.

(A) Breeding strategy and conditions for induction of CreERT2 activity. **(B)** WISH for *Sox2* ($n = 4$ embryos per genotype). *Sox2* expression was clearly down-regulated in the posterior neuropore of $T^{CreERT2/+}; Sox2^{fl/fl}$ embryos ($n = 4/4$), and to a lesser extent in $T^{CreERT2/+}; Sox2^{fl/+}$ embryos ($n = 4/4$). **(C)** WISH for *Dll1* and *Pax1* ($n = 4$ embryos each) indicates comparable expression between all embryos and genotype. Black dashed lines indicate the basal border of the neuroepithelium. Scale bars, 500 μm in Ba – Bb, Ca – Cb; 100 μm in Bc, Cc. Adapted from (Mugele et al., 2018).

However, *Sox2* mRNA expression in the neural tube was strongly reduced in the closed region and completely absent from the posterior neuropore in $n = 4/4$ $T^{CreERT2/+}; Sox2^{fl/fl}$ embryos (**Figure 23Em – p**). Again, expression levels of *Dll1* and *Pax1* mRNA were comparable between all genotypes without any noticeable differences (**Figure 23F**; $n = 4$ embryos per genotype), suggesting that the absence of *Sox2* does not affect mesoderm formation.

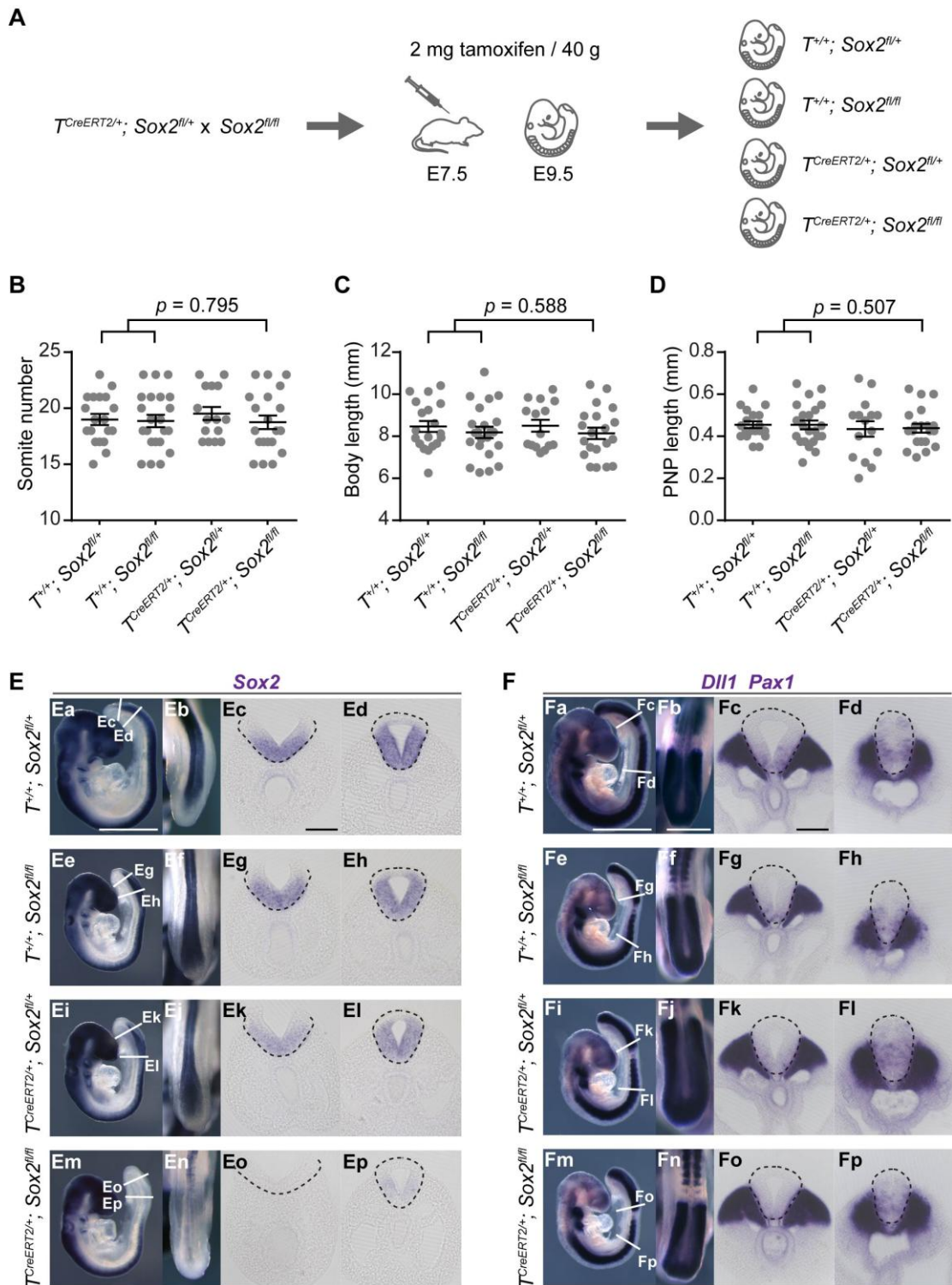


Figure 23. $T^{CreERT2/+}; Sox2^{fl/fl}$ embryos form a Sox2-negative neural tube, but axis elongation and paraxial mesoderm are not affected.

(A) Schematic of the breeding strategy and conditions for induction of CreERT2 activity. (B) Somite number, (C) body length, and (D) posterior neuropore length were not significantly different between $T^{CreERT2/+}; Sox2^{fl/fl}$ embryos and CreERT2-negative embryos. Data in B, C, and D shown as mean \pm SEM including the individual data points, with $n = 19$ $T^{+/+}; Sox2^{fl/+}$ embryos, $n = 22$ $T^{+/+}; Sox2^{fl/fl}$ embryos, $n = 15$ $T^{CreERT2/+}; Sox2^{fl/+}$ embryos, and $n = 20$ $T^{CreERT2/+}; Sox2^{fl/fl}$ embryos. Unpaired Student's *t*-test, 2-sided. (E) WISH for *Sox2* ($n = 4$ embryos per genotype). $T^{CreERT2/+}; Sox2^{fl/fl}$ embryos formed a Sox2-negative neural tube, which, however, does not exhibit any morphological abnormalities. (F) WISH for the pre-somitic mesoderm marker *Dll1* and the sclerotome marker *Pax1* ($n = 4$ embryos each) show normal mesoderm formation in all embryos and genotypes. Black dashed lines indicate the basal border of the neuroepithelium. PNP, posterior neuropore. Scale bars, 500 μ m in Ba – Bb, Ca – Cb; 100 μ m in Bc, Cc. Adapted from (Mugele et al., 2018).

3.3.6.2 $T^{CreERT2/+}; Sox2^{fl/fl}$ embryos develop a morphologically normal neural tube

To further characterise the neural tube in $T^{CreERT2/+}; Sox2^{fl/fl}$ embryos, I immuno-stained transverse sections for Sox1, Sox2, and Sox3. The embryos were treated with tamoxifen at E7.5 and collected at E9.5. I compared their expression with E9.5 WT embryos (**Figure 24**). Together with Sox2, Sox1 and Sox3 constitute the sub-family of SoxB1 transcription factors. They share a high degree of sequence homology and show overlapping expression patterns in the developing central nervous system (Collignon et al., 1996; Wood and Episkopou, 1999), suggesting possible functional redundancy. To ensure comparability, I stained and imaged all sections in parallel and used the same exposure times for both WT and $T^{CreERT2/+}; Sox2^{fl/fl}$ embryos. The sections from WISH for Sox2 shown in **Figure 24Ac, Ae, Bc, and Be** correspond to the same axial levels which were immuno-stained for Sox1 – 3 in **Figure 24Ad, Af, Bd, and Bf**, respectively. Since all three Sox antibodies were raised in the same species, I had to stain Sox1 – 3 separately on consecutive sections taken from the same embryo.

In contrast to WT embryos, which express Sox2 uniformly throughout the neuroepithelium and also in the CNH, Sox2 expression is significantly down-regulated in both the CNH and the closed neural in $n = 5/5$ $T^{CreERT2/+}; Sox2^{fl/fl}$ embryos. Although some cells in the neural tube still express Sox2 at a low level, others are completely Sox2-negative, resulting in a blotchy pattern (**Figure 24Bf**; $n = 5/5$ embryos). Sox1 was absent from the caudal end in both WT ($n = 5/5$) and $T^{CreERT2/+}; Sox2^{fl/fl}$ embryos ($n = 5/5$). To confirm that the Sox1 antibody worked, I collected brain sections from the same embryos as a positive control, which I stained simultaneously on the same slide (insets in **Figure 24Ad** and **Bd**). Similar to Sox2, Sox3 is expressed in the CNH and the neuroepithelium in WT embryos and it appears to be up-regulated in $n = 5/5$ $T^{CreERT2/+}; Sox2^{fl/fl}$ embryos compared to WT.

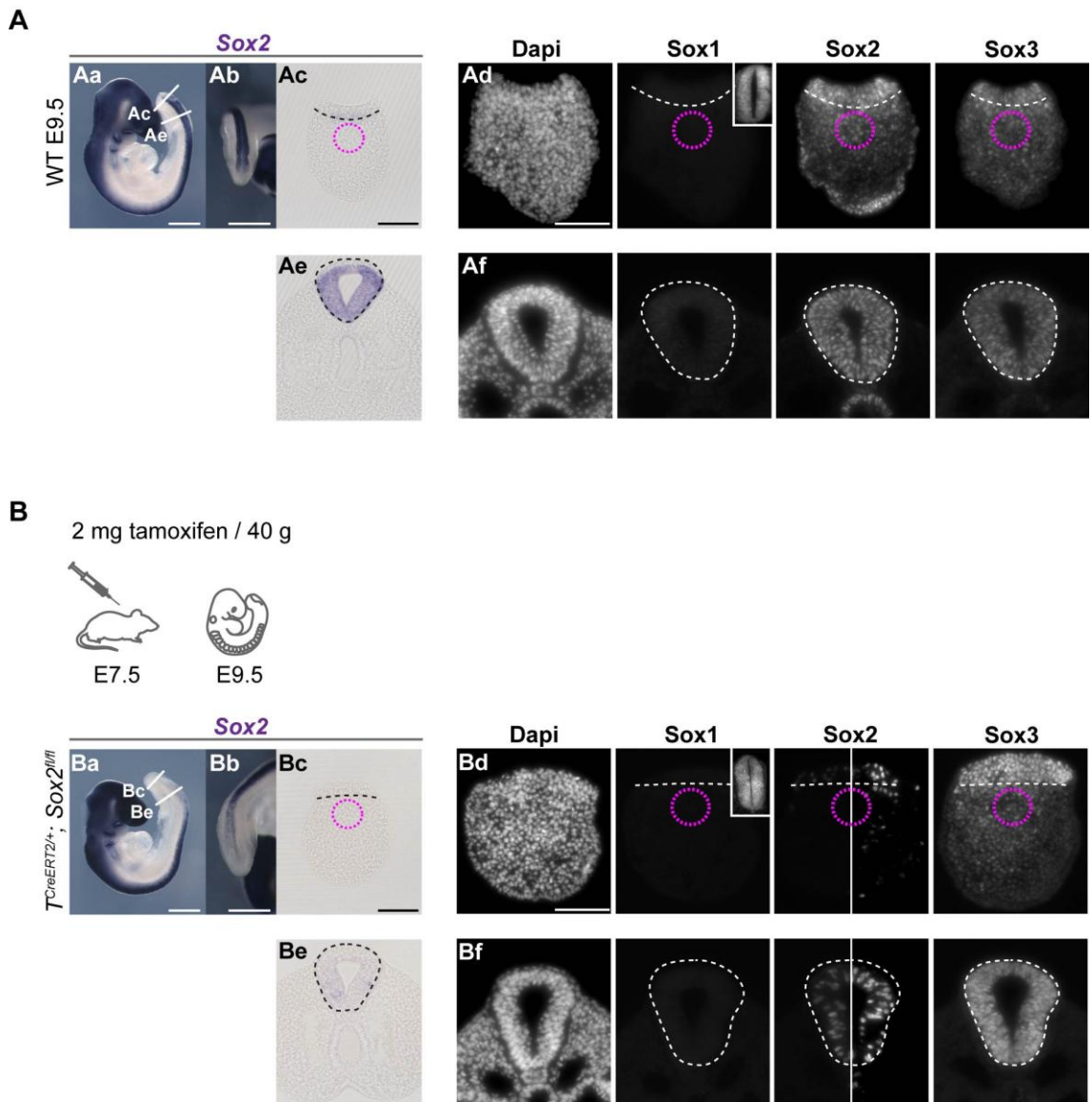


Figure 24. Sox2 protein levels are strongly reduced in the neural tube of $T^{CreERT2/+}; Sox2^{fl/fl}$ embryos. **(A)** WISH for Sox2 (n = 3 embryos; Aa – Ac, Ae) and immunostaining for Sox1, Sox2, and Sox3 in E9.5 WT embryos (n = 5 embryos; Ad, Af). **(B)** WISH for Sox2 (n = 4 embryos; Ba – Bc, Be) and immunostaining for Sox1, Sox2, and Sox3 in $T^{CreERT2/+}; Sox2^{fl/fl}$ embryos, which were treated with tamoxifen at E7.5 and collected at E9.5 (n = 5 embryos; Bd, Bf). Sox2 protein is markedly reduced in the tail bud and neural tube in n = 5/5 $T^{CreERT2/+}; Sox2^{fl/fl}$ embryos compared to WT. In Bd and Bf, Sox2 expression shown on the left hand side was imaged with the same exposure time as in Ad and Af. The right hand side of the image shows the other half of the same sections imaged with a higher exposure time revealing that Sox2 is not completely down-regulated. Sox1 is not expressed in the caudal end of neither WT nor $T^{CreERT2/+}; Sox2^{fl/fl}$ embryos (the insets show a brain section from the same embryos that were stained and imaged in parallel, confirming that the staining for Sox1 worked). Sox3 expression appears to be up-regulated in n = 5/5 $T^{CreERT2/+}; Sox2^{fl/fl}$ embryos compared to sections from WT. Pink circles in Ac – Ad and Bc – Bd outline the CNH. Black dashed lines in Ac, Ae, Bc, and Be, and white dashed lines in Ad, Af, Bd, and Bf outline the neuroepithelium. Scale bars, 500 μ m in Aa – Ab, Ba – Bb; 100 μ m in Ac – Ad, Bc – Bd. Adapted from (Mugele et al., 2018).

To achieve maximum recombination beyond the half-life of Sox2 and to address whether the resulting embryos form normal neural tubes, I crossed the same mice and

injected tamoxifen into the pregnant female at E7.5, E8.5, and E9.5. I collected the embryos at E10.5 and compared them with E10.5 WT embryos (**Figure 25**). The sections shown in **Figure 25Ac** and **Bc** were taken from the same axial level as the sections from WISH for Sox2 in **Ab** and **Bb**. All in all, I collected 15 $T^{CreERT2/+}; Sox2^{fl/fl}$ embryos and none of them displayed any neural tube defects or other morphological abnormalities.

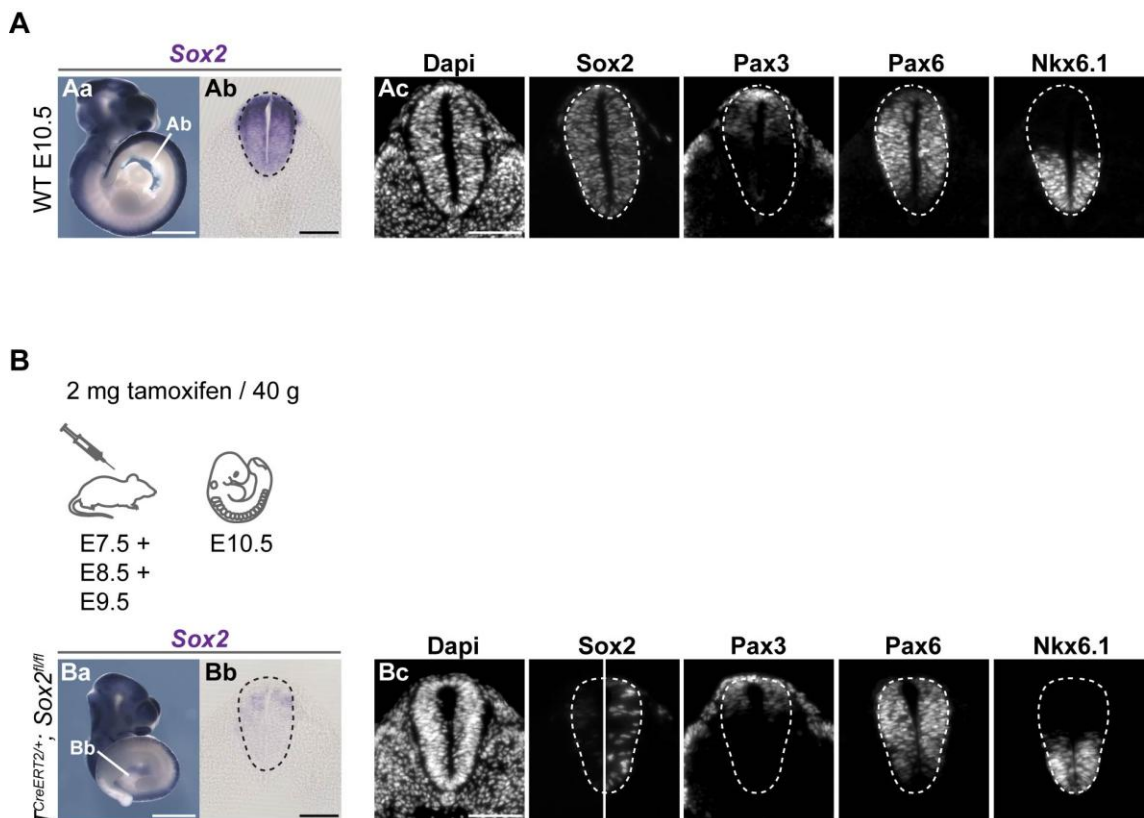


Figure 25. $T^{CreERT2/+}; Sox2^{fl/fl}$ embryos form a normal neural tube in the absence of Sox2.

(A) WISH for Sox2 (n = 3 embryos; Aa – Ab) and immunostaining for Pax3, Pax6 and Nkx6.1 in E10.5 WT embryos (n = 3 embryos; Ac). (B) WISH for Sox2 (n = 3 embryos; Ba – Bb) and immunostaining for Pax3, Pax6 and Nkx6.1 in $T^{CreERT2/+}; Sox2^{fl/fl}$ embryos, which were treated with tamoxifen at E7.5, E8.5, and E9.5, and collected at E10.5 (n = 4 embryos; Bc). Sox2 protein and mRNA levels are clearly down-regulated, yet, both were still detectable at low levels in n = 4/4 $T^{CreERT2/+}; Sox2^{fl/fl}$. In Bc, Sox2 expression shown on the left hand side was imaged with the same exposure time as in Ac. The right hand side of the image shows the other half of the same sections imaged with a higher exposure time. Black dashed lines in Ab and Bb, and white dashed lines in Ac and Bc indicate the basal border of the neuroepithelium. Scale bars, 1 mm in Aa and Ba; 100 μm in Ab – Ac, Bb – Bc. Adapted from (Mugele et al., 2018).

Both Sox2 mRNA and protein expression were further reduced compared to the results shown in **Figure 24**, yet both were still detectable (**Figure 25B**; n = 3/3 embryos for

WISH and $n = 4/4$ embryos for immunostaining). To examine whether $T^{CreERT2/+}; Sox2^{fl/fl}$ embryos form a normal neural tube, I immuno-stained them for Pax3 to label the dorsal domain of the neural tube. In addition I chose Pax6, which is expressed in the lateral neural tube, and Nkx6.1, which marks the ventral and ventro-lateral neural tube. All markers were stained together in the same section. $T^{CreERT2/+}; Sox2^{fl/fl}$ embryos ($n = 4/4$) formed all three domains in the appropriate positions, in spite of low Sox2 levels, and without any discernible differences in expression compared with WT embryos ($n = 3$).

3.3.6.3 Cell fate decision of *T*-positive cells in $T^{CreERT2/+}; Sox2^{fl/+}$ embryos

To address whether lower levels of Sox2 impact on cell fate decision in *T*-expressing cells, I crossed $T^{CreERT2/+}; Sox2^{fl/+}$ mice with the $Rosa26^{EYFP/EYFP}$ reporter line. CreERT2 activity was induced by tamoxifen injection at E8.5 and the embryos were collected 24 h later. This cross resulted in litters containing $T^{CreERT2/+}; Sox2^{+/+}; Rosa26^{EYFP/+}$ embryos (i.e. with normal Sox2 levels) and $T^{CreERT2/+}; Sox2^{fl/+}; Rosa26^{EYFP/+}$ embryos (i.e. with reduced Sox2 levels). The reporter allowed me to track descendants of *T*-positive cells and to quantify whether they ended up in the neural tube or whether they colonised the paraxial mesoderm. After collecting the litters at E9.5, I sectioned the embryos ($n = 12$ per genotype) and immuno-stained for GFP, to enhance the signal of the reporter, as well as the neural tube marker Sox2 and the pre-somitic mesoderm marker Tbx6 (**Figure 26A**). For the analysis I randomly selected five transverse sections per embryo taken from the region between the CNH and the closure point of the neural tube. Double-positive cells were counted using an in-house Fiji macro which is described in the Methods section. *T*-expressing cells which committed towards the neural lineage should co-express Sox2 and GFP. On the other hand, *T*-positive cells which adopted a mesodermal fate should be Tbx6/GFP double-positive. Note, to ensure the results were not distorted by Sox2-expressing cells in the tail bud, I only counted Sox2/GFP double-positive cells in the forming neuroepithelium. I compared the ratio of Sox2/GFP double-positive cells relative to the number of Tbx6/GFP double-positive cells between $T^{CreERT2/+}; Sox2^{+/+}; Rosa26^{EYFP/+}$ and $T^{CreERT2/+}; Sox2^{fl/+};$

Rosa26^{EYFP/+} embryos using an unpaired, two-sided Student's *t*-test (**Figure 26B**). The high *p*-value indicates that there is no evidence for a difference in the ratio of double-positive cells between both genotypes.

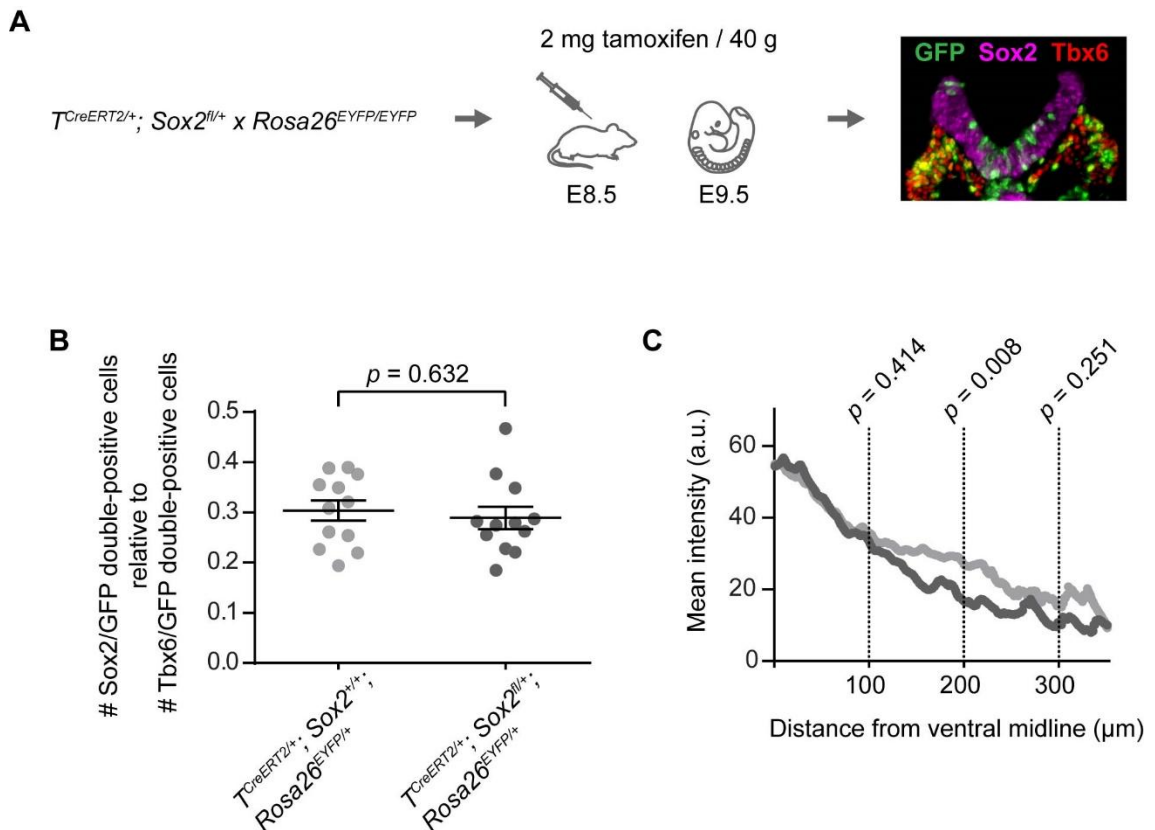


Figure 26. Down-regulation of Sox2 does not affect cell fate decision in *T*-expressing cells.

(A) Schematic of the breeding strategy and conditions for inducing CreERT2 activity. **(B)** Comparison of Sox2/GFP double-positive cells relative to Tbx6/GFP double-positive cells in *T*^{CreERT2/+}; *Sox2*^{+/+}; *Rosa26*^{EYFP/+} and *T*^{CreERT2/+}; *Sox2*^{fl/+}; *Rosa26*^{EYFP/+} embryos. Cell counts were obtained from five sections per embryo and twelve embryos per genotype. Data shown as mean \pm SEM including the individual data points. Unpaired Student's *t*-test, two-sided. **(C)** Distribution of GFP-positive cells in the forming neural tube of *T*^{CreERT2/+}; *Sox2*^{+/+}; *Rosa26*^{EYFP/+} (light grey; *n* = 12 embryos) and *T*^{CreERT2/+}; *Sox2*^{fl/+}; *Rosa26*^{EYFP/+} embryos (dark grey; *n* = 12 embryos). Data shown as mean; two-sided, unpaired Student's *t*-test comparing mean fluorescence intensity at 100 μm , 200 μm and 300 μm distance from the ventral midline.

In addition to the cell counts, I also investigated how GFP-positive cells spread in the neuroepithelium using the same sections from the previous analysis. The DiO-labelling experiments described in Chapter 3.1 revealed that different domains of the neural tube derive from separate locations in the E8.5 embryo. To clarify whether Sox2 down-regulation differentially affects certain parts of the forming neural tube, I measured the

mean fluorescence intensity along the neuroepithelium in the GFP channel (**Figure 26C**). Please refer to the Methods section for details on the analysis. I compared the mean intensity between $T^{CreERT2/+}; Sox2^{+/+}; Rosa26^{EYFP/+}$ (light grey) and $T^{CreERT2/+}; Sox2^{fl/+}; Rosa26^{EYFP/+}$ embryos (dark grey) using an unpaired, two-tailed Student's *t*-test. At 100 μ m and 300 μ m distance from the ventral midline, the difference in mean fluorescence intensity between both genotypes was not significant. Yet, at 200 μ m distance, which corresponds to the lateral neuroepithelium, $T^{CreERT2/+}; Sox2^{fl/+}; Rosa26^{EYFP/+}$ embryos had a significantly lower mean intensity compared to $T^{CreERT2/+}; Sox2^{+/+}; Rosa26^{EYFP/+}$ embryos.

3.3.6.4 Tracing NMPs in $T^{CreERT2/+}; Sox2^{fl/fl}$ embryos

To test how NMPs behave in $T^{CreERT2/+}; Sox2^{fl/fl}$ embryos, I crossed $T^{CreERT2/+}; Sox2^{fl/+}$ with $Sox2^{fl/fl}$ mice, injected tamoxifen at E7.5 into the pregnant dam, and collected the litters at E8.5. Similar to the experiments in Chapter 3.1, DiO was injected into CLE region 1 and the embryos were cultured for 24 h until E9.5 to assess the resulting dye pattern (**Figure 27A**). To ensure consistency, I only included embryos which had 1 – 7 somite pairs at collection. After 24 h in culture, the embryos were relatively short considering their age, even though their somite number was normal for E9.5 embryos (**Figure 27B**; both embryos depicted here had 17 somite pairs). This is likely due to the combined stress caused by tamoxifen and embryo culture. Indeed, all embryos were affected, independent of their genotype.

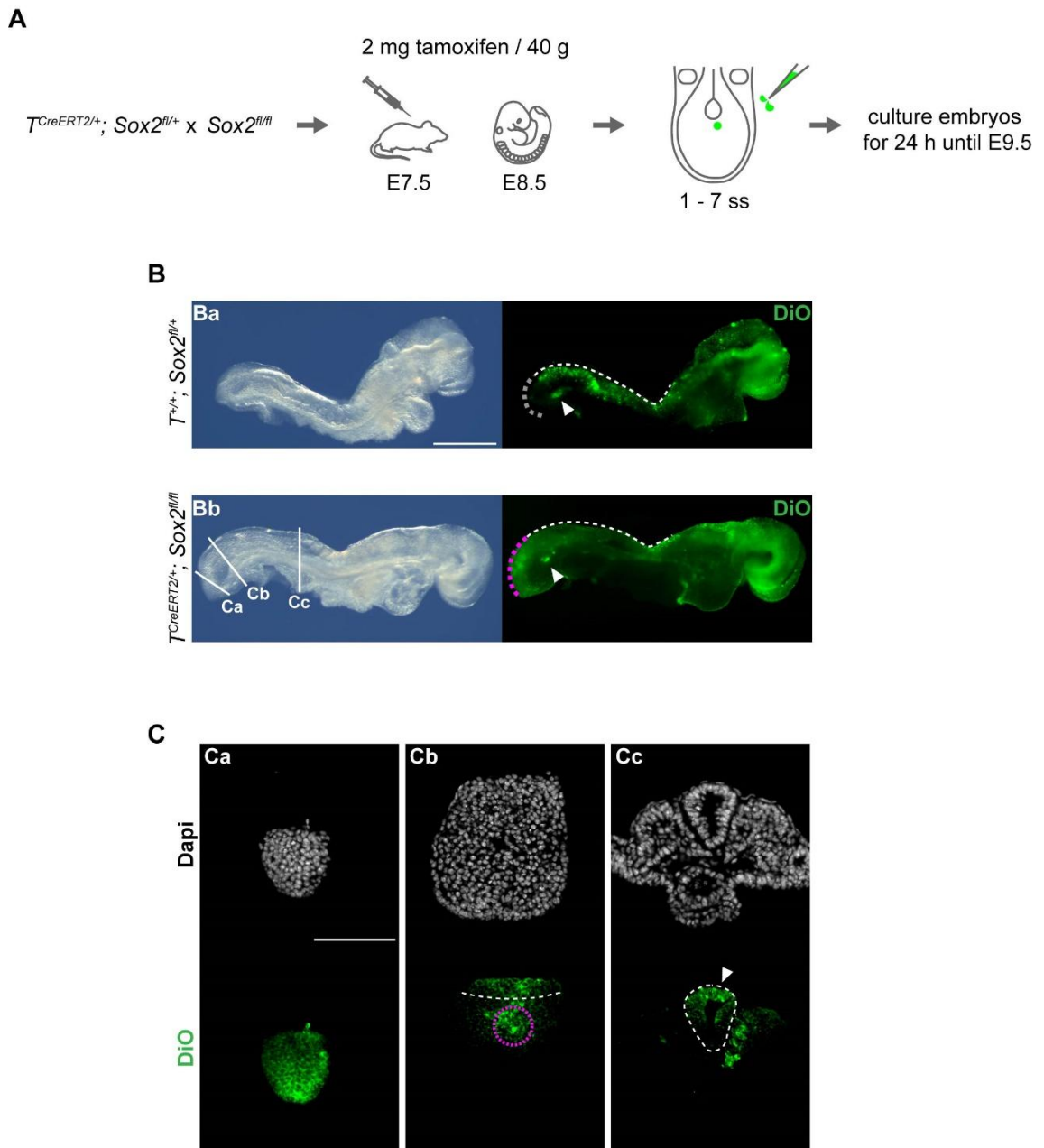


Figure 27. Cells traced from region 1 of the CLE in $T^{CreERT2/+}; Sox2^{fl/fl}$ embryos show the characteristic NMP pattern, except for DiO accumulation in the tail bud tip.

(A) Schematic showing the experimental procedure, breeding strategy, and conditions for inducing CreERT2 activity. (B) Both $T^{CreERT2/+}; Sox2^{fl/+}$ embryos (n = 8/9) and CreERT2-negative embryos (n = 6/6) displayed the typical NMP pattern, including contribution to neural tube and paraxial mesoderm along the body axis (white dashed lines in Ba, Bb) and presence of DiO-positive cells in the CNH (white arrowheads in Ba, Bb). $T^{CreERT2/+}; Sox2^{fl/fl}$ embryos also showed DiO-positive cells accumulated at the tail bud end (pink dotted line in Bb; n = 8/9), unlike CreERT2-negative embryos (grey dotted line in Ba; n = 0/6). (C) Transverse sections through a $T^{CreERT2/+}; Sox2^{fl/fl}$ embryo showing DiO-labelled cells in the tail bud tip (Ca), in the CNH (pink circle in Cb), the dorsal neural tube (white arrowhead in Cc), and paraxial mesoderm (lateral to the neural tube in Cc). White dashed lines in Cb – Cc outline the neuroepithelium. Scale bars, 500 μ m in Ba; 100 μ m in Ca. Adapted from (Mugele et al., 2018).

I compared $T^{CreERT2/+}; Sox2^{fl/fl}$ embryos (n = 9) with all CreERT2-negative embryos (n = 6) and found that 8/9 displayed the typical NMP pattern as described in Chapter 3.1:

DiO-positive cells were retained in the CNH (white arrowhead in **Figure 27Bb** and pink circle in **Cb**) and contributed to both dorsal neural tube and somites along the body axis (**Figure 27Cc**). However, $n = 8/9$ $T^{CreERT2/+}; Sox2^{fl/fl}$ embryos had DiO-positive cells accumulated in the tail bud tip (pink dashed line in **Figure 27Bb** and **Figure 27Ca**), unlike the CreERT2-negative embryos (grey dashed line in **Figure 27Ba**; $n = 0/6$).

3.3.7 Discussion: Deleting Sox2 in the T-expressing lineage

3.3.7.1 Sox2 is not expressed in NMPs

If NMPs were *Sox2/T* double-positive, deleting *Sox2* in *T*-expressing cells in the post-gastrulation embryo should compromise both neural tube and somite formation and thereby disrupt axis elongation. Yet, the embryos did not display any of these defects. Paraxial mesoderm and body axis extension were unaffected. The embryos developed a morphologically normal neural tube, which, surprisingly, was negative for *Sox2* mRNA and protein, except for a few sparse cells which expressed protein and mRNA at low levels. This suggests that *Sox2*-depletion in the *T*-expressing lineage exclusively targets cells with a neural fate.

3.3.7.2 Sox2 is not required for neural tube formation

In the developing embryo, *Sox2* mRNA and protein are expressed throughout the neural plate and the forming neural tube and expression declines as the cells differentiate and become post-mitotic (Collignon et al., 1996; Uwanogho et al., 1995; Wood and Episkopou, 1999; Zappone et al., 2000). Studies *in vivo* and *in vitro* have shown that *Sox2* knock-down in neural stem and progenitor cells interferes with their ability to self-renew and forces them to exit the cell cycle (Cavallaro et al., 2008; Gomez-Lopez et al., 2011; Graham et al., 2003; Taranova et al., 2006). It is therefore surprising that neural tube formation is unaffected in $T^{CreERT2/+}; Sox2^{fl/fl}$ embryos, especially since *Sox2* knock-out is linked to severe phenotypes. *Sox2*-deficient embryos die soon after implantation (Avilion et al., 2003). And even when *Sox2* is specifically depleted in the brain of post-gastrulation embryos, they still die before birth

(Miyagi et al., 2008). Notably, these embryos had increased levels of *Sox3* mRNA in their brains, which probably attenuated the effect of *Sox2* knock-out, although it did not prevent early lethality.

$T^{CreERT2/+}; Sox2^{fl/fl}$ embryos formed a neural tube with significantly reduced *Sox2* mRNA and protein expression. Yet, *Sox2* knock-out neither disrupted neural tube closure, nor the formation of the ventral, lateral, and dorsal gene expression domains, as judged by *Nkx6.1*, *Pax6*, and *Pax3* respectively. Moreover, *Sox2* knock-down in $T^{CreERT2/+}; Sox2^{fl/+}; Rosa26^{EYFP/+}$ embryos did not significantly influence cell fate decision in *T*-expressing cells. On the other hand, I observed that GFP-labelled cells were underrepresented in the lateral and dorso-lateral neural tube in these embryos. Although this difference was statistically significant, the actual effect size was small, perhaps because *Sox2* was not completely depleted in these experiments. Nevertheless, when I labelled NMPs in region 1 of the CLE in $T^{CreERT2/+}; Sox2^{fl/fl}$ embryos and cultured these for 24 h, the resulting phenotype was very similar to the NMP pattern in WT embryos. The only difference was that DiO-positive cells were accumulated in the tip of the tail bud. My DiO-labelling experiments presented in Chapter 3.1 (**Figure 6**) showed that cells in the caudal-most region of the embryo exclusively give rise to mesoderm. Therefore, the presence of DiO-labelled cells in the tail bud tip of $T^{CreERT2/+}; Sox2^{fl/fl}$ embryos suggests that some NMPs are no longer able to form neural tissue and therefore maintain a mesodermal fate.

All in all, these experiments demonstrate that, surprisingly, *Sox2* deletion in the *T*-expressing lineage does not disrupt embryonic development. Yet, small deviations in NMP behaviour and the colonisation pattern of the neural tube by *T*-positive cells indicate that the embryos need to compensate for the loss of *Sox2*. However, the downside of any compensatory mechanism is that it makes it more difficult to draw conclusions on the role of *Sox2* in neural tube formation. A potential candidate for this role is *Sox3*. Apart from the overlapping expressing pattern and sequence similarities between *Sox2* and *Sox3*, *Sox3* has been shown to be up-regulated in embryonic mouse brains following conditional *Sox2* knock-out (Miyagi et al., 2008). In line with

this, Sox3 protein levels appeared to be increased in the neural tube, although quantitative conclusions from immunostainings need to be treated with caution.

Another noteworthy observation from the experiments in this chapter is that I was not able to completely delete Sox2 mRNA or protein expression in the neural tube. Even after multiple tamoxifen injections over three days – which should have saturated the system – I consistently detected Sox2 mRNA, but at low levels and only in a few cells. Similarly, protein was still detectable, although very weak and only in a fraction of cells in the neural tube, whereas most of them were Sox2-negative. This finding could be explained by incomplete recombination, i.e. that only one Sox2 allele was deleted in a subset of cells. This would explain why mRNA and protein are only detectable in a subset of cells and why expression is much weaker compared to WT embryos. The recombination rate could be improved by increasing the tamoxifen concentration, however, due to drug-related side effects which limit the dose that can be administered, it is generally not possible to achieve 100% recombination. Although insufficient recombination likely contributed to the incomplete down-regulation of Sox2 mRNA and protein, another possible explanation is that a fraction of those cells which give rise to the neural tube is derived from T-negative cells. This is further supported by the patchy pattern observed after Sox2 deletion, but also by the finding that Sox2 mRNA and protein consistently persisted along the body axis and were detectable in every single section examined.

3.3.7.3 Future work

Following up on Sox2-depletion, it would be interesting to test whether $T^{CreERT2/+}; Sox2^{fl/fl}$ embryos are able undergo later stages of central nervous system development and survive until birth following multiple tamoxifen injections. Although Sox3 was found to be up-regulated in mouse embryos which had Sox2 specifically deleted in their brains (Miyagi et al., 2008), they did not survive. This underpins the crucial role of Sox2 in the development of the central nervous system, and therefore, it should be investigated in $T^{CreERT2/+}; Sox2^{fl/fl}$ embryos as well. Also, knock-down of both Sox2 and

Sox3 in the *T*-expressing lineage would clarify whether *Sox3* truly compensates for the loss of *Sox2*. If this is the case, the cross should yield a more pronounced phenotype. Yet, it should affect the neural tube only since *Sox2* and *Sox3* are not expressed in the mesoderm.

In addition, it might be worth reversing the knock-out experiment by deleting *T* in the *Sox2*-expressing lineage. My results indicate that *Sox2* acts downstream of *T* in the neuroepithelium and since *Sox2*-positive cells give rise to neural tissue only, these embryos should develop normally without any axial, neural tube, or mesoderm defects. However, it is scientifically challenging to prove the absence of an effect beyond doubt. So unless these embryos display an obvious phenotype, which is unlikely due to the reasons given above, this experiment may produce inconclusive data.

Last but not least, it would be informative to repeat the experiment on cell fate decision in *T*-expressing cells (shown in **Figure 26**) in $T^{CreERT2/+}; Sox2^{fl/fl}; Rosa26^{EYFP/+}$ embryos. Due to time constraints, I was only able to analyse $T^{CreERT2/+}; Sox2^{fl/+}; Rosa26^{EYFP/+}$, since I would have had to cross the $T^{CreERT2/+}; Sox2^{fl/+}$ line twice with the $Rosa26^{EYFP/EYFP}$ reporter to obtain $T^{CreERT2/+}; Sox2^{fl/+}; Rosa26^{EYFP/EYFP}$ mice, which I would have then crossed with the $Sox2^{fl/fl}$ mice to generate $T^{CreERT2/+}; Sox2^{fl/fl}; Rosa26^{EYFP/+}$ embryos. The breeding would have taken more than five months and since I had reached the end of my PhD, I was not able to do this experiment. However, since $T^{CreERT2/+}; Sox2^{fl/fl}$ embryos do not show any morphological defects and form a normal neural tube, they most likely counterbalance *Sox2* depletion, for example by up-regulating *Sox3*. Therefore, any effect on cell fate decision in *T*-expressing cells in these embryos is likely to be small. This is also supported by the results from the NMP labelling experiments in $T^{CreERT2/+}; Sox2^{fl/fl}$ embryos. By and large, these embryos exhibited a normal NMP pattern, except for some DiO-positive cells which were redirected to the caudal tip.

3.3.7.4 Conclusion

The experiments described in this chapter revealed that, surprisingly, *Sox2* is not required for the neural tube to form. In addition, deleting *Sox2* in the *T*-expressing lineage further supported the hypothesis that NMPs do not express *Sox2*, since mesoderm and axis elongation were unimpaired in these embryos. Hence, I have provided three independent lines of evidence which support the idea of *Sox2*-negative NMPs: First, the lineage tracing experiments revealed that *Sox2*-expressing cells give rise to neural tube but contribute only very infrequently to paraxial mesoderm in post-gastrulation embryos. Second, *Sox2* mRNA is not detectable the CNH, where NMPs are located. Finally, I showed that, in line with the previous experiments, *Sox2*-depletion in *T*-expressing cells resulted in clearly reduced *Sox2* mRNA and protein levels in the neural tube, but neither affected mesoderm formation nor axis elongation.

These findings are controversial and require extensive re-evaluation of the literature, since the majority of NMP papers define these cells based on *Sox2/T* co-expression. In the following chapter, I will discuss some of the key papers and how my results affect their conclusions. In addition, I will provide more evidence from the literature, which supports the hypothesis that NMPs are indeed *Sox2*-negative.

CHAPTER 4: THESIS DISCUSSION AND CONTROVERSY

4.1 Summary of results and new NMP model

The aim of this work was to dissect the role of NMPs in neural tube formation. For this purpose I combined classic developmental biology techniques, such as DiO-labelling, with modern approaches including laser-ablation and genetic lineage tracing.

My DiO-labelling experiments revealed that NMPs give rise to the dorsal and dorso-lateral domains of the neural tube. The ventral part, on the other hand, is derived from cells located in the NSB, the node, and directly rostral to the node. Although laser-ablation turned out to be less than ideal for studying NMP function, these experiments gave some new insights into their behaviour. Following ablation of the rostral-most CLE, cells located further caudally re-populated the NMP location and steadily provided cells for the extending body axis. This suggests that new NMPs may be continuously recruited to the rostral CLE and they do not arise just once early in development, as previously assumed (Henrique et al., 2015). Moreover, I used genetic tools to characterise *Sox2/T* double-positive cells, as the co-expression of both markers is considered a hallmark of NMPs. However, when I performed genetic lineage tracing of *Sox2*-expressing cells in post-gastrulation embryos, I stumbled across a phenotype which strongly suggests that *Sox2* is exclusively expressed in cells with a neural fate, except for a few sparse cells which ended up in the paraxial mesoderm. This was further substantiated by the finding that *Sox2* mRNA is undetectable in the CNH. In addition, depletion of *Sox2* in the *T*-expressing lineage after gastrulation resulted in reduced expression of *Sox2* mRNA and protein in the neural tube, but did not affect mesoderm formation. Based on this data, I propose an alternative NMP model as depicted in **Figure 28**: Lineage tracing *T*-expressing cells revealed that they colonise the dorsal neural tube, which is derived from the NMPs. In addition, *T* is strongly expressed both in CLE region 1 at E8.5 and the CNH at E9.5 (see **Figure 21**). This suggests that the dual-fated progenitors are *T*-positive. As they differentiate into pre-somitic mesoderm, they maintain *T* expression and activate down-stream targets, such

as *Tbx6*. However, when the NMPs adopt a neural fate and enter the neural tube, they start expressing *Sox2*, and simultaneously down-regulate *T*.

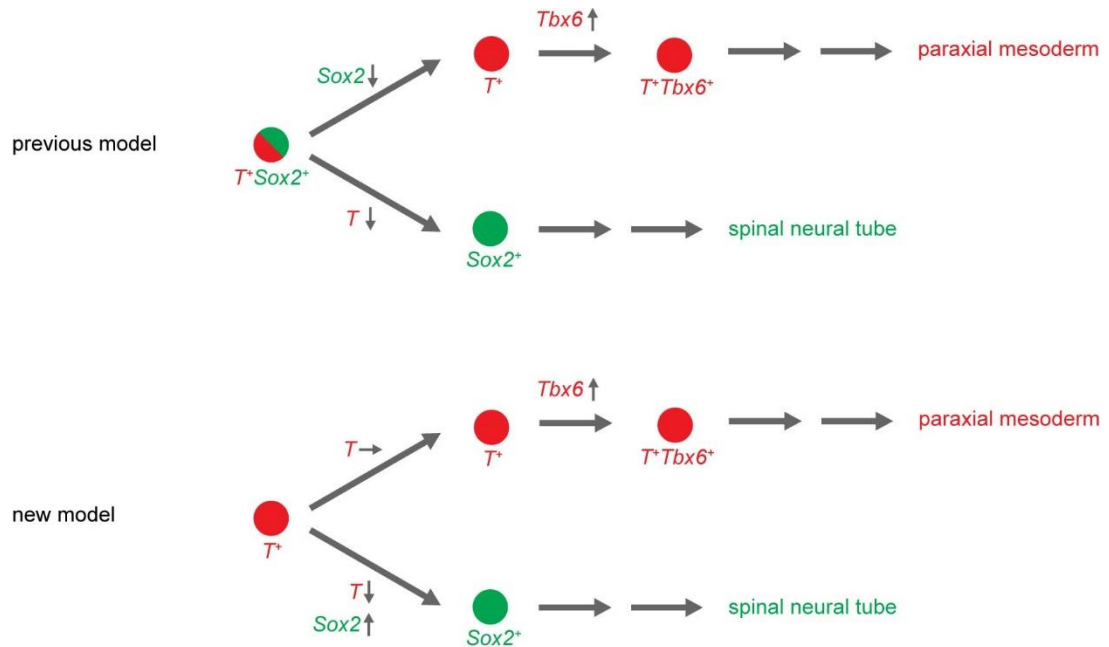


Figure 28. Current and revised NMP models.

Unlike previous assumptions, NMPs do not express *Sox2*. After gastrulation has ceased, *Sox2* expression is restricted to cells within the neural lineage, contradicting the previous NMP model. However, both spinal neural tube and paraxial mesoderm are derived from *T*-expressing cells. This suggests that NMPs down-regulate *T* and start expressing *Sox2* as they adopt a neural fate. On the other hand, as NMPs commit to form paraxial mesoderm, they maintain *T* and induce down-stream regulators, such as *Tbx6*. Adapted from (Mugele et al., 2018).

Remarkably, my DiO-labelling experiments showed that NMPs give rise to the dorsal neural tube only, although *T*-lineage tracing after the gastrulation stage revealed that derivatives of *T*-expressing cells colonise the entire neural tube, and not just the dorsal part. This suggests that the NMPs are not the only *T*-positive cell population, which gives rise to neuroepithelium. In other words, the entire spinal neural tube develops in a way which does not conform to the traditional germ layer model.

4.2 Implications for NMP research

As my findings question the validity of numerous NMP studies, I will first summarise the most common shortcomings in the literature. Afterwards, I will discuss some of the key papers in the literature focussing in particular on (i) technical concerns, (ii) alternative explanations for the findings, and (iii) how the data supports the revised NMP model.

4.2.1 Common errors in the NMP literature

4.2.1.1 Location and potency of NMPs

The most common inconsistency in the literature is the location and potency of NMPs, as discussed in Chapter 3.1.3.2. In summary, Cambray and Wilson described two long-term populations in the E8.5 embryo, which form both neural tube and paraxial mesoderm. On the one hand, cells from the NSB give rise to the ventral neural tube, paraxial mesoderm, and the notochord. On the other hand, cells in the rostral CLE populate the dorsal neural tube and paraxial mesoderm, but not the notochord (Cambray and Wilson, 2007). My DiO-labelling experiments confirmed their observations. However, several authors refer to both NSB and rostral CLE as the NMP location (Gouti et al., 2014; Henrique et al., 2015; Javali et al., 2017; Li et al., 2016; Wymeersch et al., 2016), although they harbour cells with very different behaviour. A second common mistake is that many assume that the entire CLE contains NMPs (Henrique et al., 2015; Koch et al., 2017; Kondoh and Takemoto, 2012; Rodrigo Albors et al., 2016; Takemoto et al., 2011; Yoshida et al., 2014), yet, Cambray and Wilson located them in the rostral CLE only. My labelling experiments further showed that long-term progenitors are found only in region 1 of the CLE. A third source of error is the disagreement regarding the location of the CNH, which can be found directly caudal to the extending notochord and hindgut. However, sections or diagrams depicted in publications often show regions which are located rostral to the CNH (Cambray and Wilson, 2007; Gouti et al., 2017; Rodrigo Albors et al., 2016; Wilson et al., 2009; Wymeersch et al., 2016).

These issues raise a question about which cells these researchers have studied: The NMPs in the rostral CLE? The axial stem/progenitor cells in the NSB? Cells from the pre-neural tube? Or cells from the CLE other than the NMPs? There is no straightforward answer to this issue since each of these papers needs to be re-assessed individually. However, it is likely that their results were obtained from a blend of different cell populations.

Another problem arising from these findings refers to the retrospective clonal analysis performed by Tzouanacou and colleagues (Tzouanacou et al., 2009), which is generally believed to prove that neural tube and paraxial mesoderm arise from one shared progenitor. However, their methodology does not allow any conclusions to be drawn about the region of origin of the clones in their study, which could have arisen from the NMPs in region 1, or the axial stem/progenitor cells in the NSB, or even from elsewhere. Only a few sections are provided in the paper and no clear information is given either on the location of labelled cells in the neural tube or on contribution to the notochord, both of which might have identified the site of origin of the clones. Indeed, Tzouanacou et al.'s data are consistent with there being two or even more cell populations in the caudal embryo, which give rise to both neural tube and paraxial mesoderm. This hypothesis receives support from my DiO-labelling experiments. Therefore, while the Tzouanacou et al. study suggests that both neural and mesodermal cells can arise from mitotic division of a single progenitor, it does not *per se* demonstrate the existence of NMPs, as a defined location-specific cell sub-population.

4.2.1.2 Timing

Since it is not entirely clear when NMPs emerge and until when they persist in the tail bud, timing is a crucial aspect. The grafting experiments described by Cambrey and Wilson show that cells which provide long-term contribution to the elongating neural tube and somites are located in the NSB and the rostral CLE in E8.5 mouse embryos (Cambrey and Wilson, 2007). This time point correlates well with other data: Perantoni

and colleagues traced *T*-expressing cells in the early embryo and discovered that these cells started colonising the neural tube from around the level of the sixth somite onwards (Perantoni et al., 2005). In addition, the study by Tzouanacou et al., which used retrospective analysis of clonal descendants, defined a similar axial level as the rostral limit of neuro-mesodermal clones (Tzouanacou et al., 2009). Yet, in spite of the consistent data, some researchers speculate that the NMPs might emerge earlier (Henrique et al., 2015).

Cambray and Wilson found that CNH cells from embryos up to E12.5 could be successfully transplanted to E8.5 embryos where they gave rise to paraxial mesoderm and neural tube and eventually colonised the CNH. In addition, these transplants maintained their potency over several generations of serial grafting (Cambray and Wilson, 2002). This time point also fits well with the cessation of body axis elongation, which occurs around E13.0. Wymeersch and colleagues propose that NMPs persist until E13.5, however, this is solely based on overlapping Sox2/T protein expression in the tail bud (Wymeersch et al., 2016).

In light of these findings, it is important to study NMPs within this time frame to ensure the results can be attributed to these cells. However, this is not always the case. Chalamalasetty et al. aimed to investigate how increased *Msgn1* levels affect cell fate decision (neural versus mesodermal) in NMPs (Chalamalasetty et al., 2014). For this purpose, they over-expressed *Msgn1* in the *T*-domain from E6.5 onwards and analysed the resulting embryos at E9.5 (see Figure 7 of their paper). In other words, they induced *Msgn1* expression 48 h before NMPs start contributing to the axial tissues and therefore likely created a phenotype which is not linked to the dual-fated progenitors.

A similar problem applies to the work published by Garriock and colleagues (Garriock et al., 2015), who intended to analyse how *Ctnnb1* gain- and loss-of-function regulates the differentiation of NMPs into mesodermal and neural tissues (see Figures 3 and 4 of their paper; note: *Ctnnb1* is the gene which encodes β -catenin). For these experiments, they used an inducible CreERT2 driver line to modify β -catenin levels

specifically in *T*-expressing cells. However, in both cases they induced CreERT2 activity at E6.5 and analysed the embryos at E9.5 and E10.5, respectively, which means they likely targeted cells other than NMPs.

A third study, which emphasises the importance of timing, was published by Li et al. (Li et al., 2016). They wanted to address how enhanced Wnt signalling, which they observed in mouse embryos that are deficient in the ten-eleven translocation (TET) enzymes Tet1, Tet2, and Tet3, affects differentiation of NMPs (see Figures 5 and 6 of their paper). Yet, they analysed E8.0 – E8.5 embryos only, which were likely too young. In addition, their analysis of NMP potency was solely based on co-expression of *T* and Sox2 protein, which is problematic as discussed earlier.

4.2.1.3 Sox2/T co-expression

My data strongly suggest that NMPs are Sox2-negative. However, a considerable proportion of the NMP literature is based on the assumption that these cells are defined by *T/Sox2* co-expression. This issue was extensively discussed in Chapter 3.3. It is indeed surprising that the hypothesis, that NMPs co-express both markers, has not been properly tested so far, although these experiments were relatively straight forward to do. As a consequence, those studies which defined NMPs as a *Sox2/T* double-positive population did likely not capture the true NMPs and therefore do not provide reliable information on these dual-fated progenitors. In the following, I will discuss some of the key papers and provide an alternative interpretation of their data, which further reinforces the revised NMP model.

4.2.2 Further support in the literature for the revised NMP model

4.2.2.1 In vivo studies

Long before Cambray and Wilson's grafting experiment ignited the field of NMP research, it was well known from various knock-out mouse models that the formation of neuroepithelium and somites are interlinked. For example, *Tbx6* null embryos develop ectopic neural tubes instead of paraxial mesoderm (Chapman and Papaioannou,

1998). Similarly, *Wnt3a* knock-out mouse embryos stop forming somites but at same time develop an ectopic neural tube which lies ventral to the primary neural tube (Takada et al., 1994; Yoshikawa et al., 1997). In the last few years, many more genes have been linked to the NMPs as they affect both the neural and mesodermal lineages when mutated (reviewed in (Wilson et al., 2009)). However, a subset of these mutants, which target genes that are required for mesoderm differentiation, stands out from the rest. These include *Tbx6*, *Wnt3a*, and *Fgfr1* (Ciruna et al., 1997) knock-out embryos, as well as the *T* hypomorph mutant (Cogliatti, 1986; Gruneberg, 1958; Herrmann, 1991): These embryos exhibit pre-mature axis truncation and they completely fail to form paraxial mesoderm from the level of the sixth somite onwards – which coincides with the same axial level from which *T*-expressing cells start colonising the neural tube (Perantoni et al., 2005). Instead of somites, these mutant embryos form ectopic neural tubes. This phenotype suggests that the dual-fated progenitors cannot adopt a mesodermal fate in these embryos. Therefore, they can only give rise to neural tissue. In other words, neural tubes are formed at the expense of somites. According to the old NMP model, the progenitors co-express *Sox2* and *T*, which maintains the undifferentiated stage. However, if both markers were truly equipollent, the transition should be possible in the opposite direction as well, i.e. the formation of excess mesodermal tissue at the expense of the neural tube from the sixth somite onwards. Although I performed a thorough literature search, I was not able to identify any mutants which fulfil these criteria. Retinoic acid (RA) is often referred to as an example of the reverse phenotype, since RA is specifically required for neural development (Diez del Corral et al., 2003) and mutant embryos also display axis truncation. Yet, both RA over-expression (Abu-Abed et al., 2001; Sakai et al., 2001) and disruption of RA signalling by deleting retinoic acid receptor γ (Iulianella et al., 1999) equally affect neural tube and somites. Among other defects, they exhibit down-regulation of *T* and *Wnt3a* in the tail bud, malformation of vertebrae, and spina bifida. Hence, the absence of a mouse mutant with a “reversed phenotype” – excessive mesoderm in place of

neural tissue – is consistent with the finding from my work that *Sox2* acts downstream of the mesodermal progenitors, supporting the revised NMP model.

Takemoto and colleagues (Takemoto et al., 2011) further examined the formation of ectopic neural tubes. However, the explanation given here is an alternative interpretation to the conclusions drawn by the authors. In this paper, the authors studied *Tbx6* null mutant embryos, which form two ectopic neural tubes, one on each side of the primary neural tube. They found the *Sox2* enhancer N1 up-regulated in the pre-somitic mesoderm of these embryos from E8.5 onwards and deletion of the N1 enhancer in *Tbx6* null embryos prevented the formation of ectopic neural tubes. Since the enhancer is activated by Wnt and Fgf signalling (Takemoto et al., 2006; Takemoto et al., 2011), Takemoto et al. concluded that N1 acts at the level of the dual-fated progenitors by influencing cell fate decision between the neural and mesodermal lineage. However, their results also allow for a different interpretation: Figure 3 in their paper shows that the *Tbx6* null embryos form a normal-looking neural tube with all domains present (which was shown for *Wnt3a* null embryos as well (Yoshikawa et al., 1997)). This suggests that neural tube formation remains unaffected by *Tbx6* knock-out. Similarly, deletion of the enhancer N1 – either on its own or in a *Tbx6* null background – also led to the formation of a normal primary neural tube (see Figure 3 of their paper). This is surprising because if the enhancer guided fate choice in the progenitors – and in the case of *Tbx6* knock-out forced them towards the neural lineage – one would expect an abnormal neural tube, for example it might be enlarged or display an unusual morphology. In other words, what is so striking about this phenotype is the location of the ectopic neural tubes: they emerge in the same position, where *Tbx6* is usually expressed, i.e. on both sides of the primary neural tube, where eventually somites develop.

Similarly, *Wnt3a* knock-out embryos form only a single ectopic neural tube, which lies ventral to the primary one. This correlates well with the expression of *Wnt3a* in the primitive streak/node region, right underneath the developing neuroepithelium. This suggests that the location of ectopic neural tubes is related to the gene expression

domain in wild type embryos and does not occur randomly. If the N1 enhancer regulated cell fate decision in the bi-potent progenitors, why would they move to the paraxial mesoderm domain and not to the neural tube? And why do different knock-out mice consistently develop ectopic neural tubes in such specific positions? A likely explanation for this is that the cell fate decision *per se* is not affected in these mutant embryos. Otherwise, the primary neural tube would be enlarged if all progenitors and their progeny colonised it. These mutants rather suggest that early mesodermal cells maintain the ability to form neural tissue. Once they commit to the mesodermal lineage and form paraxial mesoderm, they enter the pre-somitic mesoderm compartment. However, in the absence of *Tbx6*, they fail to differentiate into somites and therefore up-regulate N1/*Sox2* to form neural tissue by default.

It is also worth noting that the ability to differentiate into ectopic neural tubes is only retained in very early pre-somitic stages, since knock-out of *Msgn1*, which regulates pre-somitic mesoderm differentiation and acts downstream of *Tbx6*, does not lead to the formation of ectopic neural tubes, although these embryos fail to form somites from the forelimb level onwards (Nowotschin et al., 2012; Yoon and Wold, 2000). On the other hand, *Cdx2* knock-out embryos display premature axis truncation and form small ectopic neural structures ventral to the primary neural tube (Chawengsaksophak et al., 2004; van de Ven et al., 2011). They do form somites, yet, they appear abnormal starting again from the sixth somite level. Moreover, RA-treated embryos, which also exhibit axial truncation, develop an extensive network of irregularly shaped, tubular structures which express neural tube markers (Shum et al., 1999). These mutants highlight that some milder forms exist and only *Fgfr1*, *Wnt3a*, *Tbx6* null embryos and the *T* hypomorph manifest the extreme phenotype, which is the complete cessation of somite formation and generation of whole ectopic neural tubes.

The ability of early mesodermal tissue to differentiate into neuroepithelium is also supported by my laser ablation experiments (see **Figure 13**), which revealed that ablation of the CLE region 1 resulted in down-regulation of the pre-somitic mesoderm

marker *Dll1* and at the same time, the embryos formed enlarged, malformed neural tubes at the affected axial level.

Nevertheless, the *in vivo* data from mouse mutants can hardly be attributed to the NMPs alone. As discussed earlier, NMPs only give rise to the dorsal neural tube. Yet, lineage tracing experiments showed that descendants of *T*-expressing cells colonise the entire neural tube and not just the dorsal domain. In line with this, the *T* hypomorph and both the *Wnt3a* and *Fgfr1* null mutant embryos display disrupted notochord formation (Ciruna et al., 1997; Cogliatti, 1986; Gruneberg, 1958; Park et al., 1989; Takada et al., 1994; Yanagisawa and Kitamura, 1975). However, notochord defects have not been reported in *Tbx6* knock-out embryos. In addition, Zhu et al. observed that *T* knock-down in notochord progenitors resulted in embryos with an ectopic neural tube instead of the notochord (Zhu et al., 2016). As the NMPs do not give rise to notochord, this suggests that other populations exist, which possess the ability to switch from a mesodermal to a neural fate. One likely cell population are the axial stem/progenitors which were originally located in the NSB in E8.5 mouse embryos, as these cells give rise to the ventral neural tube, paraxial mesoderm, and also the notochord.

Altogether, the data highlight that spinal neural tube and paraxial mesoderm are developmentally intertwined as cells expressing early mesodermal markers are able to adopt a neural fate. However, there is no conclusive evidence which shows that neural cells are able to switch to a mesodermal fate, supporting the revised NMP model, which states that *Sox2* acts further downstream exclusively in the neural lineage.

4.2.2.2 *In vitro* studies

Although the published NMP *in vitro* models are all based on the concept that the dual-fated progenitors are *Sox2/T* double-positive (Cunningham et al., 2016; Gouti et al., 2014; Lippmann et al., 2015; Tsakiridis et al., 2014; Turner et al., 2014; Verrier et al., 2018), the data from these studies actually confirm that *Sox2* and *T* cannot be stably co-expressed. In general, the different protocols follow the same strategy by treating

pluripotent stem cells (either from mouse or human) with Fgf and a Wnt agonist, until the cells start co-expressing Sox2 and T protein (“NMP stage”), as shown by immunostaining (Cunningham et al., 2016; Gouti et al., 2014; Lippmann et al., 2015; Tsakiridis et al., 2014; Turner et al., 2014; Verrier et al., 2018). Expression of Sox2 in these cells is likely due to the long half-life of Sox2 protein, which originates in the stem cells (Avilion et al., 2003; Luo et al., 2011). Indeed, Sox2 mRNA levels consistently hit rock bottom at the “NMP stage” (see Figure 7B – C in (Turner et al., 2014), Figure 2B in (Gouti et al., 2014), Figure 1B in (Cunningham et al., 2016), and Figure 2B in (Verrier et al., 2018)). In addition, these authors also measured *T* mRNA levels as the pluripotent stem cells differentiated (shown in the same Figures), and they clearly behave antagonistically to Sox2. That is, whenever *T* mRNA is the highest, Sox2 is the lowest and vice versa. Interestingly, *T* mRNA levels are the highest at the “NMP stage”.

Last but not least, Verrier et al. (Verrier et al., 2018), who used human embryonic stem cells for their study, compared genes which they found enriched at the “NMP stage” with the data set obtained by Gouti et al. (Gouti et al., 2014) from mouse embryonic stem cells and also with data from single-cell transcriptome analysis from micro-dissected cells of E8.5 and E9.5 mouse embryos (Gouti et al., 2017). The results are displayed in Figure 3C-D of their paper and notably, Sox2 is completely missing from these lists, consistent with its lack of expression in NMPs.

4.2.2.3 Conclusion

I have shown that the literature in favour of Sox2/*T* double-positive NMPs is inconclusive as it contains many inconsistencies and misconceptions. On closer examination, these studies actually support the revised model of a *T*-expressing progenitor for the spinal neural tube and somites, in line with the data presented in this thesis.

4.2.3 Impact of findings

The combined evidence from my experiments and the literature review indicate that NMPs likely express *T*, but not *Sox2*. Most of our knowledge regarding cell fate decision of NMPs and the associated gene regulatory network are based on single-cell analyses in mouse embryos (Gouti et al., 2017; Koch et al., 2017) and *in vitro* studies (Cunningham et al., 2016; Gouti et al., 2014; Lippmann et al., 2015; Tsakiridis et al., 2014; Turner et al., 2014; Verrier et al., 2018). However, all of these define NMPs based on co-expression of *Sox2* and *T*. Therefore, the data need to be re-interpreted in the light of my findings. On the other hand, the *in vitro* models are not *per se* invalid. As there is no known marker, the NMPs cannot be reliably identified within the *T* lineage. Hence, these *in vitro* systems are unsuitable for studying these dual-fated progenitors. Nevertheless, they might still be useful for modelling the development of the spinal neural tube, as it arises from cells which initially express *T*.

Altogether, the accumulated data correctly challenge the paradigm that the neural tube and paraxial mesoderm derive from two different lineages, which segregate during gastrulation. However, the findings from my thesis allow us to go even further. The lineage-tracing experiments reveal that the derivatives of *T*-expressing cells in the post-gastrulation embryo colonise the hindgut as well (white arrowheads in **Figure 14Cb – c**), which was also briefly mentioned in a previous report (Anderson et al., 2013). This finding further challenges the traditional germ layer model, according to which the hindgut is derived from the endoderm layer. In *Cdx2* knock-out embryos, the gut fails to form from the same axial level as the neural tube and paraxial mesoderm (Chawengsaksophak et al., 2004), suggesting that the formation of these three tissues is interconnected. Moreover, genetic lineage tracing further showed that derivatives from both *T*- and *Sox2*-expressing cells intermittently colonise the notochord (orange arrowheads in **Figures 14Cb – c** and **17Cc – d**), which was so far believed to be a mesoderm-derived structure (Herrmann, 1991). As it is not only the spinal neural tube which defies the paradigm of germ layer formation and specification of early embryonic

lineages, but also the hindgut and notochord, it is likely that this model does not apply to axial tissues in embryonic trunk development.

4.3 Final remarks

Ever since they were discovered, the NMPs have attracted a great deal of attention as they were considered the exception to the rule of germ layer formation, which has held true since the early 19th century. However, the excitement led to hypotheses not being tested, findings being misinterpreted, and an agglomeration of inconsistencies and technical flaws. A major point which has been ignored all along – although Cambray and Wilson described it in their initial studies – is the presence of at least two different long-term progenitor populations, which give rise to both neural tube and paraxial mesoderm: the axial stem/progenitors in the NSB, and the NMPs in the rostral CLE. The NMPs are only one piece of the puzzle, as they only give rise to the dorsal neural tube. Therefore, the NMPs alone cannot explain why the entire neural tube is populated by derivatives of *T*-expressing cells. Similarly, they do not fully explain why *Tbx6*, *Wnt3a* and other knock-out embryos form ectopic neural tubes instead of somites – a complete neural tube with dorsal, lateral, and ventral domain markers being expressed in the correct positions. The bigger picture, which has been overlooked, is that the NMPs are not the only exception to the germ layer model. Instead, the accumulated data suggests that this long-held paradigm does by no means apply to trunk development. The formation of the spinal neural tube, and most likely other organs as well, such as the hindgut, do not conform to it. Therefore, the concept of germ layers and their derivatives, as well as the definition of germ layers based on their molecular signature, need to be revised.

These findings indicate that embryonic lineages are much more versatile than expected. This offers new opportunities to improve differentiation protocols for stem cells, both for clinical use and for disease modelling *in vitro*. Most importantly, we will

be able to better understand embryonic development of the axial tissues and related birth defects by taking these new insights into account.

REFERENCES

- Abu-Abed, S., Dolle, P., Metzger, D., Beckett, B., Chambon, P. and Petkovich, M., 2001. The retinoic acid-metabolizing enzyme, CYP26A1, is essential for normal hindbrain patterning, vertebral identity, and development of posterior structures. *Genes Dev.* 15, 226-40.
- Adamska, M., Degnan, S.M., Green, K.M., Adamski, M., Craigie, A., Larroux, C. and Degnan, B.M., 2007. Wnt and TGF-beta expression in the sponge *Amphimedon queenslandica* and the origin of metazoan embryonic patterning. *PLoS One.* 2, e1031.
- Amin, S., Neijts, R., Simmini, S., van Rooijen, C., Tan, S.C., Kester, L., van Oudenaarden, A., Creighton, M.P. and Deschamps, J., 2016. Cdx and T Brachyury Co-activate Growth Signaling in the Embryonic Axial Progenitor Niche. *Cell Rep.* 17, 3165-3177.
- Anderson, M.J., Naiche, L.A., Wilson, C.P., Elder, C., Swing, D.A. and Lewandoski, M., 2013. TCreERT2, a transgenic mouse line for temporal control of Cre-mediated recombination in lineages emerging from the primitive streak or tail bud. *PLoS One.* 8, e62479.
- Andoniadou, C.L., Matsushima, D., Mousavy Gharavy, S.N., Signore, M., Mackintosh, A.I., Schaeffer, M., Gaston-Massuet, C., Mollard, P., Jacques, T.S., Le Tissier, P., Dattani, M.T., Pevny, L.H. and Martinez-Barbera, J.P., 2013. Sox2(+) stem/progenitor cells in the adult mouse pituitary support organ homeostasis and have tumor-inducing potential. *Cell Stem Cell.* 13, 433-45.
- Avilion, A.A., Nicolis, S.K., Pevny, L.H., Perez, L., Vivian, N. and Lovell-Badge, R., 2003. Multipotent cell lineages in early mouse development depend on SOX2 function. *Genes Dev.* 17, 126-40.
- Beddington, R.S., 1994. Induction of a second neural axis by the mouse node. *Development.* 120, 613-20.
- Bettenhausen, B., Hrabe de Angelis, M., Simon, D., Guenet, J.L. and Gossler, A., 1995. Transient and restricted expression during mouse embryogenesis of Dll1, a murine gene closely related to *Drosophila* Delta. *Development.* 121, 2407-18.
- Bolognesi, R., Beermann, A., Farzana, L., Wittkopp, N., Lutz, R., Balavoine, G., Brown, S.J. and Schroder, R., 2008a. *Tribolium* Wnts: evidence for a larger repertoire in insects with overlapping expression patterns that suggest multiple redundant functions in embryogenesis. *Dev Genes Evol.* 218, 193-202.
- Bolognesi, R., Farzana, L., Fischer, T.D. and Brown, S.J., 2008b. Multiple Wnt genes are required for segmentation in the short-germ embryo of *Tribolium castaneum*. *Curr Biol.* 18, 1624-9.
- Brown, J.M. and Storey, K.G., 2000. A region of the vertebrate neural plate in which neighbouring cells can adopt neural or epidermal fates. *Curr Biol.* 10, 869-72.
- Cambray, N. and Wilson, V., 2002. Axial progenitors with extensive potency are localised to the mouse chordoneural hinge. *Development.* 129, 4855-66.
- Cambray, N. and Wilson, V., 2007. Two distinct sources for a population of maturing axial progenitors. *Development.* 134, 2829-40.

- Cavallaro, M., Mariani, J., Lancini, C., Latorre, E., Caccia, R., Gullo, F., Valotta, M., DeBiasi, S., Spinardi, L., Ronchi, A., Wanke, E., Brunelli, S., Favaro, R., Ottolenghi, S. and Nicolis, S.K., 2008. Impaired generation of mature neurons by neural stem cells from hypomorphic Sox2 mutants. *Development*. 135, 541-57.
- Chalamalasetty, R.B., Garriock, R.J., Dunty, W.C., Jr., Kennedy, M.W., Jailwala, P., Si, H. and Yamaguchi, T.P., 2014. Mesogenin 1 is a master regulator of paraxial presomitic mesoderm differentiation. *Development*. 141, 4285-97.
- Chapman, D.L. and Papaioannou, V.E., 1998. Three neural tubes in mouse embryos with mutations in the T-box gene Tbx6. *Nature*. 391, 695-7.
- Chawengsaksophak, K., de Graaff, W., Rossant, J., Deschamps, J. and Beck, F., 2004. Cdx2 is essential for axial elongation in mouse development. *Proc Natl Acad Sci U S A*. 101, 7641-5.
- Chesley, P., 1935. Development of the short-tailed mutant in the house mouse. *Journal of Experimental Zoology*. 70, 429-459.
- Ciruna, B.G., Schwartz, L., Harpal, K., Yamaguchi, T.P. and Rossant, J., 1997. Chimeric analysis of fibroblast growth factor receptor-1 (Fgfr1) function: a role for FGFR1 in morphogenetic movement through the primitive streak. *Development*. 124, 2829-41.
- Cogliatti, S.B., 1986. Diplomyelia: caudal duplication of the neural tube in mice. *Teratology*. 34, 343-52.
- Collignon, J., Sockanathan, S., Hacker, A., Cohen-Tannoudji, M., Norris, D., Rastan, S., Stevanovic, M., Goodfellow, P.N. and Lovell-Badge, R., 1996. A comparison of the properties of Sox-3 with Sry and two related genes, Sox-1 and Sox-2. *Development*. 122, 509-20.
- Cooke, J. and Zeeman, E.C., 1976. A clock and wavefront model for control of the number of repeated structures during animal morphogenesis. *J Theor Biol*. 58, 455-76.
- Copf, T., Schroder, R. and Averof, M., 2004. Ancestral role of caudal genes in axis elongation and segmentation. *Proc Natl Acad Sci U S A*. 101, 17711-5.
- Copp, A., Cogram, P., Fleming, A., Gerrelli, D., Henderson, D., Hynes, A., Kolatsi-Joannou, M., Murdoch, J. and Ybot-Gonzalez, P., 2000. Neurulation and neural tube closure defects. *Methods Mol Biol*. 136, 135-60.
- Copp, A.J., Greene, N.D. and Murdoch, J.N., 2003. The genetic basis of mammalian neurulation. *Nat Rev Genet*. 4, 784-93.
- Corallo, D., Trapani, V. and Bonaldo, P., 2015. The notochord: structure and functions. *Cell Mol Life Sci*. 72, 2989-3008.
- Criley, B.B., 1969. Analysis of embryonic sources and mechanisms of development of posterior levels of chick neural tubes. *J Morphol*. 128, 465-501.
- Cunningham, T.J., Colas, A. and Duyster, G., 2016. Early molecular events during retinoic acid induced differentiation of neuromesodermal progenitors. *Biol Open*. 5, 1821-1833.

- Cunningham, T.J., Kumar, S., Yamaguchi, T.P. and Duester, G., 2015. Wnt8a and Wnt3a cooperate in the axial stem cell niche to promote mammalian body axis extension. *Dev Dyn.* 244, 797-807.
- Danielian, P.S., Muccino, D., Rowitch, D.H., Michael, S.K. and McMahon, A.P., 1998. Modification of gene activity in mouse embryos in utero by a tamoxifen-inducible form of Cre recombinase. *Curr Biol.* 8, 1323-6.
- Davis, R.L. and Kirschner, M.W., 2000. The fate of cells in the tailbud of *Xenopus laevis*. *Development.* 127, 255-67.
- Delfino-Machin, M., Lunn, J.S., Breitkreuz, D.N., Akai, J. and Storey, K.G., 2005. Specification and maintenance of the spinal cord stem zone. *Development.* 132, 4273-83.
- Dequeant, M.L. and Pourquie, O., 2008. Segmental patterning of the vertebrate embryonic axis. *Nat Rev Genet.* 9, 370-82.
- Diez del Corral, R., Olivera-Martinez, I., Goriely, A., Gale, E., Maden, M. and Storey, K., 2003. Opposing FGF and retinoid pathways control ventral neural pattern, neuronal differentiation, and segmentation during body axis extension. *Neuron.* 40, 65-79.
- Dobrovolskaia-Zavadskaia, N., 1927. Sur la mortification spontanee de la queue chez la souris nouveau-nee et sur l'existence d'un caractere hereditaire "non viable". *Crit. Rev. Soc. Biol.*, 114-116.
- Dunty, W.C., Jr., Kennedy, M.W., Chalamalasetty, R.B., Campbell, K. and Yamaguchi, T.P., 2014. Transcriptional profiling of Wnt3a mutants identifies Sp transcription factors as essential effectors of the Wnt/beta-catenin pathway in neuromesodermal stem cells. *PLoS One.* 9, e87018.
- Dymecki, S.M. and Kim, J.C., 2007. Molecular neuroanatomy's "Three Gs": a primer. *Neuron.* 54, 17-34.
- Echelard, Y., Epstein, D.J., St-Jacques, B., Shen, L., Mohler, J., McMahon, J.A. and McMahon, A.P., 1993. Sonic hedgehog, a member of a family of putative signaling molecules, is implicated in the regulation of CNS polarity. *Cell.* 75, 1417-30.
- Fan, C.M. and Tessier-Lavigne, M., 1994. Patterning of mammalian somites by surface ectoderm and notochord: evidence for sclerotome induction by a hedgehog homolog. *Cell.* 79, 1175-86.
- Feil, S., Valtcheva, N. and Feil, R., 2009. Inducible Cre mice. *Methods Mol Biol.* 530, 343-63.
- Fraser, A., 1882. On the Inversion of the Blastodermic Layers in the Rat and Mouse. *Proc R Soc.* 34, 430-437.
- Fujimoto, H. and Yanagisawa, K.O., 1983. Defects in the archenteron of mouse embryos homozygous for the T-mutation. *Differentiation.* 25, 44-7.
- Gardner, R.L., 1978. The relationship between cell lineage and differentiation in the early mouse embryo. *Results Probl Cell Differ.* 9, 205-41.

- Gardner, R.L. and Rossant, J., 1979. Investigation of the fate of 4-5 day post-coitum mouse inner cell mass cells by blastocyst injection. *J Embryol Exp Morphol.* 52, 141-52.
- Garriock, R.J., Chalamalasetty, R.B., Kennedy, M.W., Canizales, L.C., Lewandoski, M. and Yamaguchi, T.P., 2015. Lineage tracing of neuromesodermal progenitors reveals novel Wnt-dependent roles in trunk progenitor cell maintenance and differentiation. *Development.* 142, 1628-38.
- Geelen, J.A. and Langman, J., 1979. Ultrastructural observations on closure of the neural tube in the mouse. *Anat Embryol (Berl).* 156, 73-88.
- Gentsch, G.E., Owens, N.D., Martin, S.R., Piccinelli, P., Faial, T., Trotter, M.W., Gilchrist, M.J. and Smith, J.C., 2013. In vivo T-box transcription factor profiling reveals joint regulation of embryonic neuromesodermal bipotency. *Cell Rep.* 4, 1185-96.
- Gluecksohn-Schoenheimer, S., 1938. The Development of Two Tailless Mutants in the House Mouse. *Genetics.* 23, 573-84.
- Golden, J.A. and Chernoff, G.F., 1993. Intermittent pattern of neural tube closure in two strains of mice. *Teratology.* 47, 73-80.
- Gomez-Lopez, S., Wiskow, O., Favaro, R., Nicolis, S.K., Price, D.J., Pollard, S.M. and Smith, A., 2011. Sox2 and Pax6 maintain the proliferative and developmental potential of gliogenic neural stem cells In vitro. *Glia.* 59, 1588-99.
- Gomez, C., Ozbudak, E.M., Wunderlich, J., Baumann, D., Lewis, J. and Pourquie, O., 2008. Control of segment number in vertebrate embryos. *Nature.* 454, 335-9.
- Gont, L.K., Steinbeisser, H., Blumberg, B. and de Robertis, E.M., 1993. Tail formation as a continuation of gastrulation: the multiple cell populations of the *Xenopus* tailbud derive from the late blastopore lip. *Development.* 119, 991-1004.
- Goto, H., Kimmey, S.C., Row, R.H., Matus, D.Q. and Martin, B.L., 2017. FGF and canonical Wnt signaling cooperate to induce paraxial mesoderm from tailbud neuromesodermal progenitors through regulation of a two-step epithelial to mesenchymal transition. *Development.* 144, 1412-1424.
- Gouti, M., Delile, J., Stamatakis, D., Wymeersch, F.J., Huang, Y., Kleinjung, J., Wilson, V. and Briscoe, J., 2017. A Gene Regulatory Network Balances Neural and Mesoderm Specification during Vertebrate Trunk Development. *Dev Cell.* 41, 243-261.
- Gouti, M., Tsakiridis, A., Wymeersch, F.J., Huang, Y., Kleinjung, J., Wilson, V. and Briscoe, J., 2014. In vitro generation of neuromesodermal progenitors reveals distinct roles for wnt signalling in the specification of spinal cord and paraxial mesoderm identity. *PLoS Biol.* 12, e1001937.
- Graham, V., Khudyakov, J., Ellis, P. and Pevny, L., 2003. SOX2 functions to maintain neural progenitor identity. *Neuron.* 39, 749-65.
- Gray, J. and Ross, M.E., 2011. Neural tube closure in mouse whole embryo culture. *J Vis Exp.* e3132.

- Griffith, C.M. and Sanders, E.J., 1991. Effects of extracellular matrix components on the differentiation of chick embryo tail bud mesenchyme in culture. *Differentiation*. 47, 61-8.
- Gruneberg, H., 1958. Genetical studies on the skeleton of the mouse. XXIII. The development of brachyury and anury. *J Embryol Exp Morphol*. 6, 424-43.
- Harland, R., 2000. Neural induction. *Curr Opin Genet Dev*. 10, 357-62.
- Henderson, D.J., Conway, S.J. and Copp, A.J., 1999. Rib truncations and fusions in the Sp2H mouse reveal a role for Pax3 in specification of the ventro-lateral and posterior parts of the somite. *Dev Biol*. 209, 143-58.
- Henrique, D., Abranches, E., Verrier, L. and Storey, K.G., 2015. Neuromesodermal progenitors and the making of the spinal cord. *Development*. 142, 2864-75.
- Herrmann, B.G., 1991. Expression pattern of the Brachyury gene in whole-mount TWis/TWis mutant embryos. *Development*. 113, 913-7.
- Hobmayer, B., Rentzsch, F., Kuhn, K., Happel, C.M., von Laue, C.C., Snyder, P., Rothbacher, U. and Holstein, T.W., 2000. WNT signalling molecules act in axis formation in the diploblastic metazoan Hydra. *Nature*. 407, 186-9.
- Hofmann, M., Schuster-Gossler, K., Watabe-Rudolph, M., Aulehla, A., Herrmann, B.G. and Gossler, A., 2004. WNT signaling, in synergy with T/TBX6, controls Notch signaling by regulating Dll1 expression in the presomitic mesoderm of mouse embryos. *Genes Dev*. 18, 2712-7.
- Holmdahl, D.E., 1925. Die erste Entwicklung des Körpers bei den Vögeln und Säugetieren, inkl. dem Menschen, besonders mit Rücksicht auf die Bildung des Rückenmarks, des Zöloms und der entodermalen Kloake nebst einem Exkurs über die Entstehung der Spina bifida in der Lumbosakral region. *Anatomischer Anzeiger*. 59, 393-396.
- Iulianella, A., Beckett, B., Petkovich, M. and Lohnes, D., 1999. A molecular basis for retinoic acid-induced axial truncation. *Dev Biol*. 205, 33-48.
- Jacobson, A.G. and Tam, P.P., 1982. Cephalic neurulation in the mouse embryo analyzed by SEM and morphometry. *Anat Rec*. 203, 375-96.
- Javali, A., Misra, A., Leonavicius, K., Acharyya, D., Vyas, B. and Sambasivan, R., 2017. Co-expression of Tbx6 and Sox2 identifies a novel transient neuromesoderm progenitor cell state. *Development*. 144, 4522-4529.
- Ji, J., Yu, Y., Li, Z.L., Chen, M.Y., Deng, R., Huang, X., Wang, G.F., Zhang, M.X., Yang, Q., Ravichandran, S., Feng, G.K., Xu, X.L., Yang, C.L., Qiu, M.Z., Jiao, L., Yang, D. and Zhu, X.F., 2018. XIAP Limits Autophagic Degradation of Sox2 and Is A Therapeutic Target in Nasopharyngeal Carcinoma Stem Cells. *Theranostics*. 8, 1494-1510.
- Johnson, R.L., Laufer, E., Riddle, R.D. and Tabin, C., 1994. Ectopic expression of Sonic hedgehog alters dorsal-ventral patterning of somites. *Cell*. 79, 1165-73.
- Jurberg, A.D., Aires, R., Varela-Lasheras, I., Novoa, A. and Mallo, M., 2013. Switching axial progenitors from producing trunk to tail tissues in vertebrate embryos. *Dev Cell*. 25, 451-62.

- Keller, R., 2002. Shaping the vertebrate body plan by polarized embryonic cell movements. *Science*. 298, 1950-4.
- Keller, R., Davidson, L., Edlund, A., Elul, T., Ezin, M., Shook, D. and Skoglund, P., 2000. Mechanisms of convergence and extension by cell intercalation. *Philos Trans R Soc Lond B Biol Sci*. 355, 897-922.
- Kingsbury, B.F., 1932. The 'law' of cephalocaudal differential growth in its application to the nervous system. *Journal of Comparative Neurology*. 56, 431-463.
- Kispert, A. and Herrmann, B.G., 1994. Immunohistochemical analysis of the Brachyury protein in wild-type and mutant mouse embryos. *Dev Biol*. 161, 179-93.
- Koch, F., Scholze, M., Wittler, L., Schifferl, D., Sudheer, S., Grote, P., Timmermann, B., Macura, K. and Herrmann, B.G., 2017. Antagonistic Activities of Sox2 and Brachyury Control the Fate Choice of Neuro-Mesodermal Progenitors. *Dev Cell*. 42, 514-526.e7.
- Kölliker, A., 1884. Die embryonalen Keimblätter und die Gewebe. *Zeitschrift für wissenschaftliche Zoologie*. 40, 179-213.
- Kondoh, H. and Takemoto, T., 2012. Axial stem cells deriving both posterior neural and mesodermal tissues during gastrulation. *Curr Opin Genet Dev*. 22, 374-80.
- Koseki, H., Wallin, J., Wilting, J., Mizutani, Y., Kispert, A., Ebensperger, C., Herrmann, B.G., Christ, B. and Balling, R., 1993. A role for Pax-1 as a mediator of notochordal signals during the dorsoventral specification of vertebrae. *Development*. 119, 649-60.
- Krol, A.J., Roellig, D., Dequeant, M.L., Tassy, O., Glynn, E., Hattem, G., Mushegian, A., Oates, A.C. and Pourquie, O., 2011. Evolutionary plasticity of segmentation clock networks. *Development*. 138, 2783-92.
- Kusserow, A., Pang, K., Sturm, C., Hroudá, M., Lentfer, J., Schmidt, H.A., Technau, U., von Haeseler, A., Hobmayer, B., Martindale, M.Q. and Holstein, T.W., 2005. Unexpected complexity of the Wnt gene family in a sea anemone. *Nature*. 433, 156-60.
- Kwon, G.S., Viotti, M. and Hadjantonakis, A.K., 2008. The endoderm of the mouse embryo arises by dynamic widespread intercalation of embryonic and extraembryonic lineages. *Dev Cell*. 15, 509-20.
- Lawson, K.A., Meneses, J.J. and Pedersen, R.A., 1986. Cell fate and cell lineage in the endoderm of the presomite mouse embryo, studied with an intracellular tracer. *Dev Biol*. 115, 325-39.
- Lawson, K.A., Meneses, J.J. and Pedersen, R.A., 1991. Clonal analysis of epiblast fate during germ layer formation in the mouse embryo. *Development*. 113, 891-911.
- Lawson, K.A. and Pedersen, R.A., 1992. Clonal analysis of cell fate during gastrulation and early neurulation in the mouse. *Ciba Found Symp*. 165, 3-21.
- Lee, J.Y., Lee, S.H., Heo, S.H., Kim, K.S., Kim, C., Kim, D.K., Ko, J.J. and Park, K.S., 2015. Novel Function of Lysine Methyltransferase G9a in the Regulation of Sox2 Protein Stability. *PLoS One*. 10, e0141118.

- Lee, P.N., Pang, K., Matus, D.Q. and Martindale, M.Q., 2006. A WNT of things to come: evolution of Wnt signaling and polarity in cnidarians. *Semin Cell Dev Biol.* 17, 157-67.
- Li, X., Yue, X., Pastor, W.A., Lin, L., Georges, R., Chavez, L., Evans, S.M. and Rao, A., 2016. Tet proteins influence the balance between neuroectodermal and mesodermal fate choice by inhibiting Wnt signaling. *Proc Natl Acad Sci U S A.* 113, e8267-e8276.
- Lippmann, E.S., Williams, C.E., Ruhl, D.A., Estevez-Silva, M.C., Chapman, E.R., Coon, J.J. and Ashton, R.S., 2015. Deterministic HOX patterning in human pluripotent stem cell-derived neuroectoderm. *Stem Cell Reports.* 4, 632-44.
- Lolas, M., Valenzuela, P.D., Tjian, R. and Liu, Z., 2014. Charting Brachyury-mediated developmental pathways during early mouse embryogenesis. *Proc Natl Acad Sci U S A.* 111, 4478-83.
- Luo, Z., Xu, X., Gu, P., Lonard, D., Gunaratne, P.H., Cooney, A.J. and Azencott, R., 2011. miRNA regulatory circuits in ES cells differentiation: a chemical kinetics modeling approach. *PLoS One.* 6, e23263.
- Martin, B.L., 2016. Factors that coordinate mesoderm specification from neuromesodermal progenitors with segmentation during vertebrate axial extension. *Semin Cell Dev Biol.* 49, 59-67.
- Martin, B.L. and Kimelman, D., 2008. Regulation of canonical Wnt signaling by Brachyury is essential for posterior mesoderm formation. *Dev Cell.* 15, 121-33.
- Martin, B.L. and Kimelman, D., 2012. Canonical Wnt signaling dynamically controls multiple stem cell fate decisions during vertebrate body formation. *Dev Cell.* 22, 223-32.
- McGrew, M.J., Sherman, A., Lillico, S.G., Ellard, F.M., Radcliffe, P.A., Gilhooley, H.J., Mitrophanous, K.A., Cambray, N., Wilson, V. and Sang, H., 2008. Localised axial progenitor cell populations in the avian tail bud are not committed to a posterior Hox identity. *Development.* 135, 2289-99.
- McMahon, J.A., Takada, S., Zimmerman, L.B., Fan, C.M., Harland, R.M. and McMahon, A.P., 1998. Noggin-mediated antagonism of BMP signaling is required for growth and patterning of the neural tube and somite. *Genes Dev.* 12, 1438-52.
- McShane, S.G., Mole, M.A., Savery, D., Greene, N.D., Tam, P.P. and Copp, A.J., 2015. Cellular basis of neuroepithelial bending during mouse spinal neural tube closure. *Dev Biol.* 404, 113-24.
- Miyagi, S., Masui, S., Niwa, H., Saito, T., Shimazaki, T., Okano, H., Nishimoto, M., Muramatsu, M., Iwama, A. and Okuda, A., 2008. Consequence of the loss of Sox2 in the developing brain of the mouse. *FEBS Lett.* 582, 2811-5.
- Morriss-Kay, G.M., 1981. Growth and development of pattern in the cranial neural epithelium of rat embryos during neurulation. *J Embryol Exp Morphol.* 65 Suppl, 225-41.
- Mugele, D., Moulding, D.A., Savery, D., Molè, M.A., Greene, N.D.E., Martinez-Barbera, J.P. and Copp, A.J., 2018. Genetic approaches in mice demonstrate that neuro-

mesodermal progenitors express T/Brachyury but not Sox2. Manuscript submitted for publication.

- Muzumdar, M.D., Tasic, B., Miyamichi, K., Li, L. and Luo, L., 2007. A global double-fluorescent Cre reporter mouse. *Genesis*. 45, 593-605.
- Nagy, L.M. and Carroll, S., 1994. Conservation of wingless patterning functions in the short-germ embryos of *Tribolium castaneum*. *Nature*. 367, 460-3.
- Nichols, S.A., Dirks, W., Pearse, J.S. and King, N., 2006. Early evolution of animal cell signaling and adhesion genes. *Proc Natl Acad Sci U S A*. 103, 12451-6.
- Nowotschin, S., Ferrer-Vaquer, A., Concepcion, D., Papaioannou, V.E. and Hadjantonakis, A.K., 2012. Interaction of Wnt3a, Msn1 and Tbx6 in neural versus paraxial mesoderm lineage commitment and paraxial mesoderm differentiation in the mouse embryo. *Dev Biol*. 367, 1-14.
- Olivera-Martinez, I., Harada, H., Halley, P.A. and Storey, K.G., 2012. Loss of FGF-dependent mesoderm identity and rise of endogenous retinoid signalling determine cessation of body axis elongation. *PLoS Biol*. 10, e1001415.
- Pai, Y.J., Abdullah, N.L., Mohd-Zin, S.W., Mohammed, R.S., Rolo, A., Greene, N.D., Abdul-Aziz, N.M. and Copp, A.J., 2012. Epithelial fusion during neural tube morphogenesis. *Birth Defects Res A Clin Mol Teratol*. 94, 817-23.
- Pander, C.H., 1817. Beiträge zur Entwicklungsgeschichte de Hühnchens im Eye, H. L. Brönnner, Würzburg.
- Park, C.H., Pruitt, J.H. and Bennett, D., 1989. A mouse model for neural tube defects: the curtailed (Tc) mutation produces spina bifida occulta in Tc/+ animals and spina bifida with meningomyelocele in Tc/t. *Teratology*. 39, 303-12.
- Pasteels, J., 1939. La formation de la queue chez les Vertébrés. *Annales De La Société Royale Zoologique De Belgique*. 70, 33-51.
- Pasteels, J., 1942. New observations concerning the maps of presumptive areas of the young amphibian gastrula (*Amblystoma* and *Discoglossus*). *J Exp Zool*. 89, 255-281.
- Pasteels, J., 1943. Proliférations et croissance dans la gastrulation et la formation de la queue de Vertébrés. *Arch Biol*. 54, 1-51.
- Perantoni, A.O., Timofeeva, O., Naillat, F., Richman, C., Pajni-Underwood, S., Wilson, C., Vainio, S., Dove, L.F. and Lewandoski, M., 2005. Inactivation of FGF8 in early mesoderm reveals an essential role in kidney development. *Development*. 132, 3859-71.
- Pevny, L.H. and Lovell-Badge, R., 1997. Sox genes find their feet. *Curr Opin Genet Dev*. 7, 338-44.
- Placzek, M., Yamada, T., Tessier-Lavigne, M., Jessell, T. and Dodd, J., 1991. Control of dorsoventral pattern in vertebrate neural development: induction and polarizing properties of the floor plate. *Dev Suppl. Suppl 2*, 105-22.
- Poelmann, R.E., 1981a. The formation of the embryonic mesoderm in the early post-implantation mouse embryo. *Anat Embryol (Berl)*. 162, 29-40.

- Poelmann, R.E., 1981b. The head-process and the formation of the definitive endoderm in the mouse embryo. *Anat Embryol (Berl)*. 162, 41-9.
- Pyrgaki, C., Trainor, P., Hadjantonakis, A.K. and Niswander, L., 2010. Dynamic imaging of mammalian neural tube closure. *Dev Biol*. 344, 941-7.
- Remak, R., 1855. *Untersuchungen über die Entwicklung der Wirbelthiere*, Berlin: G. Reimer.
- Rodrigo Albers, A., Halley, P.A. and Storey, K.G., 2016. Fate mapping caudal lateral epiblast reveals continuous contribution to neural and mesodermal lineages and the origin of secondary neural tube. *bioRxiv*.
- Rolo, A., Savery, D., Escuin, S., de Castro, S.C., Armer, H.E., Munro, P.M., Mole, M.A., Greene, N.D. and Copp, A.J., 2016. Regulation of cell protrusions by small GTPases during fusion of the neural folds. *Elife*. 5, e13273.
- Rosenquist, G.C., 1971. The location of the pregut endoderm in the chick embryo at the primitive streak stage as determined by radioautographic mapping. *Dev Biol*. 26, 323-35.
- Row, R.H., Tsotras, S.R., Goto, H. and Martin, B.L., 2016. The zebrafish tailbud contains two independent populations of midline progenitor cells that maintain long-term germ layer plasticity and differentiate based on local signaling cues. *Development*. 143, 244-54.
- Ryan, J.F. and Baxevanis, A.D., 2007. Hox, Wnt, and the evolution of the primary body axis: insights from the early-divergent phyla. *Biol Direct*. 2, 37.
- Sakai, Y., 1989. Neurulation in the mouse: manner and timing of neural tube closure. *Anat Rec*. 223, 194-203.
- Sakai, Y., Meno, C., Fujii, H., Nishino, J., Shiratori, H., Saijoh, Y., Rossant, J. and Hamada, H., 2001. The retinoic acid-inactivating enzyme CYP26 is essential for establishing an uneven distribution of retinoic acid along the antero-posterior axis within the mouse embryo. *Genes Dev*. 15, 213-25.
- Sausedo, R.A. and Schoenwolf, G.C., 1994. Quantitative analyses of cell behaviors underlying notochord formation and extension in mouse embryos. *Anat Rec*. 239, 103-12.
- Schindelin, J., Arganda-Carreras, I., Frise, E., Kaynig, V., Longair, M., Pietzsch, T., Preibisch, S., Rueden, C., Saalfeld, S., Schmid, B., Tinevez, J.Y., White, D.J., Hartenstein, V., Eliceiri, K., Tomancak, P. and Cardona, A., 2012. Fiji: an open-source platform for biological-image analysis. *Nat Methods*. 9, 676-82.
- Schoenwolf, G.C., 1978. Effects of complete tail bud extirpation on early development of the posterior region of the chick embryo. *Anat Rec*. 192, 289-95.
- Schoenwolf, G.C., 1984. Histological and ultrastructural studies of secondary neurulation in mouse embryos. *Am J Anat*. 169, 361-76.
- Schoenwolf, G.C., 1992. Morphological and mapping studies of the paranodal and postnodal levels of the neural plate during chick neurulation. *Anat Rec*. 233, 281-90.

- Schulz, C., Schroder, R., Hausdorf, B., Wolff, C. and Tautz, D., 1998. A caudal homologue in the short germ band beetle *Tribolium* shows similarities to both, the *Drosophila* and the vertebrate caudal expression patterns. *Dev Genes Evol.* 208, 283-9.
- Searle, A.G., 1966. Curtailed, a new dominant T-allele in the house mouse. *Genet Res.* 7, 86-95.
- Shaham, O., Smith, A.N., Robinson, M.L., Taketo, M.M., Lang, R.A. and Ashery-Padan, R., 2009. Pax6 is essential for lens fiber cell differentiation. *Development.* 136, 2567-78.
- Shinmyo, Y., Mito, T., Matsushita, T., Sarashina, I., Miyawaki, K., Ohuchi, H. and Noji, S., 2005. caudal is required for gnathal and thoracic patterning and for posterior elongation in the intermediate-germband cricket *Gryllus bimaculatus*. *Mech Dev.* 122, 231-9.
- Shum, A.S. and Copp, A.J., 1996. Regional differences in morphogenesis of the neuroepithelium suggest multiple mechanisms of spinal neurulation in the mouse. *Anat Embryol (Berl).* 194, 65-73.
- Shum, A.S., Poon, L.L., Tang, W.W., Koide, T., Chan, B.W., Leung, Y.C., Shiroishi, T. and Copp, A.J., 1999. Retinoic acid induces down-regulation of Wnt-3a, apoptosis and diversion of tail bud cells to a neural fate in the mouse embryo. *Mech Dev.* 84, 17-30.
- Sobotta, J., 1902. Die Entwicklung des Eies der Maus vom Schlusse der Furchungsperiode bis zum Auftreten der Amniosfalten. *Archiv für mikroskopische Anatomie.* 61, 274-330.
- Sobotta, J., 1911. Die Entwicklung des Eies der Maus vom ersten Auftreten des Mesoderms an bis zur Ausbildung der Embryonalanlage und dem Auftreten der Allantois. *Archiv für mikroskopische Anatomie.* 78, 271-352.
- Srinivas, S., Watanabe, T., Lin, C.S., William, C.M., Tanabe, Y., Jessell, T.M. and Costantini, F., 2001. Cre reporter strains produced by targeted insertion of EYFP and ECFP into the ROSA26 locus. *BMC Dev Biol.* 1, 4.
- Sulik, K., Dehart, D.B., Ilangaki, T., Carson, J.L., Vrablic, T., Gesteland, K. and Schoenwolf, G.C., 1994. Morphogenesis of the murine node and notochordal plate. *Dev Dyn.* 201, 260-78.
- Takada, S., Stark, K.L., Shea, M.J., Vassileva, G., McMahon, J.A. and McMahon, A.P., 1994. Wnt-3a regulates somite and tailbud formation in the mouse embryo. *Genes Dev.* 8, 174-89.
- Takemoto, T., Uchikawa, M., Kamachi, Y. and Kondoh, H., 2006. Convergence of Wnt and FGF signals in the genesis of posterior neural plate through activation of the Sox2 enhancer N-1. *Development.* 133, 297-306.
- Takemoto, T., Uchikawa, M., Yoshida, M., Bell, D.M., Lovell-Badge, R., Papaioannou, V.E. and Kondoh, H., 2011. Tbx6-dependent Sox2 regulation determines neural or mesodermal fate in axial stem cells. *Nature.* 470, 394-8.
- Tam, P.P. and Beddington, R.S., 1987. The formation of mesodermal tissues in the mouse embryo during gastrulation and early organogenesis. *Development.* 99, 109-26.

- Tam, P.P., Williams, E.A. and Chan, W.Y., 1993. Gastrulation in the mouse embryo: ultrastructural and molecular aspects of germ layer morphogenesis. *Microsc Res Tech.* 26, 301-28.
- Taniguchi, Y., Kurth, T., Weiche, S., Reichelt, S., Tazaki, A., Perike, S., Kappert, V. and Epperlein, H.H., 2017. The posterior neural plate in axolotl gives rise to neural tube or turns anteriorly to form somites of the tail and posterior trunk. *Dev Biol.* 422, 155-170.
- Taranova, O.V., Magness, S.T., Fagan, B.M., Wu, Y., Surzenko, N., Hutton, S.R. and Pevny, L.H., 2006. SOX2 is a dose-dependent regulator of retinal neural progenitor competence. *Genes Dev.* 20, 1187-202.
- Technau, U., Rudd, S., Maxwell, P., Gordon, P.M., Saina, M., Grasso, L.C., Hayward, D.C., Sensen, C.W., Saint, R., Holstein, T.W., Ball, E.E. and Miller, D.J., 2005. Maintenance of ancestral complexity and non-metazoan genes in two basal cnidarians. *Trends Genet.* 21, 633-9.
- Tsakiridis, A., Huang, Y., Blin, G., Skylaki, S., Wymeersch, F., Osorno, R., Economou, C., Karagianni, E., Zhao, S., Lowell, S. and Wilson, V., 2014. Distinct Wnt-driven primitive streak-like populations reflect in vivo lineage precursors. *Development.* 141, 1209-21.
- Tsakiridis, A. and Wilson, V., 2015. Assessing the bipotency of in vitro-derived neuromesodermal progenitors.
- Turner, D.A., Hayward, P.C., Baillie-Johnson, P., Rue, P., Broome, R., Faunes, F. and Martinez Arias, A., 2014. Wnt/beta-catenin and FGF signalling direct the specification and maintenance of a neuromesodermal axial progenitor in ensembles of mouse embryonic stem cells. *Development.* 141, 4243-53.
- Tzouanacou, E., Wegener, A., Wymeersch, F.J., Wilson, V. and Nicolas, J.F., 2009. Redefining the progression of lineage segregations during mammalian embryogenesis by clonal analysis. *Dev Cell.* 17, 365-76.
- Uwanogho, D., Rex, M., Cartwright, E.J., Pearl, G., Healy, C., Scotting, P.J. and Sharpe, P.T., 1995. Embryonic expression of the chicken Sox2, Sox3 and Sox11 genes suggests an interactive role in neuronal development. *Mech Dev.* 49, 23-36.
- van de Ven, C., Bialecka, M., Neijts, R., Young, T., Rowland, J.E., Stringer, E.J., Van Rooijen, C., Meijlink, F., Novoa, A., Freund, J.N., Mallo, M., Beck, F. and Deschamps, J., 2011. Concerted involvement of Cdx/Hox genes and Wnt signaling in morphogenesis of the caudal neural tube and cloacal derivatives from the posterior growth zone. *Development.* 138, 3451-62.
- van Straaten, H.W., Hekking, J.W., Copp, A.J. and Bernfield, M., 1992. Deceleration and acceleration in the rate of posterior neuropore closure during neurulation in the curly tail (ct) mouse embryo. *Anat Embryol (Berl).* 185, 169-74.
- Verrier, L., Davidson, L., Gierlinski, M., Dady, A. and Storey, K.G., 2018. Neural differentiation, selection and transcriptomic profiling of human neuromesodermal progenitor-like cells in vitro. *Development.* 145, pii: dev166215.

- Vogt, W., 1926. Über Wachstum und Gestaltungsbewegungen am hinteren Körperende der Amphibien. *Anat Anz.* 61, 62 - 75.
- Wang, F., Flanagan, J., Su, N., Wang, L.C., Bui, S., Nielson, A., Wu, X., Vo, H.T., Ma, X.J. and Luo, Y., 2012. RNAscope: a novel in situ RNA analysis platform for formalin-fixed, paraffin-embedded tissues. *J Mol Diagn.* 14, 22-9.
- Waterman, R.E., 1976. Topographical changes along the neural fold associated with neurulation in the hamster and mouse. *Am J Anat.* 146, 151-71.
- Waterman, R.E., 1979. Scanning electron microscope studies of central nervous system development. *Birth Defects Orig Artic Ser.* 15, 55-77.
- Wilkinson, D.G., Bhatt, S. and Herrmann, B.G., 1990. Expression pattern of the mouse T gene and its role in mesoderm formation. *Nature.* 343, 657-9.
- Wilson, D.B. and Finta, L.A., 1980. Early development of the brain and spinal cord in dysraphic mice. *Anatomy and Embryology.* 160, 315-326.
- Wilson, V. and Beddington, R.S., 1996. Cell fate and morphogenetic movement in the late mouse primitive streak. *Mech Dev.* 55, 79-89.
- Wilson, V., Olivera-Martinez, I. and Storey, K.G., 2009. Stem cells, signals and vertebrate body axis extension. *Development.* 136, 1591-604.
- Wittler, L., Shin, E.H., Grote, P., Kispert, A., Beckers, A., Gossler, A., Werber, M. and Herrmann, B.G., 2007. Expression of *Mgn1* in the presomitic mesoderm is controlled by synergism of WNT signalling and *Tbx6*. *EMBO Rep.* 8, 784-9.
- Wood, H.B. and Episkopou, V., 1999. Comparative expression of the mouse *Sox1*, *Sox2* and *Sox3* genes from pre-gastrulation to early somite stages. *Mech Dev.* 86, 197-201.
- Wymeersch, F.J., Huang, Y., Blin, G., Cambray, N., Wilkie, R., Wong, F.C. and Wilson, V., 2016. Position-dependent plasticity of distinct progenitor types in the primitive streak. *Elife.* 5, e10042.
- Yamaguchi, T.P., Takada, S., Yoshikawa, Y., Wu, N. and McMahon, A.P., 1999. T (Brachyury) is a direct target of *Wnt3a* during paraxial mesoderm specification. *Genes Dev.* 13, 3185-90.
- Yamanaka, Y., Tamplin, O.J., Beckers, A., Gossler, A. and Rossant, J., 2007. Live imaging and genetic analysis of mouse notochord formation reveals regional morphogenetic mechanisms. *Dev Cell.* 13, 884-96.
- Yanagisawa, K.O., Fujimoto, H. and Urushihara, H., 1981. Effects of the brachyury (T) mutation on morphogenetic movement in the mouse embryo. *Dev Biol.* 87, 242-8.
- Yanagisawa, K.O. and Kitamura, K., 1975. Effects of the brachyury (T) mutation on mitotic activity in the neural tube. *Dev Biol.* 47, 433-8.
- Ybot-Gonzalez, P., Cogram, P., Gerrelli, D. and Copp, A.J., 2002. Sonic hedgehog and the molecular regulation of mouse neural tube closure. *Development.* 129, 2507-17.

- Ybot-Gonzalez, P., Savery, D., Gerrelli, D., Signore, M., Mitchell, C.E., Faux, C.H., Greene, N.D. and Copp, A.J., 2007. Convergent extension, planar-cell-polarity signalling and initiation of mouse neural tube closure. *Development*. 134, 789-99.
- Yoon, J.K. and Wold, B., 2000. The bHLH regulator pMesogenin1 is required for maturation and segmentation of paraxial mesoderm. *Genes Dev*. 14, 3204-14.
- Yoshida, M., Uchikawa, M., Rizzoti, K., Lovell-Badge, R., Takemoto, T. and Kondoh, H., 2014. Regulation of mesodermal precursor production by low-level expression of B1 Sox genes in the caudal lateral epiblast. *Mech Dev*. 132, 59-68.
- Yoshikawa, Y., Fujimori, T., McMahon, A.P. and Takada, S., 1997. Evidence that absence of Wnt-3a signaling promotes neuralization instead of paraxial mesoderm development in the mouse. *Dev Biol*. 183, 234-42.
- Zappone, M.V., Galli, R., Catena, R., Meani, N., De Biasi, S., Mattei, E., Tiveron, C., Vescovi, A.L., Lovell-Badge, R., Ottolenghi, S. and Nicolis, S.K., 2000. Sox2 regulatory sequences direct expression of a (beta)-geo transgene to telencephalic neural stem cells and precursors of the mouse embryo, revealing regionalization of gene expression in CNS stem cells. *Development*. 127, 2367-82.
- Zhu, J., Kwan, K.M. and Mackem, S., 2016. Putative oncogene Brachyury (T) is essential to specify cell fate but dispensable for notochord progenitor proliferation and EMT. *Proc Natl Acad Sci U S A*. 113, 3820-5.